Heat Transfer Characteristics of Supercritical Cycle of Carbon Dioxide in a Horizontal Tube

(수평관내 이산화탄소의 초임계 사이클 중의 열전달 특성에 관한 연구)

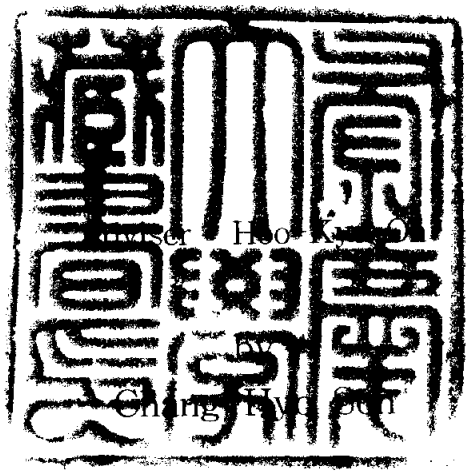

A thesis submitted in partial fulfillment of the requirements for the degree of

Doctor of Philosophy

in the Department of Refrigeration and Air Conditioning Engineering, Graduate School, Pukyong National University

August 2004

손창효의 공학박사 학위논문을 인준함

2004년 8월 일

주 심	공학박사	김 종 수	
부 심	공학박사	김 영 수	
위 원	공학박사	최 광 환	
위 원	공학박사	정 시 영	
위 원	공학박사	오 후 규	

Heat Transfer Characteristics of Supercritical Cycle of Carbon Dioxide in a Horizontal Tube

A Dissertation
by
Chang-Hyo Son

Approved by :

Dean of Graduate School

Chairman

Member

Member

Member

Member

August 20, 2004

CONTENTS

Heat Transfer Characteristics of Supercritical Cycle of Carbon Dioxide in a Horizontal Tube

Chang Hyo Son

Department of Refrigeration & Air Conditioning Engineering,
Graduate School, Pukyong National University

Abstract

몬트리올 의정서 채택 이후, 오존층 파괴 및 지구 온난화 등의 문제를 해결하기 위하여, 이에 영향을 미치는 물질들의 생산 및 사용을 규제하고 있다. 기존 열에너지 이용기기의 냉매로 널리 사용되어온 CFCs 물질은 선진국의 경우 1996년부터는 사용하지 않고 있다. 개발 도상국에서 필수 용도로 제한된 양만을 생산하여 한시적으로 개발도상국으로 수출하고 있다. 몬트리올 의정서 채택 이후, CFCs의 생산 중단과 HCFCs의 점차적인 규제로 말미암아 표준 냉동사이클 및 기기에 적합한 HFCs계를 개발하는 것과 생체학적으로 안전한 자연냉매를 이용하는 연구가 세계 각국에서 활발히 이루어지고 있는데, CO_2는 자동차 에어콘 및 급탕기에 적용할 수 있는 대표적인 자연냉매이다.

CO_2(R 744)는 1800년도 후반부터 선박에서의 냉동, 건물에서의 공조시스템 및 일반적인 냉동시스템의 냉매로 널리 쓰여져 왔으나 프레온 냉매의 등장 이후에 그 사용이 급격히 감소하였다. 그러나 최근 환경문제가 중요시되면서 CO_2는 자동냉매로서 재사용되기 위한 연구가 활성화되고 있다. CO_2는 무독성,

비가연성의 환경 친화적인 냉매로 냉동기유 및 일반 기기재료와도 호환성이 좋다. CO_2는 임계 압력이 약 74bar 이고, 임계온도는 약 31℃로서 대기와 열교환을 할 때 임계점 보다 높은 온도에서 열교환하게 된다. 그러므로 초임계 압력에서 냉각하게 되고, 이때 큰 온도하강을 고려하여야 하며, 효율적인 에너지 사용을 위한 방안을 모색하여야 한다. CO_2를 작동매체로 사용할 때 체적 냉동능력(VCR)이 높고, 압력강하가 작기 때문에 에너지 소비도 줄일 수 있고, 컴팩트한 열교환기도 제작할 수 있는 이점이 있다. 또한 시스템 압력이 종래의 증기 압축 냉동시스템보다 매우 높다. 높은 압력은 단점이 될 수 있지만 장점이 될 수도 있다. 이런 이유로 CO_2를 작동유체로 사용하는 경우에 열교환기의 적절한 설계가 요구된다. 따라서, 본고에서는 CO_2용 증발기와 가스 냉각기 설계를 위한 기초자료를 제공하고자 CO_2를 냉매로 사용하여 임계와 초임계 압력에서 열전달과 압력강하 특성에 대해서 연구하고자 하였다.

본 논문의 실험은 CO_2의 증발과 가스 냉각으로 크게 나누어지며, 우선 증발 실험장치는 마그네틱 기어펌프로 구동되는 냉매 순환루프로 구성된다. 냉매 순환루프의 주요 구성품은 수액기, 마그네틱 기어펌프, 질량 유량계, 예열기, 시험부(증발기) 등으로 구성된다. 증발 시험을 위한 시험부는 내경이 7.75 mm 이고, 길이가 5 m인 스텐레스관이다. 실험은 포화온도가 -5, 0, 5℃이고, 열유속이 10, 20, 30, 40 kW/m^2이며, 질량유속은 200, 300, 400, 500 kg/m^2s의 범위에서 수행되었다. 증발 실험의 주요 결과를 요약하면 다음과 같다. 증발압력강하를 종래의 상관식들과 비교했을 때, 큰 이탈정도를 보였다. 그 중에서 Choi와 Domanski(1968) 상관식과 13.9%이내에서 좋은 일치를 보였다. 그리고, 열전달 계수는 다른 상관식들과 많은 차이를 보였으며, 그 중에서 Jung 등의 상관식이 21.6%이내에서 가장 좋은 일치를 보였다.

냉각 실험장치는 내관으로 냉매가 흐르고, 환상공간으로 냉각수가 유동하는

대향류 형태의 이중관식 열교환기이다. 내관은 스테인레스관으로 내경이 7.75 mm이고, 전체길이는 6000 mm이다. 실험은 가스 냉각기의 입구압력은 7.5에서 12 MPa까지 0.5 MPa씩 증가하고, 질량유속은 200에서 500 kg/m^{2}s까지의 범위내에서 수행하였다. 가스 냉각기내 CO_2의 압력강하는 종래의 Blasius 상관식과 4.8%이내에서 좋은 일치를 보였다. 그리고 열전달 계수는 타 상관식들과 다소 많은 차이를 보였지만, 그 중에서 Bringer와 Smith 상관식과 가장 좋은 일치를 보였다. 그러나, 여전히 본 실험결과와는 큰 차이를 보였으므로, 본 실험자료를 바탕으로 초임계 영역에서 쉽게 적용할 수 있는 새로운 상관식을 제안하였다.

주요서: 가스냉각, 히트 펌프, 초임계 열전달 계수, 초임계 압력강하

LIST OF TABLES, FIGURES AND PHOTOGRAPHS

FIGURES

TABLES

PHOTOGRAPHS

NOMENCLATURE

SYMBOLS

A	Area	m^2
A_1, A_2	Coefficients in Petuhkov-Kirillov's correlation	
B	Parameter in Krasnoshchekov et al.'s correlation, Parameter in Chisholm' correlation	
C	Constant defined Eq. (3.18)	
COP	Coefficients of performance	
c_p	Specific heat at constant pressure	kJ/kg·K
$\overline{c_p}$	Mean specific heat at constant pressure	kJ/kg·K
$c_{p,i}$	Integrated mean specific heat at constant pressure	kJ/kg·K
d	Diameter	m
exp	Exponent	
E	Constant in Gungor Winterton's correlation	
f	Friction factor	
f_n	Friction factor defined in Eq. (3.29)	
F	Constant in Shah's correlation	
F_{fl}	Parameter depending on fluid	
F_p	Parameter of Jung's correlation	
g	Gravity acceleration	m/s^2

G	Mass velocity	$kg/m^2 \cdot s$
h	Heat transfer coefficient	$kW/m^2 \cdot K$
H_1, H_2, H_3	Constants in Friedel's correlation	
i	Enthalpy	kJ/kg
i_{fg}	Latent heat	kJ/kg
I	Input ampere of preheater	A
J	Parameter in Krasnoshchekov et al.'s correlation	
k	Thermal conductivity	$kW/m \cdot K$
L	Tube length	m
M	Mass flow rate	kg/h
n	Number of local tube	
N	Constant in Shah's correlation	
P	Pressure	MPa
Q	Heat capacity	kW
q	Heat flux	kW/m^2
R_n	Relative roughness of tubes	
S	Suppression factor	
s	Parameter in Petro Popov's correlation	
T	Temperature	K
V	Input voltage of preheater	V
W	Molecular weight	kg/kmol
x	Quality	
Y	Chisholm's parameter	

z	Tube length	m
Z	Parameter in Shah's correlation	
$\left(\frac{dP}{dz}\right)_f$	Pressure drop due to friction	
$\left(\frac{dP}{dz}\right)_a$	Pressure drop due to acceleration	

GREEK SYMBOLS

Δ	Difference	
μ	Dynamic viscosity	Pa·s
ν	Specific volume	m^3/kg
ρ	Density	kg/m^3
ζ	Efficiency of preheater	
σ	Surface tension, Deviation	
Ψ	Parameter in Shah's correlation	
X_{tt}	Lockhart Martinelli parameter	
Φ	Two phase multiplier	

DIMENSIONLESS NUMBERS

Bo	Boiling number
Co	Convection number
Fr	Froude number
Ga	Galileo number
Nu	Nusselt number

Pr	Prandtl number
Re	Reynolds number
We	Weber number

SUBSCRIPTS

abs	Absolute
avg	Average
b	Bulk
bottom	Bottom
bs	Bubble suppression
cal	Calculated
cb	Convective boiling
CBD	Convective boiling dominant
cp	Critical point
cs	Source water of condenser
e	Evaporator
eq	Equivalent
es	Source water of gas cooler
exp	Experimental
gc	Gas cooler
h	Homogeneous model
i	Inner
in	Inlet

l	Liquid, Flow of the liquid phase alone in the tube
lo	Total flow having the liquid properties
loc	Local
m	Mean
nb	Nucleate boiling
NBD	Nucleate boiling dominant
o	Outer
out	Outlet
pc	Pseudo critical point
pool	Pool boiling
re	Refrigerant
rp	Reduced pressure
sat	Saturation
side	Side
top	Top
tp	Two phase
TP	Triple point
v	Vapor, Flow of the vapor phase alone in the tube
v0	Total flow having the vapor properties
VCR	Volumetric capacity for refrigerating
w	Wall
x	Reference

CHAPTER 1

INTRODUCTION

1.1 BACKGROUND OF THE STUDY

CFCs and HCFCs, which are thermodynamically superior and safe refrigerants, have been used widely as working fluids for refrigerator and air conditioner since the 1930s. But nowadays these refrigerants are so called 'greenhouse gases', artificial substances have a higher ozone depletion potential(ODP) and global warming potential(GWP). Ozone depletion was to be suppressed by the international agreement of Montreal Protocol and the cure for global warming was prepared by Kyoto protocol. The heart of the Montreal Protocol is restricting the production and consumption of ozone depletion substances. The regulation prohibiting the use of CFCs as refrigerants by industrialized nations is currently in effect, and guidelines for phasing out HCFCs as refrigerants in the future have already been agreed upon by many nations. This has prompted researchers worldwide to investigate the feasibility of natural refrigerants in novel refrigeration cycles.

The description 'natural' implies their presence in the environment form biological and geological sources. In other words, the natural refrigerants are naturally occurring substances, namely, carbon dioxide(CO_2), nitrogen(N_2), helium(He), and water(H_2O) represent a further 'natural' alternative. These natural refrigerants have a zero ozone depletion potential(ODP), and most of them also have zero GWP. However, some of

them are flammable and/or toxic.

Among these natural refrigerants, CO_2 is not a new refrigerant and has a successful history of the use as a refrigerant. It has many advantages as a working fluid. Namely, the most relevant characteristics of CO_2 are no toxicity, inflammability, no ODP and no GWP, if CO_2 is recovered, and economical efficiency. Moreover, because CO_2 has the high VCR(volumetric capacity for refrigerants) and working pressure, it is possible to make a system compact.[1]

Recent research on CO_2 has been focused on the development of a supercritical cycle. Most of the recent investigations of CO_2 as working fluid have included a thermodynamic analysis of supercritical cycle. However, relatively few study have been performed to measure heat transfer coefficient and pressure drop during evaporation and heat rejection of CO_2. While a great deal of research has been conducted to determine the heat transfer coefficient and pressure drop during evaporation and condensation of fluorocarbon refrigerant, comparatively few investigations have been performed for CO_2. Therefore, more comprehensive and fundamental study for major components is required to develop the enhanced refrigeration system. Especially, to design heat exchanger for CO_2 during evaporation and cooling process, the basic data for heat transfer and pressure drop characteristics of CO_2 are necessary. The purpose of this study is to offer the heat transfer and pressure drop characteristics during evaporation and cooling of CO_2.

1.2 CHARACTERISTICS OF CO_2

This section deals with the properties of CO_2 which are of importance for the system design, especially for heat transfer and pressure drop calculations. Additionally, a comparison of CO_2 with the R-12, R-22, R-134a, R-717, R-290 and R-410A is presented.

1.2.1 Critical point of CO_2

Critical point is a state at which it is impossible to distinguish certainly liquid phase from gas phase and is defined as liquid-like state or gas like state. Namely, no liquefaction will take place above its supercritical region and no gas will be formed above its critical point. The region where pressure and temperature are higher than the critical values can be defined as the supercritical point, and the region where pressure and temperature are lower than the critical values can be defined as the subcritical point

Fig. 1.1 depicts pressure and temperature diagram for critical point and triple point of CO_2. As can be seen from this figure, a refrigerator and air conditioner using CO_2 will always operate close to the critical point. Outside the saturation line no phase change can be observed, the fluid becomes single-phase and any limits between liquid and vapor are arbitrary. The region where pressure and temperature are higher than the critical values can be defined as the supercritical region.

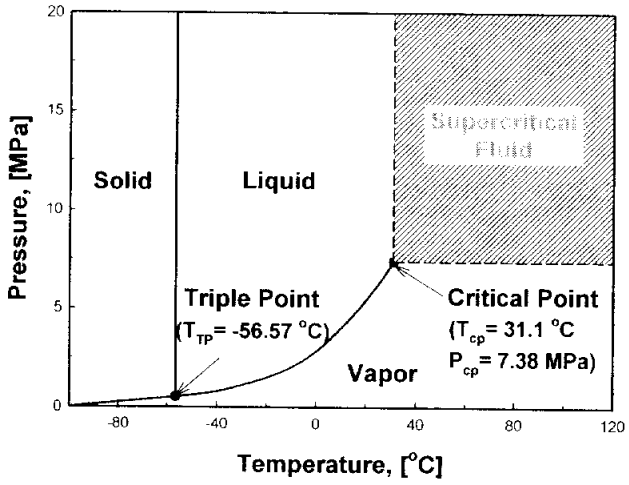

Fig. 1.1 Pressure and temperature diagram for critical point and triple point of CO_2.

1.2.2 Thermophysical properties of CO_2

The thermophysical properties of CO_2 are, of course, extremely important in determining the heat transfer and pressure drop during the cooling and evaporation process of CO_2. They can be usually classified as thermodynamic properties and transport properties. The main thermodynamic properties include density, specific heat, enthalpy and entropy. The main transport properties include thermal conductivity and viscosity.

Fig. 1.2 shows how the selected thermodynamic properties of CO_2, which are calculated by REFPROP(version 6.02)[2], change during the supercritical gas cooling process. Fig. 1.2 (a) and (b) depict the variation of density and specific heat with respect to refrigerant temperature. The density decreases

rapidly with temperature near the critical point. The specific heat increases extremely in the vicinity of critical point, and these enhancement is higher as gas cooling pressure increases. This rapid increase, which is only observed near the critical point, is called a critical enhancement.[3] The region where the specific heat attains a maximum for a specified pressure is called the pseudocritical region or transposed critical region. The temperature of these region is called the pseudocritical temperature.[4]

Fig. 1.2 (c) and (d) display the variation of thermal conductivity and viscosity. The thermal conductivity increases sharply near the critical point. The critical enhancement of the thermal conductivity is stronger than that of the viscosity. The critical enhancement of the thermal conductivity is observed in a larger range of temperatures and pressures around the critical point, while the critical enhancement of the viscosity is confined to a very small region around the critical point.[5] As the pressure approaches the critical temperature, these variations become severe. This results from the fact that no boundary exists between the liquid and gas phase.

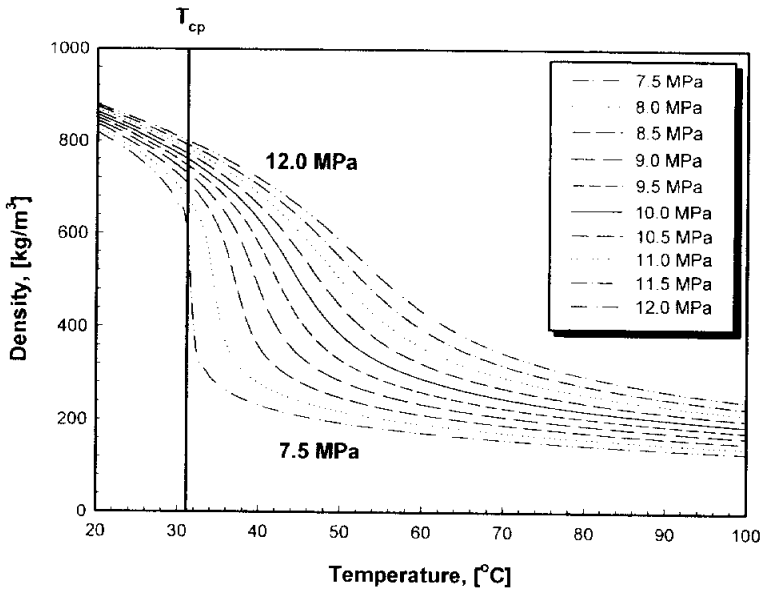

(a) Density

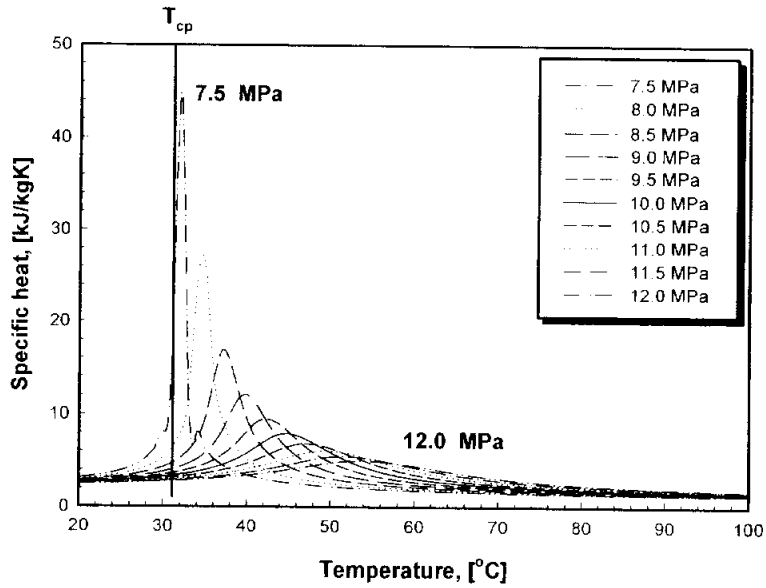

(b) Specific heat

Fig. 1.2 Thermophysical properties of supercritical CO_2 (continued).

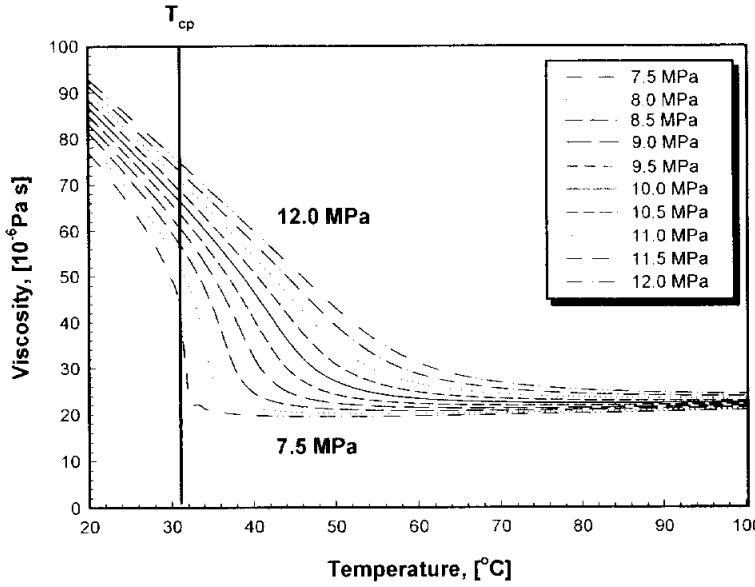

(c) Viscosity

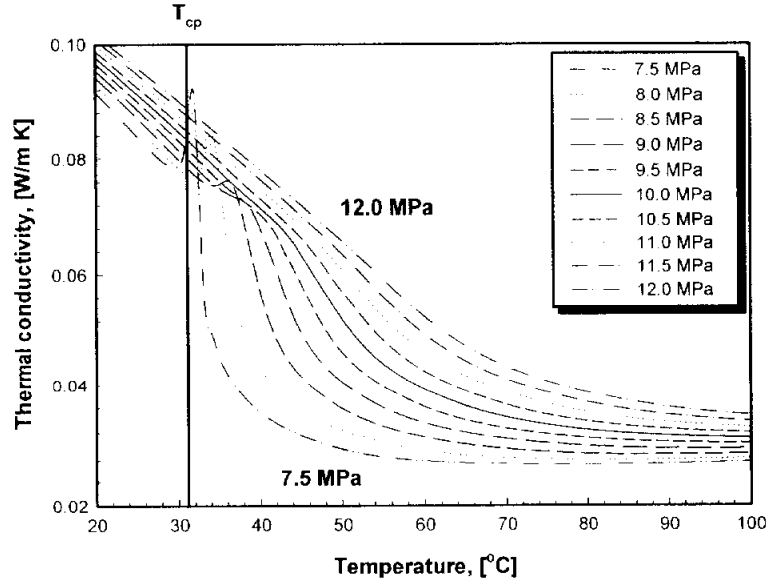

(d) Thermal conductivity

Fig. 1.2 Thermophysical properties of supercritical CO_2.

Variation of Prandtl number($Pr = c_p \mu / k$) with respect to pressure and temperature in shown in Fig. 1.3. As one can see, the Prandtl number has a maximum at the pseudocritical temperature. This is caused by the maximum of the isobaric heat capacity. The dependence of the Prandtl number on the temperature changes with pressure. In the supercritical region, Prandtl number becomes higher with system pressure, while the maximum value decreases. This fact leads to a strongly varying local heat transfer coefficient depending on temperature and pressure. Therefore, although no phase change takes place in the supercritical point, it has been difficult to design a gas cooler and to predict a system performance in a supercritical region. This is because no application of representative single phase flow correlations which can describe the heat transfer characteristics and pressure drop over a range of conditions.

The Prandtl number varies with pressure and temperature of supercritical CO_2 near the critical region. Its variation also has a peak at the pseudocritical temperature as for specific heat, and this peak increases as the pressure approaches the critical point. The Prandtl number represents the ratio between momentum diffusivity and thermal diffusivity and it usually relates the relative thickness of velocity and thermal boundary layers in the constant property case. For fluid flow with heat transfer in the critical region, the Prandtl number is not constant, but varies with temperature and pressure, which means that the ratio of diffusivities in momentum and energy is locally different.

In case of mass flux of 200 kg/m^{2}s, the Reynolds number($Re = G_{re} d_i / \mu$)

with respect to temperature and pressure at the supercritical conditions is shown in Fig. 1.4. As presented in Fig. 1.4, the Reynolds number at the same temperature increases with gas cooling pressure and it has a maximum at the critical point. This means that the heat transfer coefficient has a peak at the pseudocritical point and it decreases dramatically after the critical region.

Fig. 1.5 depicts the comparison of saturation temperature of CO_2 with that of some refrigerants with respect to refrigerant pressure. The CO_2 saturation pressure is about 4 to 12 times higher. For instance, the saturation pressure at 0℃ is 3.49 MPa for CO_2, 0.8 MPa for R-410A and 0.3 to 0.5 MPa for the others. Fig. 1.6 represents the comparison of volumetric capacity of CO_2 with that of some refrigerants. The volumetric capacity for refrigerant, VCR, is defined as the product of the enthalpy of total evaporation and vapor density. For temperatures higher than 22℃, it decreases strongly with temperature ; at the critical temperature it is zero by definition. For temperature lower than 30℃, a VCR of CO_2 is highest. at 0℃, it has a value of 22650 kJ/m^3 for CO_2 and for the others it is below 6700 kJ/m^3. Therefore, due to the advantageous properties of CO_2, system components become compact.

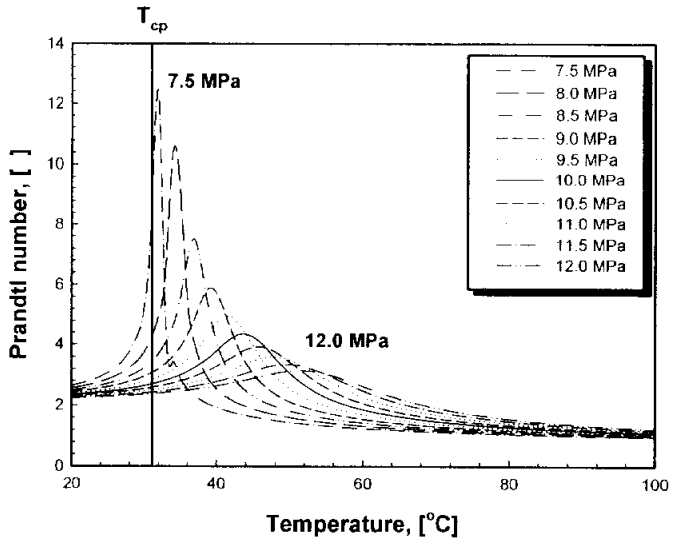

Fig. 1.3 Variation of Prandtl number with respect to temperature and pressure of supercritical CO_2.

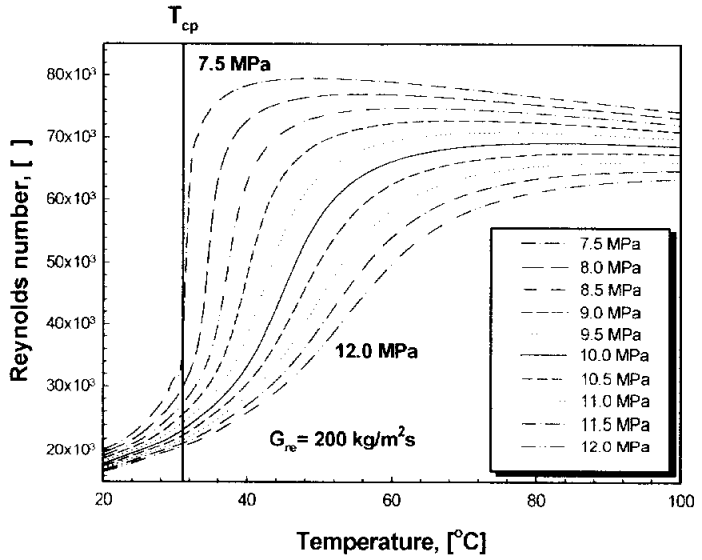

Fig. 1.4 Variation of Reynolds number with respect to temperature and pressure of supercritical CO_2.

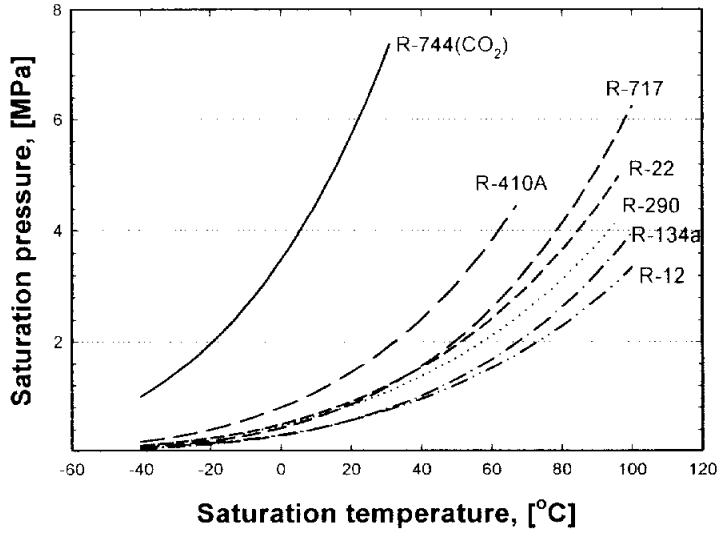

Fig. 1.5 Comparison of the saturation temperature of CO_2 with that of some refrigerants.

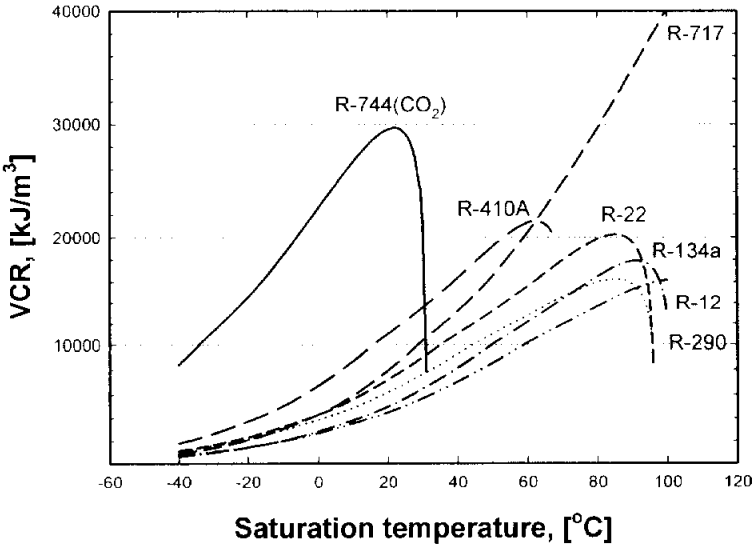

Fig. 1.6 Comparison of the volumetric refrigeration capacity of CO_2 with that of some refrigerants.

1.2.3 Comparison with other refrigerants

This section gives comparisons of the characteristics and properties of the CFC 12, the HCFC 22, the HFC 134a and the binary HFC blend R 410A with the natural substances ammonia(R 717), propane(R 290) and CO_2(R 744). Some important data for the comparison can be found in Table 1.1. The most relevant characteristics of CO_2 are non-toxic, incombustible, no ODP, no GWP and cheap. From a thermodynamic point of view, the main differences to other refrigerants are the low critical temperature and the high critical pressure.

The most important difference to other refrigerants is that the heat rejection process occurs over the critical point. Furthermore, the saturation temperature of CO_2 is about 4 to 12 times higher. Additionally, because of the high operation pressure in a supercritical point, the design technique of heat exchanger is required for the high pressure higher than 15 MPa. However, because the CO_2 refrigerant density is higher as a operation pressure increases, the volumetric flow rate of CO_2 is about one-third of other refrigerants. In case of applying the conventional heat exchanger to a small diameter tube, the heat transfer in a small diameter is improved. Therefore, the main component of refrigeration and air conditioner can be compact.

Table 1.1 Characteristics and properties of some refrigerants[6]

Refrigerant		R-12 CFC	R-22 HCFC	R-134a HFC	R-410A HFC-HFC	R-717	R-290	R-744
Chemical Formula		CCl_2F_2	$CHClF_2$	CH_2FCF_3	CH_2F_2/CHF_2CF_3	NH_3	C_3H_8	CO_2
Natural Substance?		No	No	No	No	Yes	Yes	Yes
ODP		1.0	0.05	0	0	0	0	0
GWP	100년	7,100	1,600	1,200	1,730	0	3	1(0)
	20년	7,100	4,200	3,100	-	0	-	1(0)
TLV* [ppm]		1,000	1,000	1,000	1,000	25	1,000	2,500
IDLH**ppm]		50,000	-	-		500	20,000	50,000
Maximum charge[vol %]		4.0	4.2	-		-	0.44	5.5
per room volume [kg/m^3]		0.2	0.15		-		0.008	0.1
Flammable or explosive?		No	No	No	No	Yes	Yes	No
Toxic/irritation decomposition products?		Yes	Yes	Yes	-	No	No	No
Relative price (approximately)		1	1	3~5	5	0.2	0.1	0.1
Molar mass (kg/kmol)		120.92	86.48	102.03	72.6	17.03	44.1	44.01
Critical parameter	temperature (℃)	112.0	96.2	101.2	72.5/84.9	132.3	96.7	31.1
	pressure (MPa)	4.16	4.99	4.07	4.95	11.33	4.24	7.38
Normal boiling point [℃]		-29.8	-40.8	-26.2	-52.7	-33.3	-42.1	-78.5

TLV*: Threshold Limit Value The refrigeration concentration limit in air or a normal 8 hour work day, will not cause an adverse effect in most people.

IDLH**: Immediately Dangerous to life or Health Maximum level from which one could escape within 30 minutes without impairing symptoms or any irreversible health effects.

1.3 REVIEW OF PREVIOUS WORKS

1.3.1 evaporation heat transfer and pressure drop

In the early 1990's, researches on CO_2 have been focused on the development of a supercritical cycle. However, relatively few investigations have been conducted on the in-tube heat transfer and pressure drop of CO_2.

Kuo and Wang[7] compared the measured evaporation heat transfer coefficient for CO_2 in a smooth tube and micro-fin tube with inner diameter tube of 9.52 mm. The experiments were conducted at the evaporation temperature of 6℃ and 10℃, mass flux of 100 to 300 kg/m^{2}s and heat flux of 6 to 14 kW/m^2. They showed that the heat transfer coefficient is influenced by heat flux, mass flux and evaporation pressure.

Yuan et al.[8] present the comparison of the measured evaporation heat transfer coefficient for CO_2 in a smooth tube with inner diameter of 6 mm. The experimental conditions in their study are following range of variables : the evaporation temperature is 283 K, mass fluxes range from 160 to 320 kg/m^{2}s, the heat fluxes vary from 10 to 20 kW/m^2. The evaporation heat transfer coefficient increases with mass flux and heat flux of refrigerant and decreases as vapor quality increases. Their experimental data showed relatively good agreement with correlation predicted by Gungor-Winterton.[9] The deviation of experimental data and their correlation is less than 10 %.

Hihara and Tanaka[10] showed the boiling heat transfer coefficients and pressure drops of CO_2 in a horizontally smooth tube of whose inner

diameter is 0.1 mm. Experimental conditions are as following ; evaporating temperature is 15℃, heat flux is between 9 and 36 kW/m^2, and mass flux is from 360 to 1449 kg/m^{2}s. The heat transfer coefficient is dependent on heat flux but mass flow rate does not affect it. The vapor quality at the onset of dryout is a function of mass flow rate. In this experimental conditions, the heat transfer coefficients did not agree with the existing equation because the effects of forced convective vaporization were little. Moreover, the pressure drops were much lower than predicted results using the experimental equation that has been generally used.

Choi et al.[11] experimentally investigated the evaporation heat transfer coefficient of CO_2 in a horizontally smooth tube, of whose inner diameter is 7.75 mm. Mass fluxes are controlled at 212, 318, 424 and 530 kg/m^{2}s, heat fluxes are adjusted at 12, 16, 20, 23 and 27 kW/m^2, and evaporating temperature is regulated at 0, 3.4, 6.7 and 10.5 ℃. The evaporating heat transfer coefficient increases with mass flux and heat flux, but it decreases with vapor quality. The measured evaporation heat transfer coefficient at the top, side and bottom of inside wall tube decreases as quality increases. They explained that this is because of the small surface tension of vapor phase of CO_2.

Aoki et al.[12] experimentally investigated the boiling heat transfer coefficients and pressure drops for flow of CO_2 in a horizontal tube, of which inner diameter is 1.0 mm. The experimental conditions are in the following ranges : evaporation temperature is 0℃, mass flux is from 100 to 800 kg/m^{2}s, heat flux is from 5 to 40 kW/m^2, and the quality is from 0.1

to 0.8. As a result, the experimental values of the frictional pressure drop are smaller than that given by Chisholm Larid's correlation. In the boiling heat transfer coefficient of CO_2, the nucleate boiling is predominant when the mass flux is low and the forced convection evaporation is predominant when the mass flux is high. Thus it can be assumed that the mechanism of boiling heat transfer of CO_2 in a small tube is similar to that in a tube of relatively large diameter.

Based on the experimental results of Bredesen et al.[13], Hwang and Radermacher[4] investigated the applicability of six commonly used empirical correlations reported by Chen[14](1966), Bennett Chen[15](1980), Gungor Winterton (1986), Shah(1976), Schrock Grossman[16](1959) and Liu Winterton (1991). It was found that all the six correlations had a large deviation (from 80 to 20%) from the experiments. They proposed a new empirical model which is the modified Bennett Chen correlation for CO_2 flow boiling in horizontal smooth tubes. They claimed that the new correlation could predict the heat transfer coefficients consistent with Bredesen's results to within a mean deviation of 14%.

If the previous studies are summarized, the researches on heat transfer coefficient of CO_2 in evaporator are rare and sparse. The evaporation heat transfer coefficient of CO_2 in a horizontal tube decreases with quality. This results from the low surface tension of CO_2. In comparison with the existing correlations, due to the activation of nucleate boiling and suppression of convective boiling. Their experimental data has relatively large deviation to the existing correlations for the evaporation heat transfer

and the pressure drop of CO_2.

Table 1.2 Preview study on CO_2 evaporator

Author	Test tube				T_{sat} [MPa]	G_{re} [kg/m^{2}s]	q_{re} [kW/m^2]	Geometry
	Material	d_i [mm]	t [mm]	L [m]				
Kuo & Wang		9.52				100~300	6~14	S.T., M.T.
Yuan et al.	Al	6			10	160~320	10~20	S.T.
Hihara & Tanaki		1			15	360, 720, 1449	9, 18, 36	S.T.
Choi		0.775			0, 3.4, 6.7, 10.5	212, 318, 424, 530	12, 16, 20, 23, 27	S.T.
Aoki et al.		1		0.12	0	100~800	5~40	S.T

M.T. : Micro fin Tube, S.T. : Smooth Tube,

1.3.2 Cooling heat transfer and pressure drop

Hashimoto et al.[17] investigated the heat transfer coefficient of CO_2 in horizontal copper tube, which has inner diameter tube of 4 mm and outer diameter tube of 8 mm. The length of test section is 4 m. The correlation predicted by Petukhov Gnielinski is about 22 to 40% lower than the experimental data. The correlation predicted by Krasnoshchekov is about 20 to 30% lower than experimental data. This phenomenon is remarkable at the pseudocritical temperature. They explained that the large property variations at near critical point are not included in their correlation in supercritical region.

Rieberer[6] investigated the heat transfer coefficient during the cooling process of CO_2 in a tube with an inner diameter of 7.8 mm. For the mass flux of 751 kg/m^{2}s, in the temperature range of 40.2 to 34.3℃, the measured value is only 50% of the calculated mean value in the corresponding heat exchanger section. For higher temperature, the measured value is higher. At higher mass flux(936 and 1004 kg/m^{2}s), the differences between calculations and measurement are negligible in all sections. Even the peaks are detected very well in the measurements. The lowest heat coefficient occurs in the supercritical region. In the liquid region(T_w<31℃), the heat transfer coefficient is in the range of 3500 to 4500 W/m^{2}K. For measured mass velocity of 1038 kg/m^{2}s, the fit of the measured and calculated heat transfer coefficient is not very good. Comparing the value at 10 MPa with those at 8 MPa, one can see the lower maximum heat transfer coefficient. Pressure drop measurements are

compared with calculations according to the correlation of Colebrook White. For a test run with a CO_2 inlet pressure of 8.33 MPa and a mass velocity of 940 and 1040 kg/m^{2}s, the measured mean values follow the calculated values very well.

Gao and Honda[18] experimentally investigated the heat transfer characteristics of CO_2 inside horizontal tubes which are used as a gas cooler of a CO_2 heat pump system. The CO_2 flows through the inner tube of 5 mm in I.D. and 8 mm in O.D. The gas cooler is 6 m in length, which are divided into 6 subsections respectively. The mass flow rate ranged from 330 to 680 kg/m^{2}s, pressure of gas cooler varied from 7.6 to 9.6 MPa and saturation temperature ranged from -4 to 4℃. The local heat transfer coefficient in the gas cooler has been compared with the Gnielinski' correlation. The results show that the local heat transfer coefficient of gas cooler agrees well with the correlation except for that at the region near pseudocritical temperature, while that at the region near pseudocritical temperature is higher than the correlation.

Based on Gnielinski's correlation and Petrov-Popov[19]'s equation, Fang et al.[20] obtained the in-tube heat transfer and pressure drop model of gas cooler. When Fang[21]'s equation is compared with Petrov Popov's correlation, the predictions agree with the experimental data very well. They recommended a new correlation in the range of $3000 < Re_w < 10^6$ and $350 < q_w/G < 0$ J/kg.

Pitla et al.[22] presented and discussed the Nusselt number variations of supercritical CO_2 during in tube cooling. Based on the Favre averaged

equations using Nikuradse's mixing length model and k equation turbulence model, a new correlation is proposed. It is based on mean Nusselt numbers that are calculated using the thermophysical properties at the wall and the bulk temperature, respectively. It was seen that 85% of the heat transfer coefficient values predicted by the new correlation was accurate to within 20%. A comparison of the heat transfer coefficient calculated using the new correlation and three existing correlations found in the literature showed that the accuracy in predicting the heat transfer coefficient with the new correlation was greatly increased, especially in the pseudocritical region.

In order to obtain the data for designing and optimizing air conditioning systems using a CO_2 refrigerant, Mori et al[23] examined the cooling heat transfer characteristics of CO_2 at a supercritical pressure condition 9.5 MPa and temperature between 20 to 70℃. The obtained data revealed that heat transfer coefficient increased with mass flux and the maximum heat transfer coefficients were obtained at 45℃. Two layer models for flow field near the tube wall were proposed the models were found to be valid according to the comparison of the predicted values with the experimental data.

If the main previous studies were summarized, the experimental results on heat transfer and pressure drop characteristics of CO_2 in a horizontal stainless steel tube are scare and rare. When comparing the experimental data with the existing correlations, the deviation increases significantly at near pseudocritical point due to the large variation of thermophysical

properties near the critical temperature. The pressure drop of CO_2 in gas cooling process showed relatively agreement to the correlation predicted by Colebrook White.

Table 1.3 Preview study on CO_2 gas cooler

Author	Test tube				P_{gc} [MPa]	G_{re} [kg/m^{2}s]	q_{re} [kW/m^2]	Geometry
	Material	d_i [mm]	t [mm]	L [m]				
Hashimoto & Iwatsubo	Cu	4	2	4	9~10.4	2016~2040		Double Pipe
Rieberer	-	7.8		15.6	8.14~10	751~1038	15~70	Double Pipe
Gao & Honda	Cu	5	1.5	6	7.6~9.6	383~464	0.1~16.5	Double Pipe
Pitla et al.	SUS	6.35	0.815	12.9	8~12	0.029~0.039 [kg/s]		Double Pipe
Mori et al.	Cu	4, 6, 8	2, 3, 4	0.8	9.5	100~500		Double Pipe

1.4 OBJECTIVE AND SUMMARY OF THIS STUDY

1.4.1 Objective of this study

With the growing awareness of the dual threats of ozone depletion and global warming, the significant research activity has been directed to the identification and development of environmentally benign refrigerants. The higher ozone depletion potential by HFCs refrigerant leads to the environmental issues of global warming. In case of the leakage of refrigerant mixture R-407 and R-410A, due to the variation in component ratio of their mixture, the system should be fully recharged. When appling the refrigerant mixture to the existing system, owing to deteriorating coefficient of performance(COP), the design of system is required newly. Therefore, in order to settle environmental problem occurred by using HCFCs and HFCs, a promising candidate must be developed urgently. Some investigators have considered the natural substances like HCs(Hydro Carbon), carbon dioxide(CO_2) and ammonia (NH_3) as a promising candidate. These natural refrigerants have zero ozone depletion potential(ODP) and the majority of them also have zero global warming potential(GWP). Among the natural refrigerants, CO_2 has advantages of no toxicity, no inflammability and economical efficiency. In addition to these advantages, CO_2 has a merit over the existing refrigerants because it has high VCR(Volumetric Capacity for Refrigerants) with a possibility to make a system compact[4].

Thus, in this study, focusing on the heat transfer and pressure drop characteristics during evaporation and gas cooling process, which will be

the foundation of the optimum design for refrigeration and air conditioner using CO_2, the objective of this study is that it offers a basic experimental data of CO_2 for optimum design of refrigeration and air conditioner.

1.4.2 Summary of this study

This thesis consists of five chapters. The summary of each chapter is as follows : In Chapter 1, the introduction, such as back ground of performing this study, previous investigations and the basic understanding of gas cooling process are described. Chapter 1 also examines fundamentals for this study and presents the main aims.

In chapter 2, experimental setup and test procedure to measure the evaporation and cooling heat transfer coefficient and pressure drop of CO_2 in a horizontal tube are presented. Heat flux, mass flux and saturation temperature are major testing parameters. The suitability of the experimental apparatus is also confirmed and the way of arranging experimental results is explained.

In chapter 3, the evaporation heat transfer coefficients and pressure drop are measured in a horizontal tube with CO_2 for several experimental conditions and the results are compared with existing correlations. Obtained heat transfer coefficient of a single evaporating tube is decreasing with increased vapor quality. The heat transfer coefficients of CO_2 are higher than those of fluorocarbon refrigerants. The pressure drop of CO_2 is much lower than that of R 22. These lower pressure drop of CO_2 is attributed to its unique thermal properties. Therefore, CO_2 has a unique characteristics

of evaporation heat transfer and pressure drop.

In chapter 4, the heat transfer coefficients and pressure drop during cooling process of CO_2 are investigated experimentally and the experimental data are compared with existing correlations. The heat transfer coefficients of supercritical CO_2 increase greatly at the pseudocritical temperature. The measured pressure drop during gas cooling process of CO_2 are observed less than 1 kPa/m. Most of the existing correlations shows a large difference with the experimental data during gas cooling process of CO_2. Appropriate correlation is presented by analyzing the experimental data. Finally, in Chapter 5, conclusions for this study summarizes.

CHAPTER 2

EXPERIMENTAL SETUP AND METHODS

2.1 EXPERIMENTS ON EVAPORATION HEAT TRANSFER

This section deals with description of test rig for evaporation heat transfer of CO_2. The experimental apparatus is equipped with measurement sensors in order to gather practical experimental data of CO_2. Here, a detailed description of the test rig, experimental method and conditions are presented.

2.1.1 Experimental apparatus

The experimental apparatus was designed and constructed to grasp the heat transfer during the evaporation process of CO_2. The test runs were concentrated on the measurement of the evaporation heat transfer coefficient and pressure drop for CO_2. Fig. 2.1 shows the schematic diagram of the experimental apparatus for evaporation heat transfer test with CO_2. Fig. 2.2 presents the detail diagram of the test section for the evaporation heat transfer test.

As shown in Fig. 2.1, the test rig is composed of magnetic gear pump, mass flowmeter, preheater, heat transfer test section, liquid receiver, subcooler and constant temperature bath. The subcooling liquid of CO_2 in receiver was circulated through the mass flowmeter by means of magnetic gear pump without compressor. The mass flowmeter is installed before the

preheater to measure the mass flux and density of CO_2 refrigerant in liquid phase. The refrigerant leaving the mass flowmeter in subcooling phase enters the preheater. Because the temperature and pressure of CO_2 is adjusted simultaneously at the preheater, the preheater is installed to obtain the desired inlet quality and pressure of CO_2 refrigerant, and the constant temperature bath is set up to control the given saturation temperature. After leaving the preheater, the CO_2 enters the test section and then it is evaporated with flowing through the tube. The CO_2 refrigerant leaving the evaporator is completely cooled down and condensed in subcooler that is cooled by brine at the temperature of 25℃ to -5℃. Owing to the simultaneous existence of vapor and liquid phase in receiver, the liquid phase of CO_2 in the bottom of receiver is circulated by magnetic gear pump. Because of heat loss from the surroundings, when CO_2 refrigerant flows through system, the state of CO_2 in system varies the two phase or superheating phase. In order to reduce heat gain and loss from the surroundings and to obtain the desired saturation temperature and quality, the tube and valve was covered with insulation material.

In the experimental apparatus, the evaporation process occurs at a preheater and the test section. In order to actively supply electronic power for the preheat with respect to mass flux variation, the preheater was divided into two section one of which has maximum power of 5 kW, separately. The heat transfer test section was designed to control the input heat by means of the auto voltage regulator that supples the maximum power of 15 kW. The preheater is installed to provide heat load to the

refrigerant of CO_2. The electronic power for the preheater was displayed on two watt transducers in order to control an electronic power for the preheater.

As can be seen in Fig. 2.2, the outer tube of the test section was made of acryl tube and the inner tube was made of stainless steel tube(SUS 316) that is the inner and outer diameter of 7.75 and 9.53 mm. The electronic power for the preheater section was regulated by the auto voltage transformer and the electronic power is provided for nicrome wire winding the outer wall of inner tube. In this study, the merit of this heating method is that it can adjust easily the experimental conditions and supply the uniform heat flux which is applied to the test section.

The stainless steel tubing for pressure measurement was electrically isolated from the test section by using the dielectric fittings which connect the main test section to the tubing for pressure measurement. The heating length of the test section is 5.0 m, and seamless stainless steel tube is used for heat transfer test section.

The outside wall temperature on the heated tube was measured by T type copper(Cu)/constantan(CuNi) thermocouple mounted at the regular interval of 500 mm along the tube as shown in Fig. 2.2. T type thermocouples to measure the temperature of the outer wall of the tube are attached at ten locations along the test section. At each point, the temperature at four circumferential locations was measured and the average values are used in calculating the heat transfer coefficient. A detailed procedure for mounting wall thermocouples is given in Fig. 2.2.

T type thermocouple to measure the refrigerant temperature was installed at the regular interval of 500 mm. The pressure in the test section inlet was measured with a precision pressure transmitter, and the refrigerant pressure difference between test section inlet and outlet was measured with a differential pressure transducer at regular interval of 500 mm.

2.1.2 Experimental conditions and method

All of the valves in the system is opened to do a leakage examination of the system, and a nitrogen gas is streamed in charging port of the system. After the enough passage of time, if there is not the leakage part in apparatus, all nitrogen gases in the system is excluded by vacuum pump and all of the valves is closed. Before charging the CO_2 in receiver, the brine temperature in chiller is maintained as 15℃. When charging the refrigerant in a receiver, the CO_2 refrigerant state in the receiver exists the liquid and vapor phase. In order to charge only the liquid phase of CO_2 refrigerant in the receiver, the brine temperature in chiller makes a lower temperature. If the brine temperature is maintained as a certain temperature of 15℃, the liquid phase of CO_2 is only charged. During charging the CO_2, when a system pressure is higher than a vessel pressure, a check valve was installed to present the refrigerant from flowing backward.

If the appropriate amount of CO_2 was charged, the main valve of a vessel is closed and the magnetic gear pump is operated. And then, a needle valve at the outlet of receiver is opened and CO_2 refrigerant flows

in the preheater. After the mass flow rate corresponding to experimental conditions is controlled by magnetic gear pump and bypass valve, it observes that system is operated at steady state conditions. When the above procedure is stably progressed, CO_2 flowing in mass flow meter is a subcooled liquid phase. The heat load, which needs to change from subcooled liquid state to saturation state, is calculated with REFROP(Version 6.01). The preheater is used to adjust the inlet vapor quality of test section and heat transfer rate supplied to the test section is calculated as following equation to consider the CO_2 refrigerant latent heat.

$$Q_e = M_{re} \cdot i_{fg} \cdot x_{out} \tag{2.1}$$

where, Q_e is the provided heat transfer rate at the test section, M_{re} is the mass flow rate of CO_2 and x_{out} is the outlet quality of preheater. If the above procedure is finished, the pressure and temperature data for test section is recorded and calculated.

The evaporation heat transfer is significantly influenced by mass flux, saturation temperature and heat flux. The experiments were conducted for various heat fluxes, mass fluxes and saturation temperature of refrigerant. The mass fluxes were adjusted at 200, 300, 400 and 500 kg/m^{2}s, the saturation temperatures were controlled at 5℃, 0℃ and 5℃, the heat fluxes were regulated at 10, 20, 30 and 40 kW/m^2 and the inlet and outlet vapor quality of test section varied from 0 to 100%. Table 2.1 presents the experimental conditions for evaporation heat transfer.

Table 2.1 Experimental conditions for evaporation heat transfer

Refrigerant	CO_2(R-744)
Test section	Horizontal stainless tube
Mass flux, kg/m^{2}s	200, 300, 400, 500
Heat flux, kW/m^2	10, 20, 30, 40
Inner diameter of test section, mm	7.75
Saturation temperature, ℃	-5, 0, 5
quality	0 ~ 100
Saturation pressure, MPa	3.04 ~ 3.96

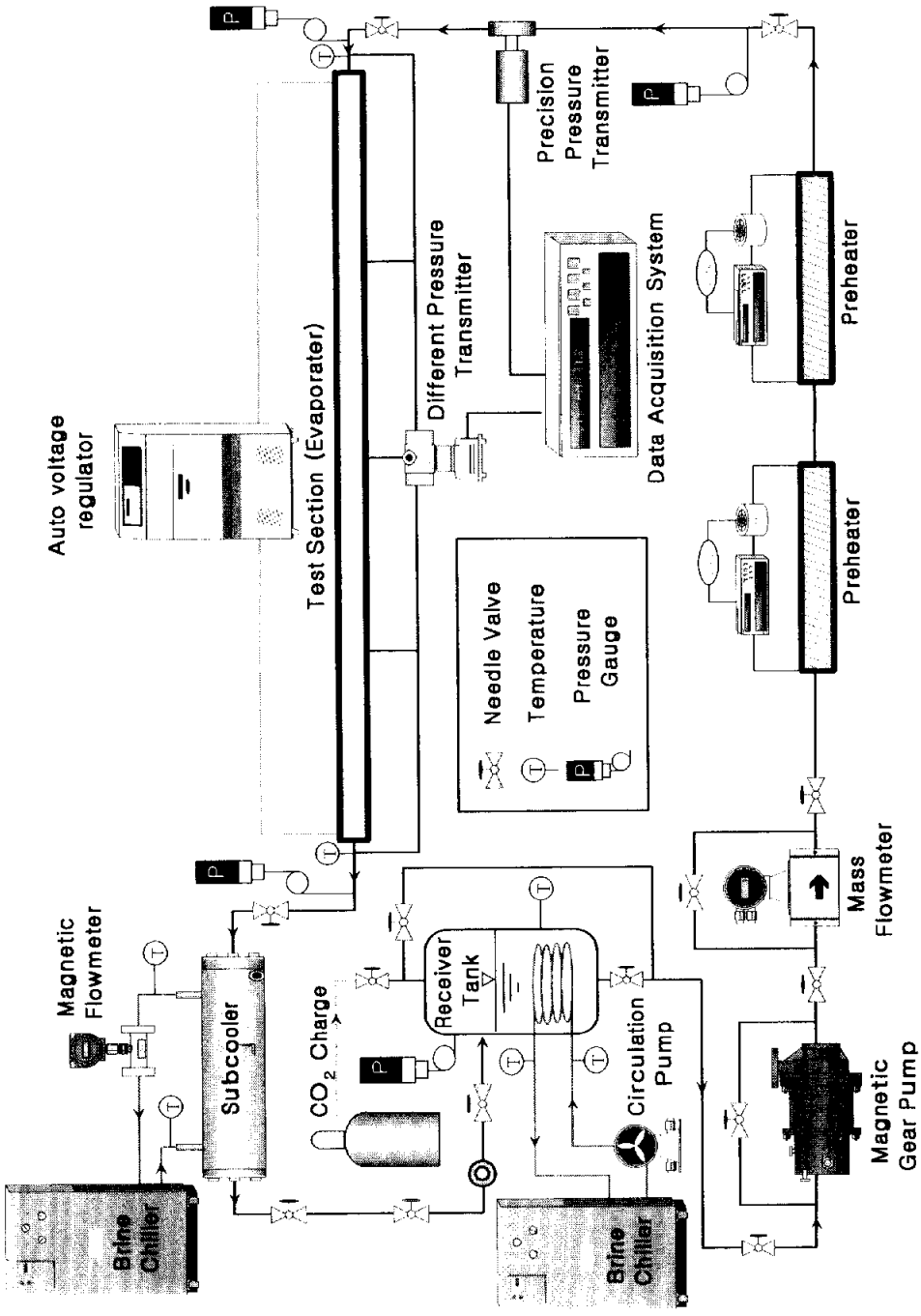

Fig. 2.1 Schematic diagram of experimental apparatus for evaporative heat transfer test with CO_2.

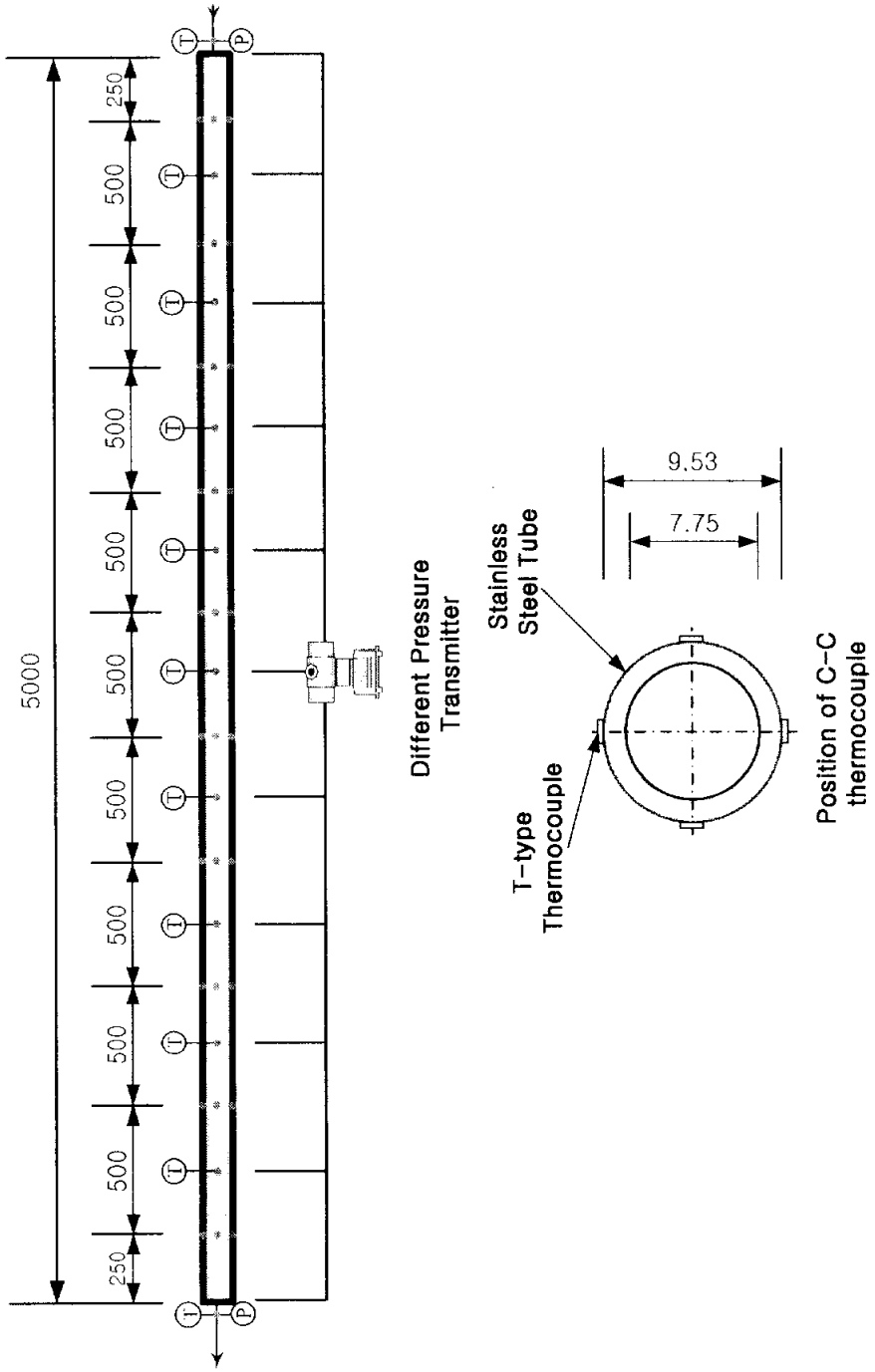

Fig. 2.2 Schematic diagram of the test section for evaporative heat transfer test.

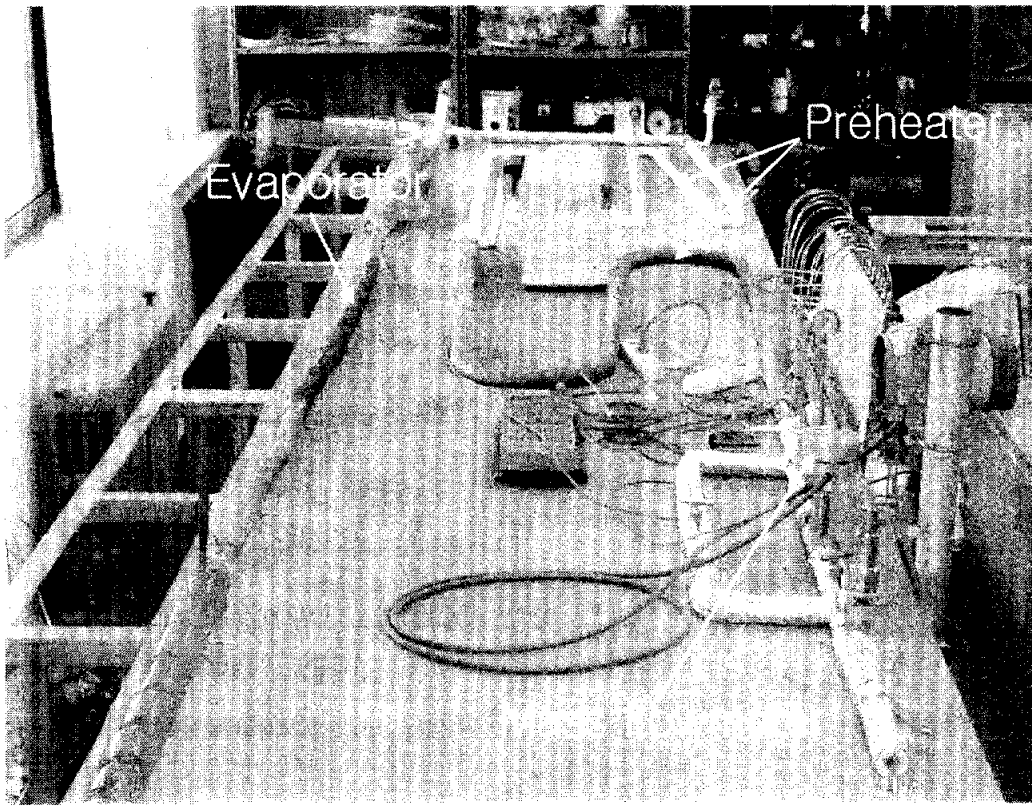

Photo. 2.1 Photograph of experimental apparatus for evaporation heat transfer test.

2.2 EXPERIMENTS ON COOLING HEAT TRANSFER

This section deals with description of test rig for the heat transfer of supercritical CO_2. The experimental apparatus is designed and constructed at laboratory. The measurements have been conducted for the experimental results of heat transfer and pressure drop during gas cooling process of CO_2. Here, a detailed description of the test rig, experimental setup, experimental method and test conditions are presented.

2.2.1 Experimental apparatus

Fig. 2.3 shows a schematic diagram of the overall experimental apparatus for the cooling heat transfer of CO_2. The facility consists of two loops and the main component of the CO_2 refrigerant loop are magnetic gear pump, preheater, test section(gas cooler), liquid receiver, and so forth. The cooling water loop for the test section is made of water circulation pump, flow meter and constant temperature bath. Fig. 2.4 presents a schematic diagram of the gas cooler. Photo. 2.1 depicts the schematic diagram of data acquisition system, gas cooler(test section) and preheater used in this experiment.

As can be seen from Fig. 2.3, CO_2 is circulated by a variable speed internal gear pump, which is driven by a magnetic coupling, and its flow rate and density are measured with a Coriolis mass flow meter. After exiting the mass flow meter, CO_2 enters a preheater heated by electricity. They elevate the fluid temperature to a desired temperature of test section. The CO_2 in the supercritical state enters the test section and then it is

cooled by the cold water flowing through the annulus. After leaving the test section, CO_2 is cooled by subcooler and then recirculates the pump.

The subcooler which is installed at the outlet of gas cooler controlled the subcooling temperature of gas cooler exit and cooled down the carbon dioxide. The temperature of cooling water for the gas cooler is controlled by the chiller, and the constant mass flow rate of coolant flows in circulation pump, mass flow meter, and gas cooler in good order. Gas cooler consists of double pipe heat exchanger in which CO_2 and water exchange heat in counter flow. A CO_2 refrigerant flows in tube and cooling water flows in annulus path counter currently to CO_2.

In order to reduce heat gain and loss from the surroundings, all test sections were insulated against external influence thoroughly with double adiabatic material. The test section consists of twelve subsections connected in series. The subsection, which is a tube in-tube counter flow heat exchanger, is shown in Fig. 2.4. An inner tube was made of stainless steel with inner diameter of 7.75 mm and outer diameter of 9.53 mm. The cross sectional view of the test section is shown in Fig. 2.4. The annulus was made by combining two pieces of acrylic blocks, each of which has semi cylindrical passage for secondary fluid. The length of the annulus for one section is 500 mm with an inner diameter of 25 mm.

As can be presents in Fig. 2.4, at inlet and outlet of the subsection, the temperature of CO_2 and cooling water were measured by T type thermocouple probe, which were directly inserted into the flow. Outer wall temperatures were measured by T type thermocouple wire, which was

fixed to the outside surface of the inner tube by thin teflon film. Three thermocouple wire were located 250 mm downstream from the inlet in the middle of the subsection to measure the wall temperatures at top, side and bottom.

The measuring locations for bulk and wall temperature of CO_2 is shown in Fig. 2.4. The temperature and pressure of CO_2 were measured equally at inlet and outlet of subsection, respectively. Outer wall temperature at the top, side and bottom was measured in the middle of subsection. A minimum interval between subsections is maintained and outer wall temperature was measured at the center of the interval. Although the measured wall temperature has an effect on more convection of coolant than conductivity. The interval between subsections decreases so that the measurement deviation is minimized.

The inlet pressure of CO_2 was measured with an precision pressure transmitter and the pressure drop in the test section was measured with a differential pressure transducer. Pressure tap locations are shown in Fig. 2.4. In order to determine the mass flow rate of CO_2, a Coriolis mass flow meter was used, which was installed in the subcooled liquid line at pump outlet as shown in Fig. 2.3. The total mass flow rate of water was measured by the mass flow meter, too. However, water flow rate of each subsection is controlled by each valve attached rotameter to distribute equal flow rate to each subsection.

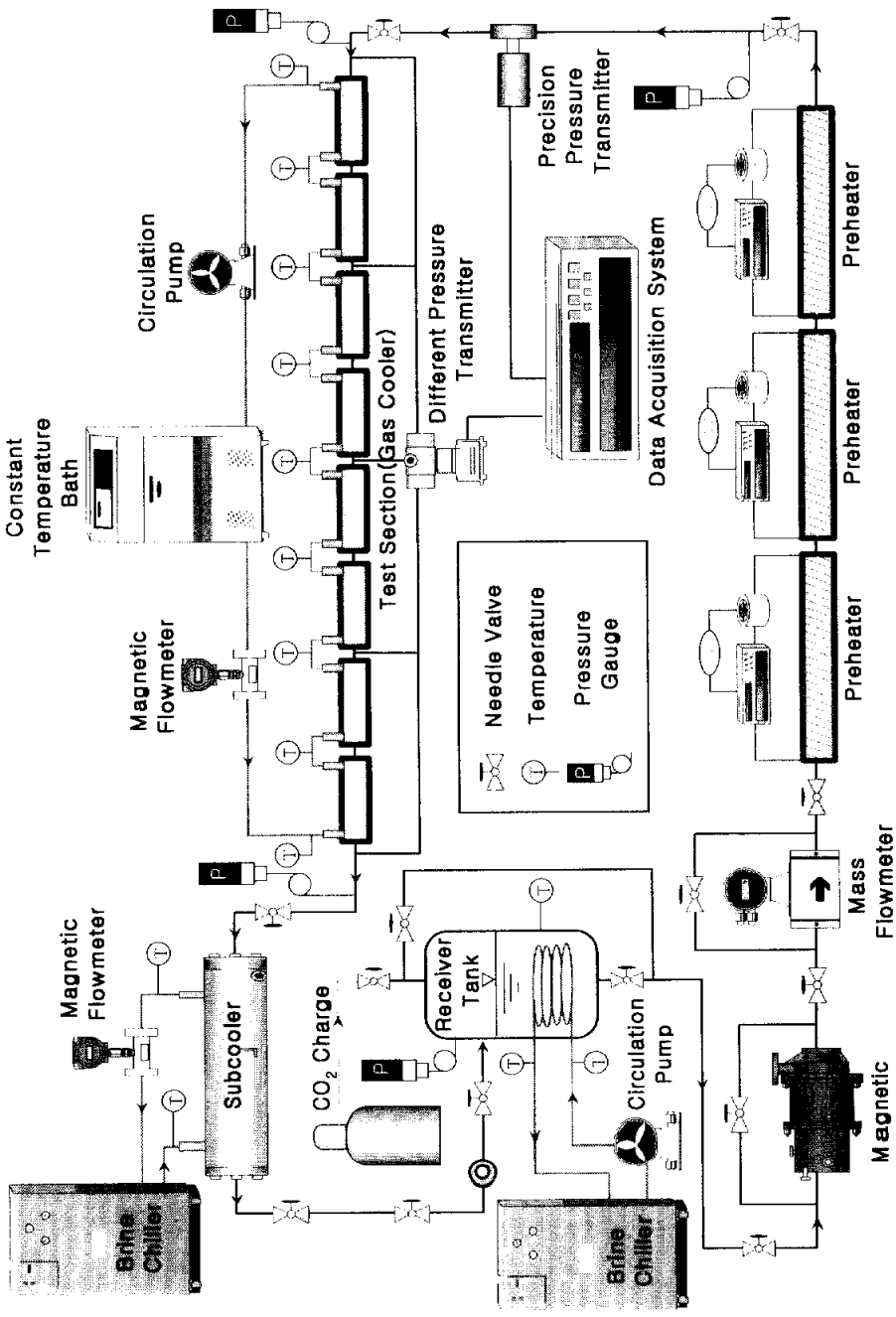

Fig. 2.3 Schematic diagram of experimental apparatus during cooling process of CO_2.

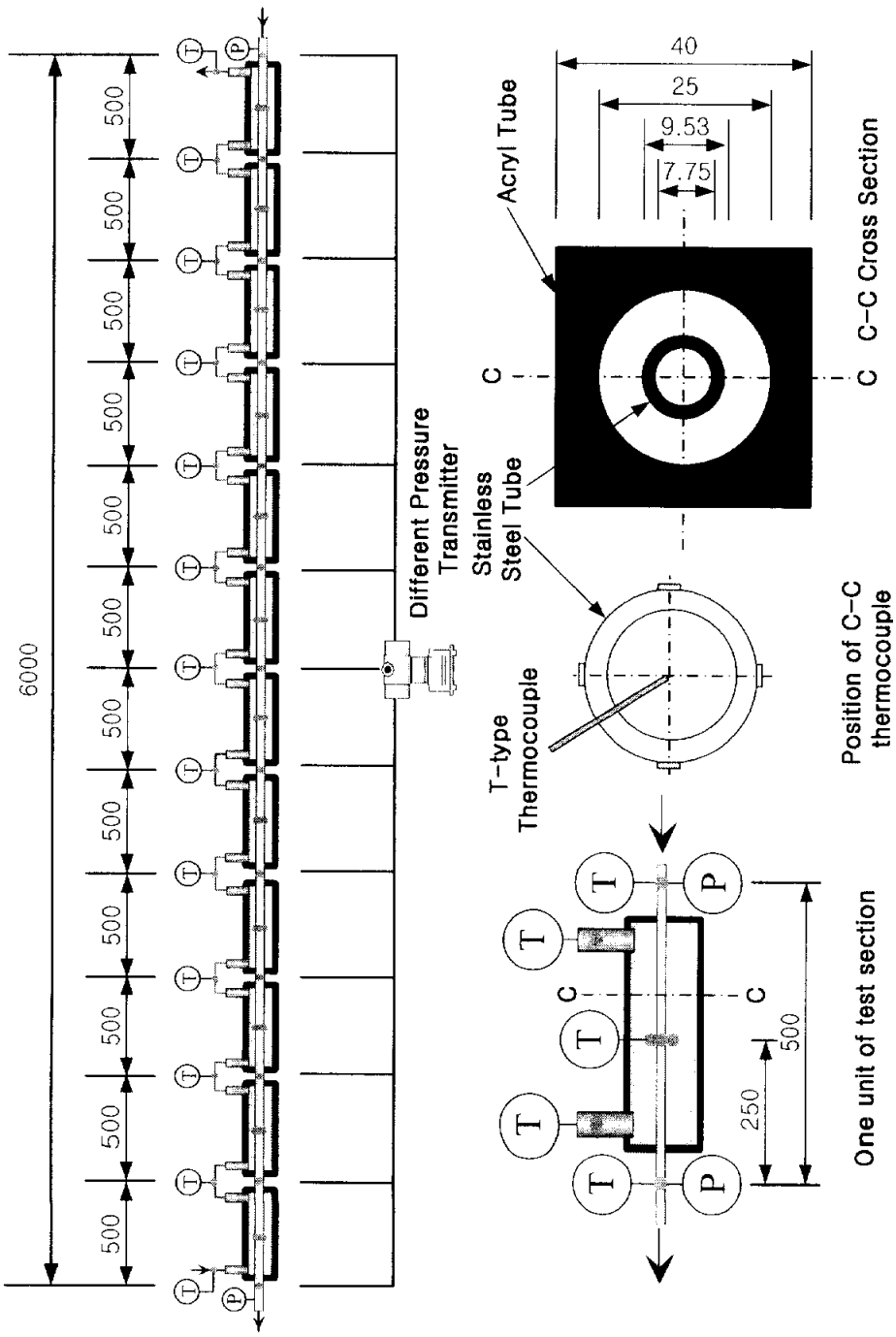

Fig. 2.4 Schematic diagram of the gas cooler.

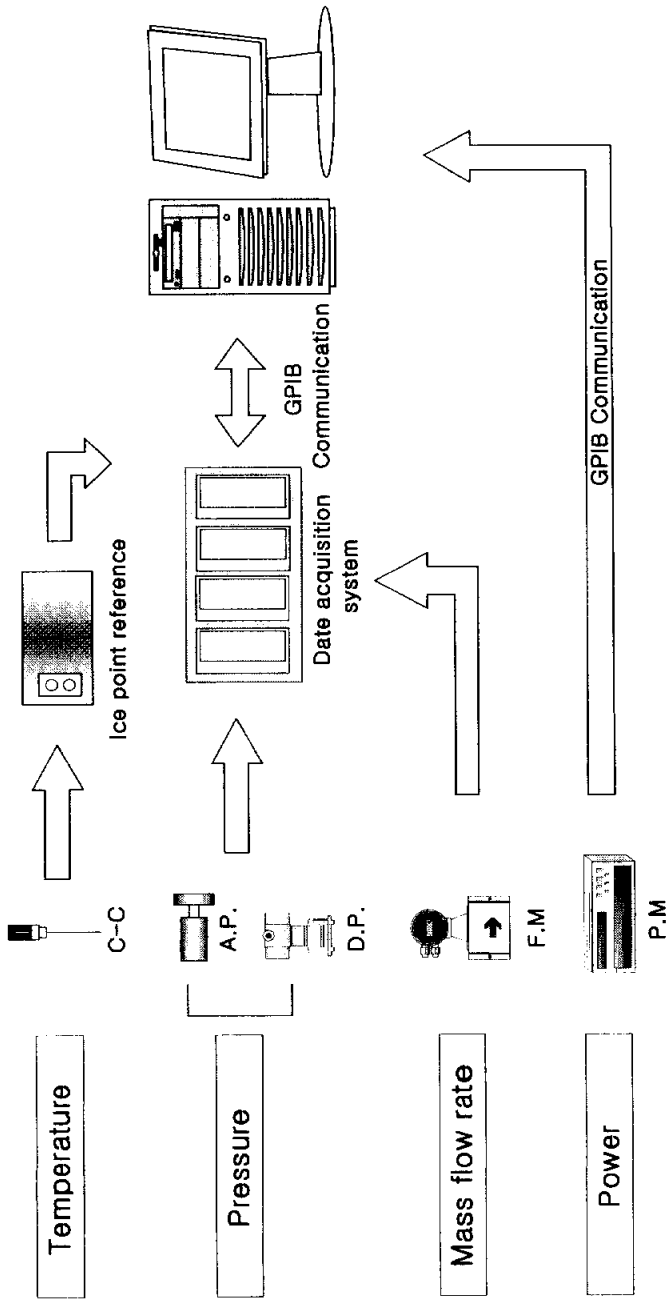

Fig. 2.5 Measurement system of temperature, pressure, mass flow rate and electric power.

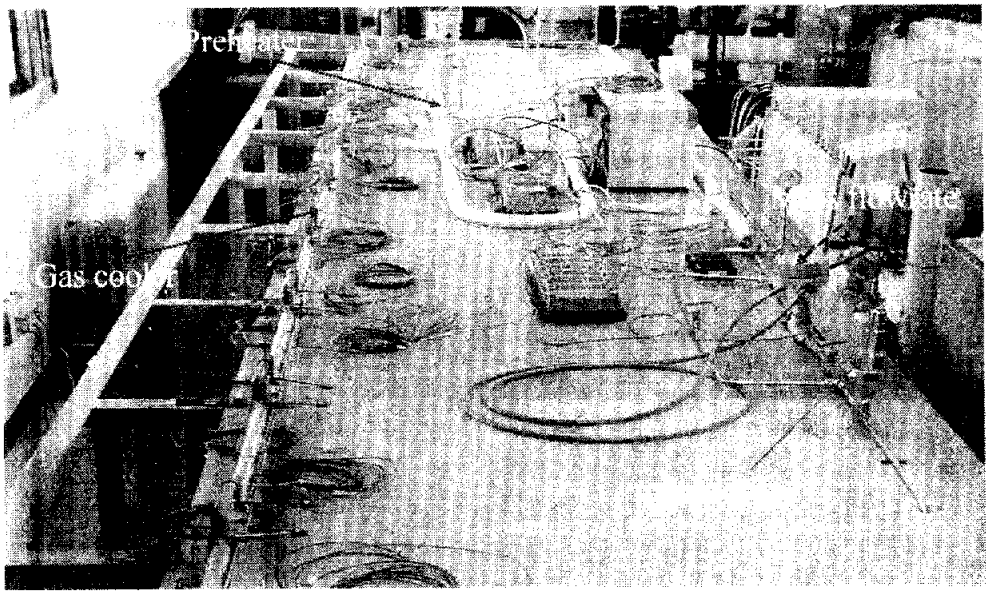

(a) Overall experimental facility

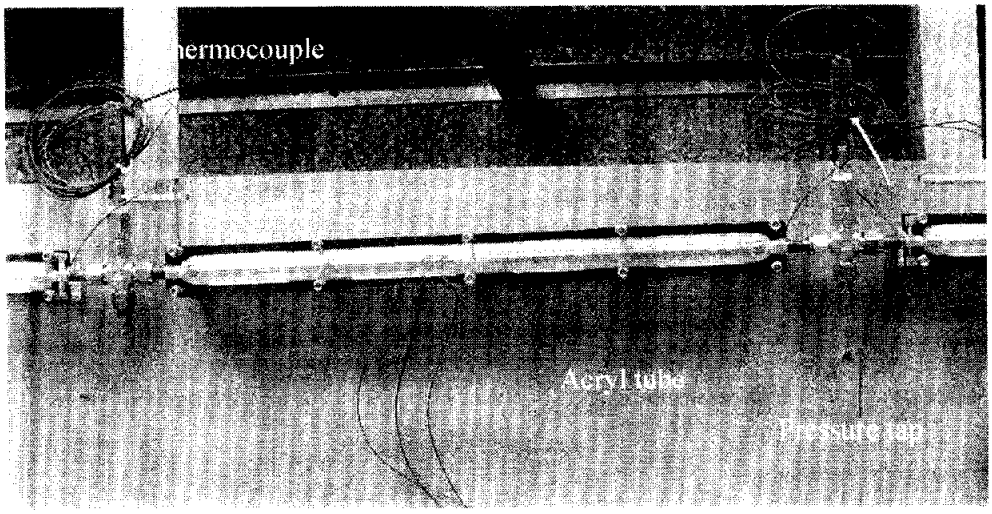

(b) Detailed diagram of the gas cooler

Photo. 2.2 Photograph of experimental apparatus for cooling heat transfer test.

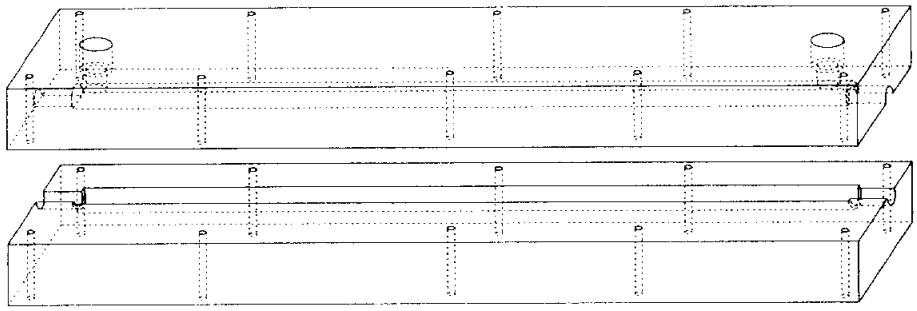

(a) Drawing of the acrylic block with cylindrical trench

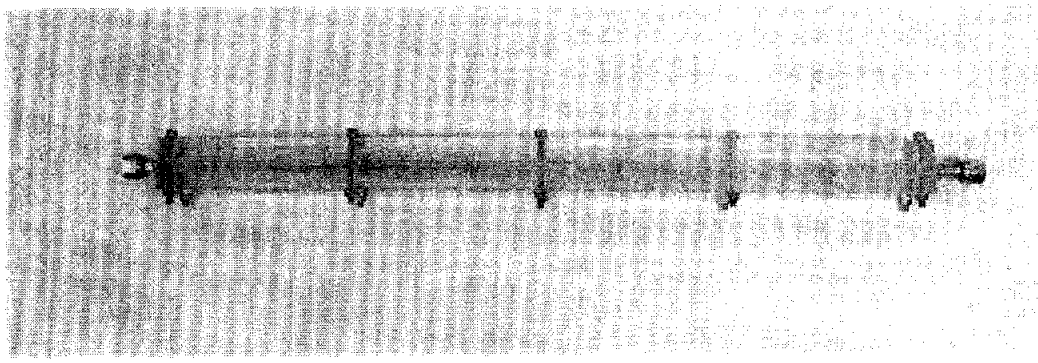

(b) Photograph of an assembly of the subsection

Photo. 2.3 Design of the annular path of the test section.

2.2.2 Experimental conditions and method

Before charging the CO_2 in a receiver, in order to do the leakage test of experimental facility, the high pressure nitrogen was injected by using an air compressor in a system. After about one day, if any leakage is not discovered in the system, all nitrogen gas is removed the system. In order to conduct a CO_2 refrigerant flow in the experimental apparatus with ease, the vacuum in the system is maintained using a vacuum pump. After charging the CO_2 in the receiver, the CO_2 liquid phase flows in system using a magnetic gear pump.

If the cooling water is maintained with a given temperature at a chiller, it flows in the gas cooler by a circulation pump. The mass flow rate of coolant could be modulated by adjusting the valve and by pass line. Ice point reference device to which thermocouples are wired is used to give an accurate reference values for temperature measurement excluding the readings from the rather inaccurate measurement by a built-in thermister.

Output signals of each equipment and sensor are gathered by using a data acquisition unit. Personal computer communicates with the data logger through GPIB(general purpose interface bus). Data scan time is set to 2 second. Fig. 2.5 shows the schematic of data acquisition system used in this experiment. All tests were run under steady state conditions. Data collection and control of the system were done by the use of computer and data acquisition system.

Table 2.2 Experimental conditions during cooling process of CO_2

Refrigerant	CO_2(R-744)
Test section	Horizontal smoothed tube
I.D. of test section, mm (O.D. of test section, mm)	7.75 (9.53)
Mass flux of refrigerant, kg/m^{2}s	200, 300, 400, 500
Inlet pressure of gas cooler, MPa	7.5 ~ 10.0
Refrigerant temperature of gas cooler, ℃	100 ~ 20
Temperature of cooling water, ℃	15

2.3 DATA REDUCTION

In the present study, The thermodynamic properties for CO_2 were obtained from the latest version of a CO_2 refrigerant property package (NIST)[2]. In order to investigate the evaporation and cooling heat transfer characteristics, it used following equations to analyze the experimental data. First, to analyze the evaporation heat transfer characteristics, the heat transfer rate between electronic power for evaporator and CO_2 refrigerant can be calculated from Eq. (2.2) and (2.3).

$$Q_{coil} = \zeta \cdot V \cdot I \tag{2.2}$$

$$Q_e = M_e \cdot (i_{e,out} - i_{e,in}) \tag{2.3}$$

where, ζ is the efficiency of auto voltage regulator in [%], V is the input voltage in [V], and I is the input ampere in [A]. M_e represents the mass flow rate of CO_2, and $i_{e,in}$ and $i_{e,out}$ are the inlet and outlet refrigerant enthalpy at subsection. The heat flux supplied by auto voltage regulator was determined as follows.

$$q_e = \frac{Q}{\pi \cdot d_i \cdot \Delta z} \tag{2.4}$$

here, Q represents the heat transfer rate calculated by Eq. (2.2) and (2.3), d_i is the inner diameter of inside tube in [m], and Δz is the length of subsection in [m].

The circumferential heat transfer coefficient of CO_2 in the evaporation process had great influence on the performance of this system. The local heat transfer coefficient in the evaporation could be evaluated by the

following equations.

$$h_{e,loc} = \frac{q_e}{T_{e,w,in} - T_e} \tag{2.5}$$

In Eq. (2.5), $h_{e,loc}$ is the heat flux to the test section and T_e is the refrigerant temperature in an evaporator, and $T_{e,w,in}$ is the inner wall temperature calculated by one dimensional steady state concentric equation from measured outer wall temperature.

$$T_{e,w,in} = T_{e,w,out} - \frac{Q_{e,loc}}{2\pi \cdot k_w \cdot \Delta z} \cdot \ln\left(\frac{d_o}{d_i}\right) \tag{2.6}$$

where d_o and d_i are the inner and outer diameter of inside tube, and k_w is the thermal conductivity of the stainless steel tube. $T_{e,w,out}$ is the outer tube wall temperature of the inner tube and it is averaged by measuring the top, side and bottom temperature.

$$T_{e,w,out} = \frac{T_{w,top} + 2T_{w,side} + T_{w,bottom}}{4} \tag{2.7}$$

where the subscript top, side and bottom stand for the top, side and bottom of the outer tube, respectively.

Equilibrium quality, x, is defined from the specific enthalpy at each thermocouple location and latent heat during evaporation as shown in Eq. (2.8). The outlet quality to the subsection can be calculated with Eq. (2.9).

$$x = \frac{\Delta i_{loc}}{i_{fg}} \tag{2.8}$$

$$x_{loc,out} = x_{in} - \frac{\pi \cdot d_i}{M_{re} \cdot i_{fg}} \cdot \int_{z_{in}}^{z_{out}} q_e dz \tag{2.9}$$

where Δi_{loc} is the refrigerant enthalpy difference of CO_2 at the inlet and outlet of subsection and i_{fg} is the refrigerant latent heat. z_{in} and z_{out} are inlet and exit of subsection, respectively. q_e is the heat flux in the evaporator calculated with Eq. (2.4), and $\pi \cdot d_i \int_{z_{in}}^{z_{out}} q_e dz$ is the cumulative sum of the subsection.

The average heat transfer coefficient at the evaporator was defined as

$$h_{e,avg} = \frac{1}{x_{out} - x_{in}} \int_{x_{in}}^{x_{out}} h_{e,loc} dx = \sum \frac{h_{e,loc}}{n} \tag{2.10}$$

In above Eq. (2.10), x_{in} and x_{out} are the inlet and outlet quality of subsection, $h_{e,loc}$ is the local heat transfer coefficient in the subsection, and n is the number of subsection.

In order to analyze the cooling heat transfer characteristics, it must be known that heat capacity, Q_{gc}, gained by cooling water flowing through the annular and heat capacity, Q_{cs}, lost by the CO_2 refrigerant flowing in tube. This equations were summarized as follows

$$Q_{cs} = M_{cs} \cdot c_{p,cs} \int_{T_{cs,in}}^{T_{cs,out}} dt \tag{2.11}$$

$$Q_{gc} = M_{gc} \cdot (i_{gc,in} - i_{gc,out}) \tag{2.12}$$

$$Q_{gc} = M_{gc} \cdot c_{p,gc} \int_{T_{gc,in}}^{T_{gc,out}} dt \tag{2.13}$$

Q_{cw} represents the heat transfer rate obtained from the flow rate of the cooling water and the temperature difference between the inlet and outlet

of the test section, and Q_{gc} is the heat transfer rate obtained from the flow rate of refrigerant and the enthalpy change between the inlet and outlet of the test section. M_{cs} and M_{gc} are the flow rate of the cooling water and refrigerant. Where $T_{cw,in}$ and $T_{cw,out}$ are the inlet and outlet coolant temperature, $T_{gc,in}$ and $T_{gc,out}$ are the CO_2 refrigerant temperature at the inlet and outer of gas cooler, $c_{p,cs}$ and $c_{p,gc}$ are the specific heat of coolant and CO_2 refrigerant, and $i_{gc,in}$ and $i_{gc,out}$ are the enthalpy of CO_2 refrigerant, respectively.

The heat flux is derived from the enthalpy change of the cooling water based on the temperature change in the test section as shown in Eq. (3.4).

$$q_{gc} = \frac{Q}{\pi \cdot d_i \cdot \Delta z} \tag{2.14}$$

where Q is the heat transfer rate calculated from Eq. (2.11) to (2.13), and Δz is the length of the test section. The circumferential heat transfer coefficient of CO_2 in the cooling process has great influence on the performance of this system. Thus, the gas cooler was divided into subsections to evaluate the local heat transfer coefficient of CO_2. This local heat transfer coefficient during gas cooling process can be calculated by the following equation.

$$h_{gc,loc} = \frac{q_{gc}}{T_{gc} - T_{gc,w,in}} \tag{2.15}$$

where $h_{gc,loc}$ represents the local heat transfer coefficient in the subsection of gas cooler, T_{gc} is the refrigerant temperature of CO_2 in gas cooler.

$T_{gc,w,in}$ is determined from the average value of the measured outside wall temperature via one dimensional heat conduction equation as shown in Eq. (2.16).

$$T_{gc,w,in} = T_{gc,w,out} + \frac{Q_{gc,sub}}{2\pi \cdot k_w \cdot \Delta z} \cdot \ln\left(\frac{d_o}{d_i}\right) \tag{2.16}$$

where $T_{gc,w,out}$ is the average value of the top, side and bottom of inner tube wall as shown in Eq. (2.17). The d_o and d_i are the inner diameter and outer diameter of the inner tube, respectively, and k_w is the thermal conductivity of stainless steel tube in [kW/m·K].

$$T_{gc,w,out} = \frac{T_{w,top} + 2T_{w,side} + T_{w,bottom}}{4} \tag{2.17}$$

In the Eq. (2.17), $T_{w,top}$, $T_{w,side}$, and $T_{w,bottom}$ are the measured temperature at the top, side and bottom of inner tube wall, respectively. T_{gc} is the average temperature at the inlet and outlet of the subsection and the bulk temperature of CO_2, T_{gc}, is calculated with Eq. (2.18).

$$T_{gc} = \frac{T_{gc,n-0.5} + T_{gc,n+0.5}}{2} \tag{2.18}$$

The mean heat transfer coefficient, $h_{gc,avg}$, during cooling process of supercritical CO_2 is calculated by Eq. (2.19).

$$h_{gc,avg} = \sum \frac{h_{gc,loc}}{n} \tag{2.19}$$

where $h_{gc,loc}$ is the local heat transfer coefficient of CO_2 calculated by Eq. (2.15), and n is the number of the subsection.

CHAPTER 3
EXPERIMENTAL RESULTS FOR EVAPORATION PROCESS OF CO_2

For the refrigeration and air conditioning system using CO_2 as working fluid, the evaporator is a main component. Hence, study on the evaporation heat transfer coefficient and pressure drop characteristics be positively necessary. Especially, because of the large variation of specific volume, specific heat, and surface tension in the evaporation heat transfer of CO_2, some researchers[24-26] present that the evaporation heat transfer of CO_2 is greatly different from that of conventional refrigerants, like HCFCs and HFCs. Due to complex flow pattern and thermophysical property, the heat transfer mechanism occurred during evaporation process of CO_2 is difficult to examine. Accurate theory for the evaporation heat transfer of CO_2 is not yet established. And, study on the evaporation heat transfer characteristics of CO_2 is limited, and few results have been published on CO_2. Therefore, in this chapter, the evaporation heat transfer coefficients and pressure drops of CO_2 are measured in a horizontal tube of inner diameter, which is 7.75 mm, and compared with the existing correlations. Based on the experimental results, the basic design data for evaporator using CO_2 as working fluid is presented.

3.1 HEAT BALANCE OF EVAPORATOR

In this section, we need to confirm the validity of the experimental apparatus by examining its heat balance of the experimental apparatus. In order to make an accurate measurement of evaporator capacity, heat balance between refrigerant flow and energy input in the test section examined and presented all measurement results in the evaporator.

Fig. 3.1 presents heat balance between the capacity of refrigerant side, Q_{re}, and the energy input, Q_{coil}, with respect to varying mass flux. Heat capacity Q_{coil} supplied with energy input was presented in the axis of ordinate and refrigerant heat capacity, Q_{re}, obtained by heating wire was shown in the axis of abscissa. The energy balance between the refrigerant side and the energy input side was calculated from equation (2.2) and (2.3), respectively. The symbol, ○, □, △ and ◇ represent the mass velocity of CO_2 for 200, 300, 400 and 500 kg/m^{2}s, respectively. As can be seen in Fig. 3.1, the results indicate that energy balance between, Q_{coil}, of Eq. (2.2) and, Q_{re}, of Eq. (2.3) is generally within ±10% for all runs. Energy balance in this study was maintained, thus, this energy balance indicated the accuracy of the experiment. All raw data acquired in the experimental apparatus showed a high level of reliability to validate the experimental results.

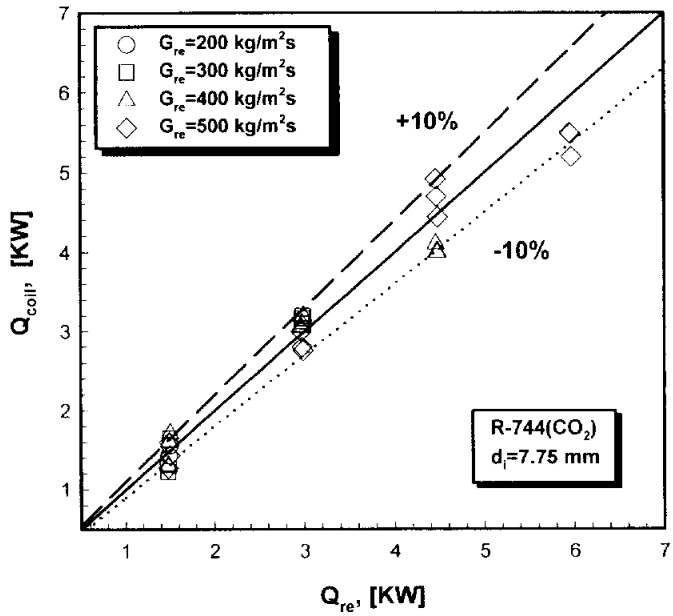

Fig. 3.1 Heat balance between the capacity of refrigerant side, Q_{re}, and the energy input, Q_{coil}, with respect to varying mass flux.

3.2 EVAPORATION HEAT TRANSFER CHARACTERISTICS

In order to examine the evaporation heat transfer characteristics of CO_2 in a horizontal tube, the experiments were conducted for various heat fluxes, mass fluxes and saturation temperature of CO_2. The saturation temperatures were controlled at -5℃, 0℃ and 5℃, mass fluxes were adjusted at 200, 300, 400 and 500 kg/m^2s, and heat fluxes were regulated at 10, 20, 30 and 40 kW/m^2.

In general, the evaporation phenomenon, which breaks out phase change from liquid state to vapor state, is divided into boiling phenomenon. But, in general, when the refrigerant temperature is above the corresponding saturation temperature, evaporation phenomenon is referred to as the process of the vapor formation at a continuous liquid surface such as interface between the liquid film and vapor core in annular flow, and boiling phenomenon is regarded to as the process of vapor formation at a heated surface and channel. Therefore, in this study, it is known that all of the process is referred to as the evaporation phenomenon.

3.2.1 Local evaporation heat transfer

The heat transfer during forced convective boiling in a horizontal tube has an effect on various factors such as mass flux, heat flux and the ratio of vapor and liquid velocity. The forced convection in a horizontal tube is divided into nucleate boiling and convective boiling. Nucleate boiling is characterized by the formation and departure of vapor bubbles at heating

surface and convective boiling is characterized by the formation of vapor bubbles at interface between the liquid film and vapor core.

In nucleate boiling, the flow pattern represents a form of bubble and slug flow at the low quality, and the heat transfer coefficient is chiefly dependent on the heat flux. On the contrary, in convective boiling, the flow pattern represents a form of annular and spray flow, and the heat transfer coefficient is primarily influenced by the mass flux. In the area of low quality, the heat transfer coefficient is chiefly dependent upon the heat flux. Downstream, the average velocity of CO_2 increases with vapor quality. The supplied heat is essentially transferred by convection from the tube wall to the vapor-liquid flow. The nucleate boiling converts into convective boiling. In the area of convective boiling, the local heat transfer coefficient is practically independent of the heat flux and is strongly dependent on the mass flux and the quality. Therefore, in order to analyze the evaporation heat transfer characteristics of CO_2, study on the influences of quality, heat flux, saturation temperature and mass flux is investigated necessarily.

(1) Effects of vapor quality

Variation of heat transfer coefficients with respect to quality at a fixed heat flux is shown in Fig. 3.2. Fig. 3.3 displays the comparison of the surface tension and viscosity of R 744(CO_2) with R 22 and R 134a. Fig. 3.3 presents that the surface tension and viscosity of CO_2 are far smaller than those of conventional refrigerants. Thus, this results explain that the

liquid layer of CO_2 surrounding the inner wall of the tube is easily broken into pieces. As can be observed in Figure 3.2, the heat transfer coefficient of CO_2 has a tendency to increase at a lower vapor quality range($x<0.1$) because void fraction increases with quality and liquid film thickness of CO_2 becomes thinner. As the evaporation proceeds with a rise of quality, the local evaporation heat transfer coefficients of CO_2 have a tendency to decrease. As shown in Fig. 3.3, this is because the liquid viscosity and surface tension of CO_2 for constant saturation temperature are about one third of R-22 and R 134a. Due to this reason, liquid film thickness surrounding the inner wall of the tube becomes thinner as quality increases, and the liquid film of CO_2 is formed at the side and bottom of inner tube due to the effect of gravity. At the top of inner tube, liquid film disappears and dryout occurs more frequently.

As for this trend mentioned in above, Yun[24] explained that two-phase flow pattern observation for flow vaporization of CO_2 in a horizontal tube of inner diameter of 6.0 mm shows a dominance of intermittent flow at lower quality and annular flow regimes at higher quality. Entrainment increases at higher vapor quality, and this, together with a very irregular liquid film, may give dryout and reduced heat transfer at moderate vapor fraction. This results show that nucleate boiling dominated at low/moderate quality, where the heat transfer coefficient increased with heat flux and temperature but was less affected by varying mass flux. Dryout effects became very important at higher mass flux and temperature, where the heat transfer coefficient dropped rapidly with increasing quality.

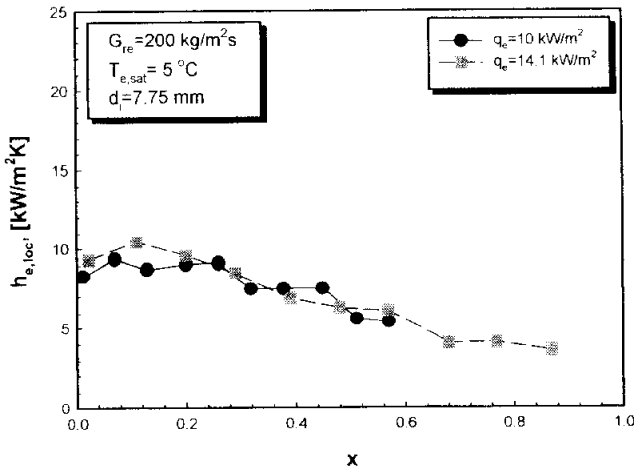

(a) G_{re}=200 kg/m^{2}s, $T_{e,sat}$=5 ℃

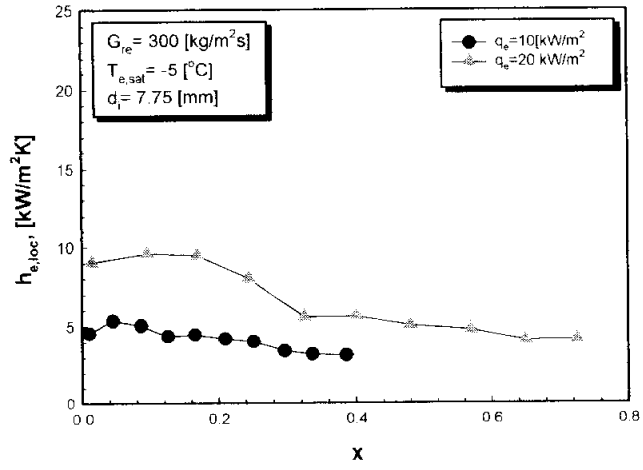

(b) G_{re}=300 kg/m^{2}s, $T_{e,sat}$=-5 ℃

Fig. 3.2 Variation of evaporating heat transfer coefficients with respect to vapor quality.

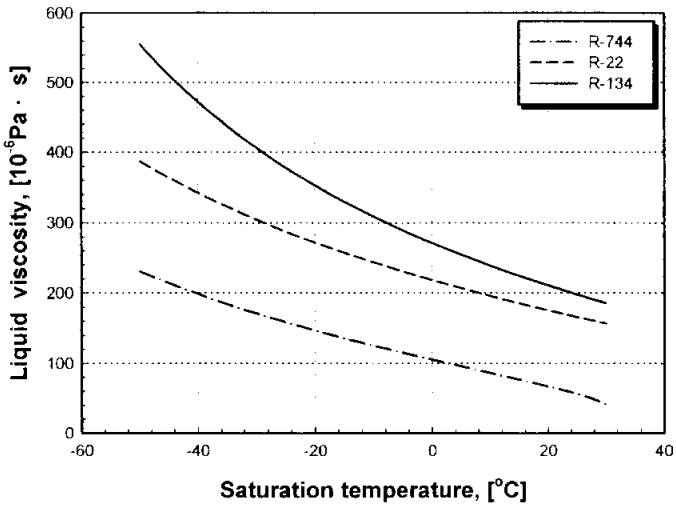

(a) Variation of liquid viscosity with respect to saturation temperature

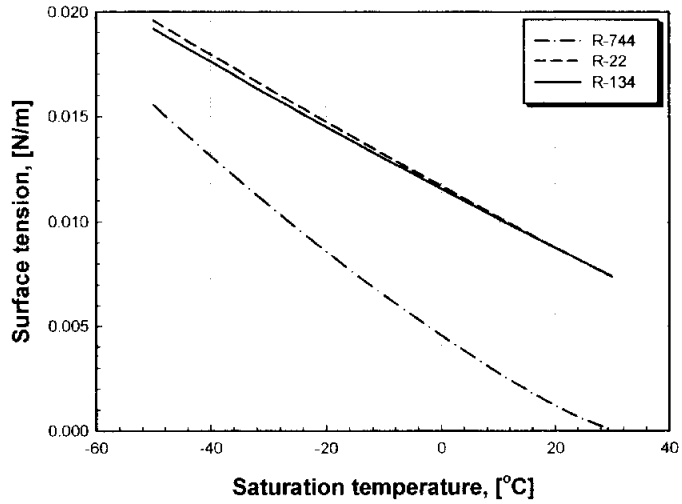

(b) Variation of surface tension with respect to saturation temperature

Fig. 3.3 Comparison of the thermophysical properties of R-744 with those of some refrigerants (R-22 and R-134a).

Fig. 3.4 presents the wall temperatures of inside tube, which are measured at the top, side and bottom, with respect to quality. At low quality region($x<0.3$), temperature of inside tube wall shows almost constant. But, at high quality region($x>0.3$), wall temperature at the top increases rapidly and wall temperature at the bottom of tube increases slowly. It is because the liquid film covering the inside tube wall becomes thinner and the liquid state of CO_2 due to gravity is maintained at the bottom of inside tube.

The local heat transfer coefficients which are measured at the top, side and bottom of the tube with respect to quality are shown in Fig. 3.5. All of the evaporation heat transfer coefficients have a tendency to decrease relatively, and at low quality, the heat transfer coefficient at the top of inside tube wall is constant and tends to decrease largely at high quality. The main causes are summarized as follows : At high quality, the liquid film surrounding the inside wall of the tube in annular flow is easily broken into pieces and the wall is essentially dry. The wall temperature of inside tube increases suddenly and the heat transfer coefficient decreases. In the evaporation process using CO_2 as working fluid, this tendency represents at all quality range, this is due to the large variation of CO_2 near the critical point.

In an evaporator using CO_2 as working fluid, the surface tension and viscosity of CO_2 with respect to saturation temperature decrease largely. Especially, the surface tension of CO_2 near the critical point is close to the zero. When the evaporation heat transfer occurs at high saturation

temperature near the critical point, the liquid film of CO_2 in annular flow is broken and the broken liquid film is built up at the bottom of inside tube due to gravity, and the heat transfer coefficient at the top of inside tube decreases dramatically.

Namely, the liquid film becomes thinner as vapor quality increases, and because of the diminished surface tension and viscosity, the liquid film covering inside tube wall is not maintained. And due to the effect of gravity, the liquid film is broken partly from the top of inside tube wall. If the vapor of CO_2 comes in contact with the area of broken liquid film, due to the reduction of vapor density and bursting of the liquid film, the effect of heat transfer reduces greatly. Therefore, in the evaporation process, the vapor of CO_2 directly comes in contact with the top of inside tube wall, and the evaporation heat transfer coefficient decreases as quality increases.

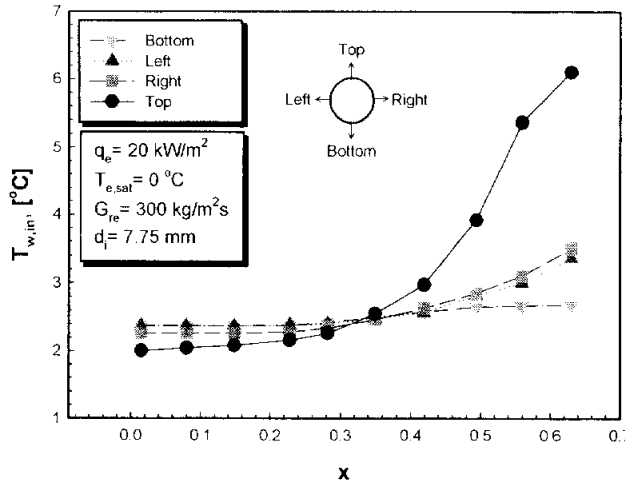

Fig. 3.4 Variation of the circumferential inner wall temperature with respect to quality (G_{re}=300 kg/m^{2}s, $T_{e,sat}$=0 ℃, q_e=20 kW/m^2).

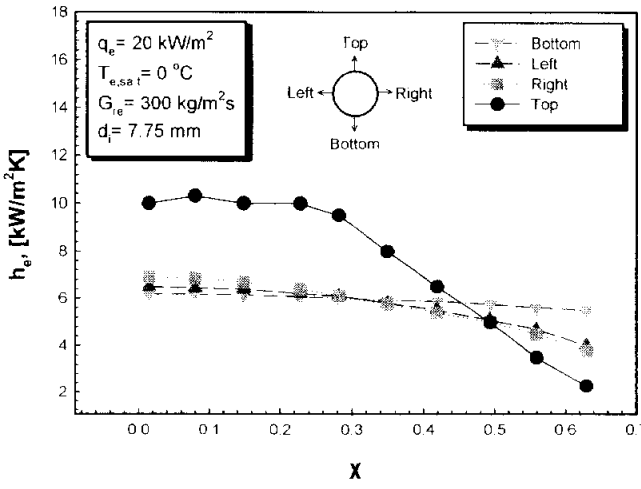

Fig. 3.5 Variation of the circumferential heat transfer coefficient with respect to quality (G_{re}=300 kg/m^{2}s, $T_{e,sat}$=0 ℃, q_e=20 kW/m^2).

(2) Effects of heat flux

Boiling phenomenon is classified into various forms by physical properties, such as vaporization enthalpy, boiling temperature, density of vapor, surface tension as well as by geometric parameter, such as microstructure and material of the heating surface. In general, the forced convective boiling heat transfer, which is occurred at the two-phase flow like vapor and liquid phase, is classified into nucleate boiling and convective boiling. The nucleate boiling is occurred chiefly at low vapor quality, and has something to do with heat flux. The convective boiling is generated at high quality and has a major effect on mass flux and quality. Hence, in this chapter, in order to analyze the evaporation heat transfer characteristics of CO_2, the effect on heat flux is investigated.

Variation of heat transfer coefficient versus quality with respect to a given mass flux is shown in Fig. 3.6. The heat transfer coefficient increases with heat flux, which is more evident over a wide range of quality. This indicates that nucleate boiling is generated even at high quality. The reason is that the ratio of specific volumes of vapor to liquid phase is smaller than that of fluorocarbon refrigerants, and then the vapor velocity is not so greater than the liquid velocity. Accordingly, the evaporation heat transfer coefficient of CO_2 has an effect on nucleate boiling at low quality as well as at high quality. Zhao et al.[27] showed that the heat transfer coefficient increased with a rise of heat flux at all qualities.

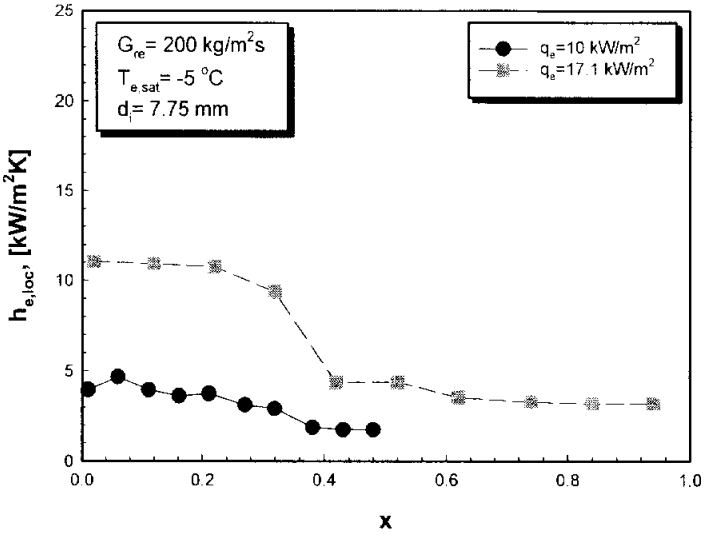

(a) G_{re}= 200 kg/m^{2}s, $T_{e,sat}$= -5 ℃

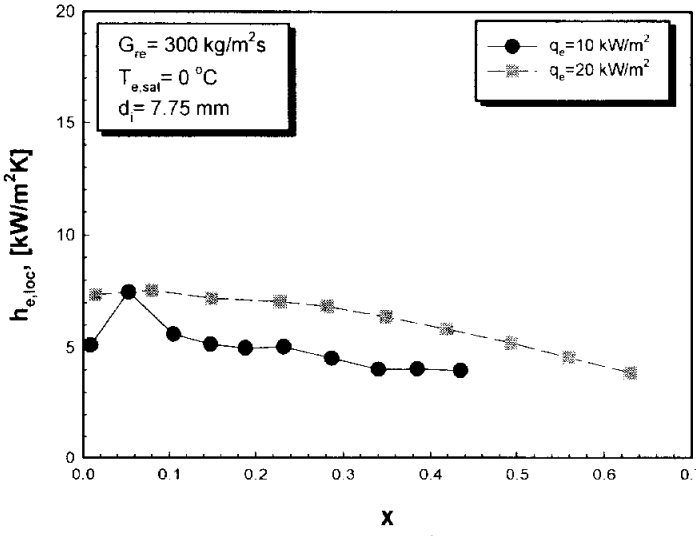

(b) G_{re}= 300 kg/m^{2}s, $T_{e,sat}$= 0 ℃

Fig. 3.6 Variation of the heat transfer coefficients for different heat fluxes at constant mass fluxes condition (continued).

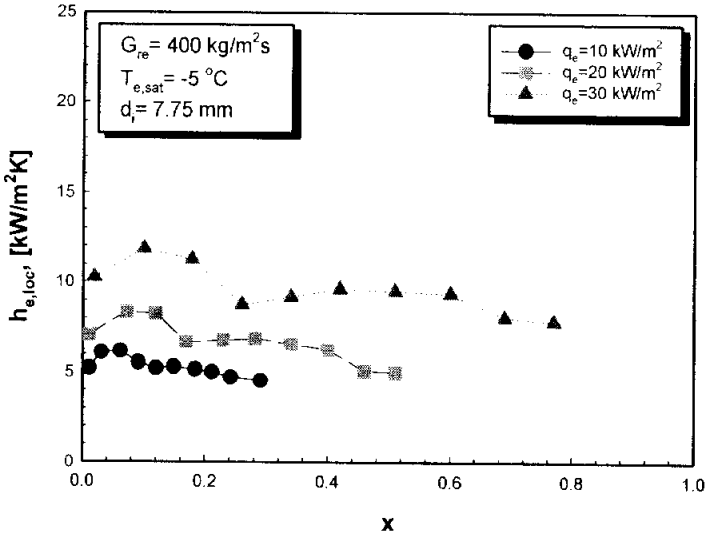

(c) G_{re}= 400 kg/m^{2}s, $T_{e,sat}$= 5 ℃

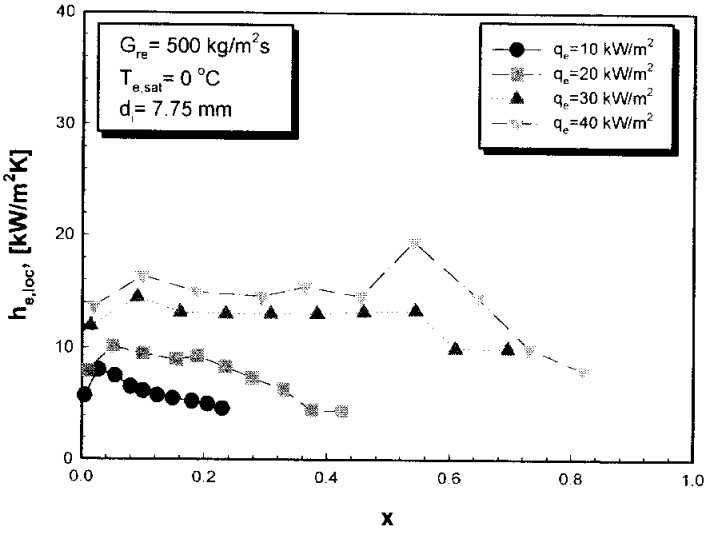

(d) G_{re}= 500 kg/m^{2}s, $T_{e,sat}$= 0 ℃

Fig. 3.6 Variation of the heat transfer coefficients for different heat fluxes at constant mass fluxes condition.

(3) Effects of mass flux

Fig. 3.7 shows the influences of varying mass flux on the heat transfer coefficient of CO_2 in a horizontal tube. As expected, the local evaporation heat transfer coefficient hardly increases as mass flux increases. Hihara Tanaka[10] also observed this trend in their experiments. Namely, because the ratio of liquid and vapor density of CO_2 is small, the heat transfer of CO_2 has an great effect on more nucleate boiling than convective boiling. Therefore, mass flux of CO_2 does not affect on nucleate boiling too much, and mass flux effect on heat transfer of CO_2 is very smaller than that of fluorocarbon refrigerant. As can be seen from Fig. 3.7 (d), for qualities above 0.3, the heat transfer coefficient increases with a rise of mass flux due to an enhancement of convective evaporation. As the mass flux increases at high quality, dry patches are rewetted and the dryout quality becomes higher.

An important consequence of the test results with varying mass flux of CO_2 is that efficient compact CO_2 evaporators for refrigeration and air conditioning application can be designed with low mass flux. Increasing mass flux does not improve heat transfer coefficient, while the added pressured drop acts negatively by reducing the local temperature difference. Another reason for selecting low mass flux is the increased critical vapor fraction. Thus, dryout can be avoided by reducing mass flux. It follows from this that the evaporator should preferably be fed with liquid only or with a low vapor quality and, if possible, the evaporator outlet condition should be kept in the wet region. A secondary advantage of liquid feeding

is that flow distribution between parallel channels can be improved especially at low mass flux.

(4) Effects of saturation temperature

Fig. 3.8 presents the variation of the heat transfer coefficients with respect to saturation temperature for a fixed mass flux. As expected, the heat transfer coefficient increases with saturation temperature of CO_2. These trend were also observed in the test results of Cho et al.[28] They showed that the heat transfer coefficients increase at all qualities as the evaporation temperature increases from 25℃ to 10℃. In nucleate boiling, the vapor bubble detach from heated surface playes an important role. As saturation temperature increases, the ratio of specific volumes of liquid to vapor is increased. Due to this reason, the buoyancy of vapor bubble increases, and the bubble detach is increased and finally, the nucleate boiling is activated.

In the Fig. 3.8, the local evaporation heat transfer coefficient has an effect on variation of saturation temperature at all the quality. Especially, at high quality, the increase in saturation temperature causes an increase of heat transfer coefficient due to activated nucleate boiling. In the Fig. 3.8 (d), the saturation temperature which changes from 0 to 5℃ has almost no influence on evaporation heat transfer coefficient at G_{re}=500 kg/m^{2}s and q_e=30 kW/m^2. This means that the heat transfer coefficient at 5℃ is lower compared to that at 0℃. The reduction in heat transfer coefficient at $T_{e,sat}$=5 may be due to reduced flow velocity caused by higher vapor

density with evaporation temperature, possibly in combination with non-equilibrium effects due to poor heat transfer between vapor and droplets. The fact that this reduction was observed at the higher mass flux and heat flux indicates that non equilibrium effects were present.

Cooper[29](1984) proposed that the nucleate boiling heat transfer coefficient is a strong function of reduced pressure, P_{rp}, which is the ratio of system pressure to critical pressure. The reduced pressure, P_{rp}, at increasing saturation temperature increases, and the density difference of vapor to liquid is decreased. In the end, due to this reason, the flow area of vapor bubble and the heat transfer coefficient of nucleate boiling increases with increasing saturation temperature.

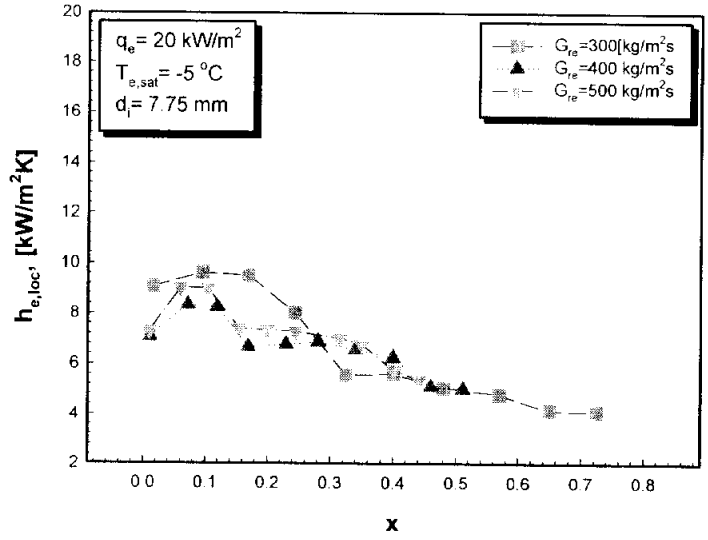

(a) q_e=20 kW/m^2, $T_{e,sat}$= 5 ℃

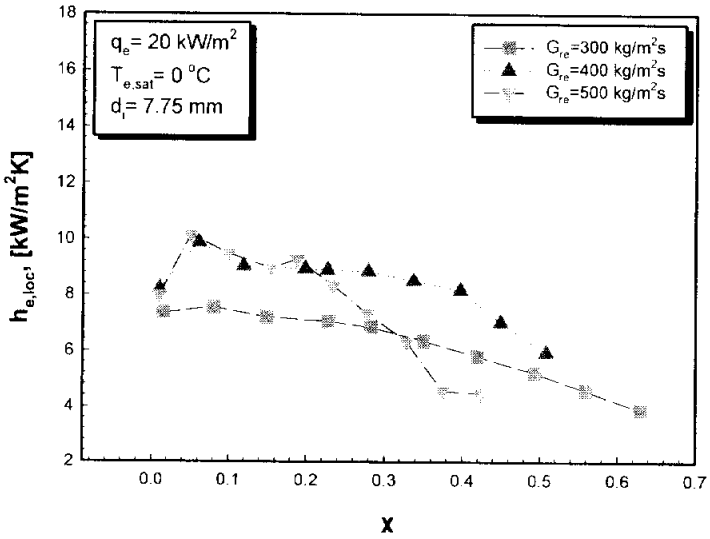

(b) q_e=20 kW/m^2, $T_{e,sat}$= 0 ℃

Fig. 3.7 Variation of the heat transfer coefficients for different mass fluxes at constant heat fluxes condition(continued).

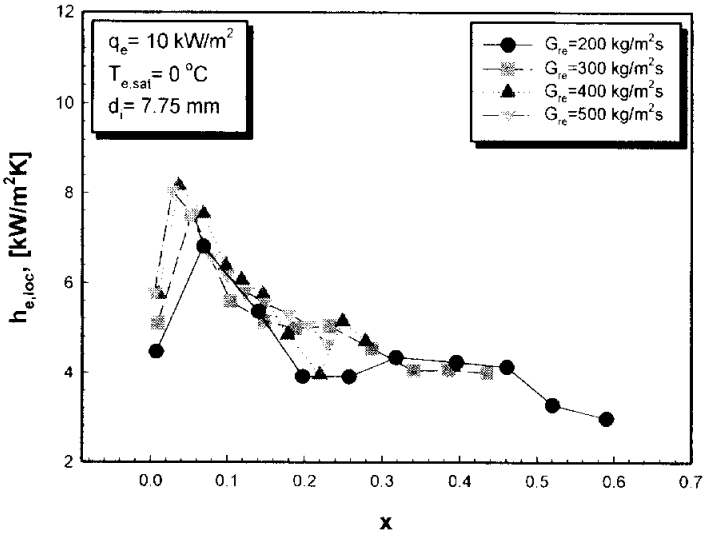

(c) q_e=10 kW/m^2, $T_{e,sat}$= 0 ℃

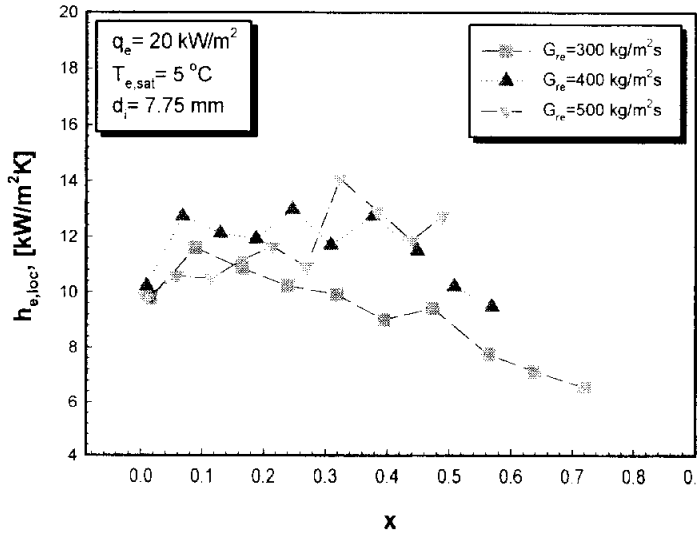

(d) q_e=20 kW/m^2, $T_{e,sat}$= 5 ℃

Fig. 3.7 Variation of the heat transfer coefficients for different mass fluxes at constant heat fluxes condition.

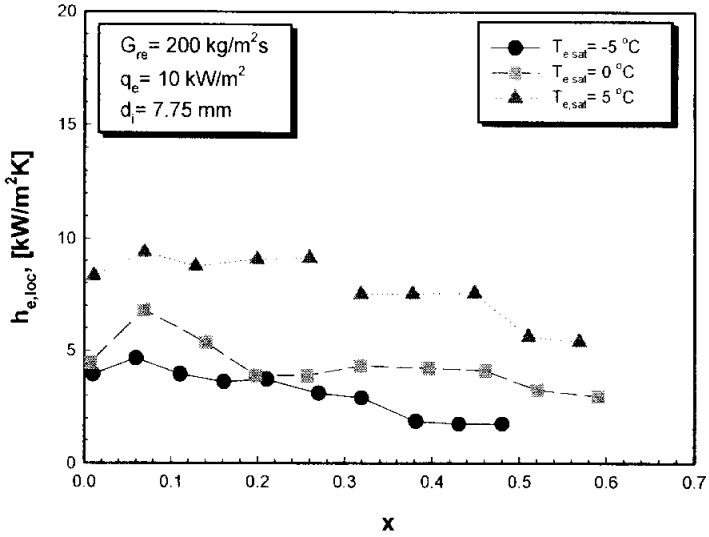

(a) G_{re}=200 kg/m^{2}s, q_e=10 kW/m^2

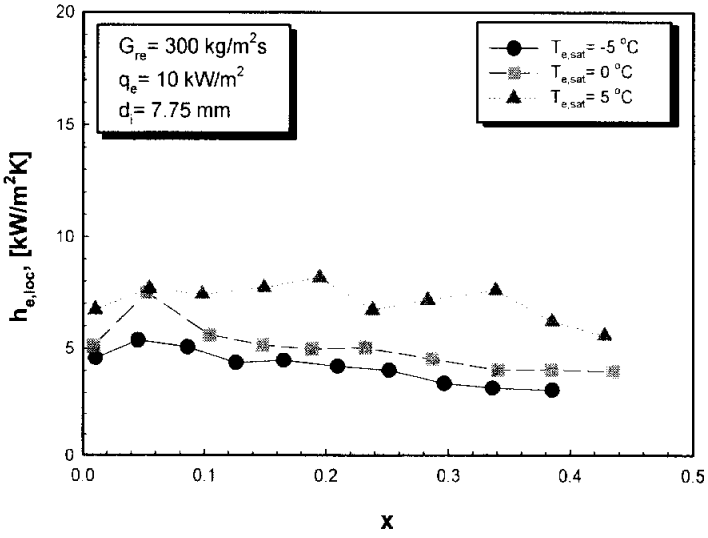

(b) G_{re}=300 kg/m^{2}s, q_e=10 kW/m^2

Fig. 3.8 Variation of the heat transfer coefficients with different saturation temperature for constant heat and mass fluxes (continued).

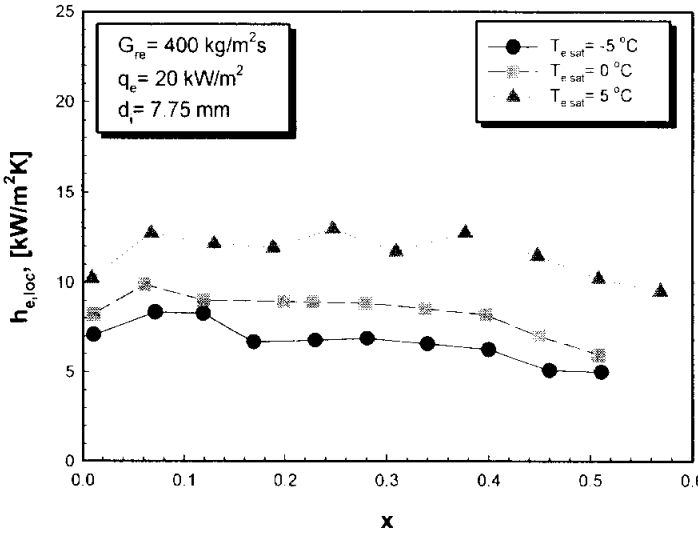

(c) G_{re}=400 kg/m^{2}s, q_e=20 kW/m^2

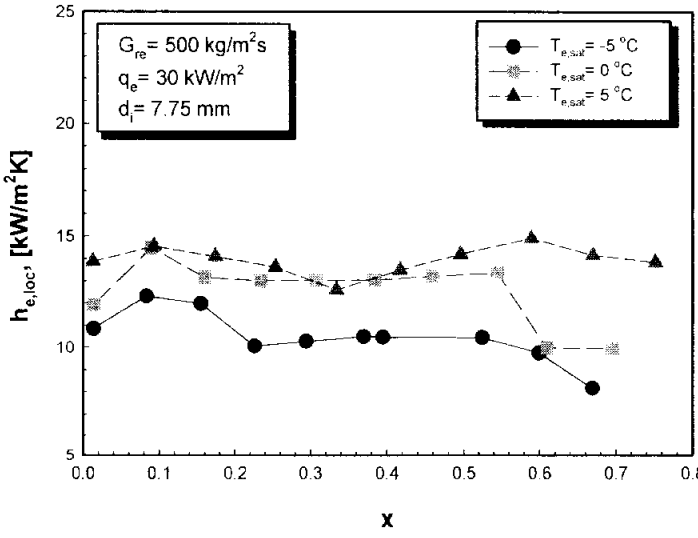

(d) G_{re}=500 kg/m^{2}s, q_e=30 kW/m^2

Fig. 3.8 Variation of the heat transfer coefficients with different saturation temperature for constant heat and mass fluxes.

3.2.2 Mean Evaporation Heat transfer

Fig. 3.9 displays variation of mean evaporation heat transfer coefficient with respect to mass flux over a wide range of experimental conditions. The mean heat transfer coefficient in evaporator could be calculated from Eq. (2.10). The inlet saturation temperature is -5℃, 0℃ and 5℃. Heat flux of CO_2 ranges from 10, 20, 30 and 40 kW/m^2. Mass flux is kept at 200, 300, 400 and 500 kg/m^{2}s. As seen in Fig. 3.9, varying mass flux has almost no influence on the mean heat transfer coefficient of CO_2 over a wide range of vapor quality. This indicates that nucleate boiling dominates over forced convection for CO_2 flow boiling in a horizontal tube. High velocity could enhance forced convection heat transfer. However, since the forced convection also suppresses nucleate boiling, the overall effect is a nearly constant heat transfer coefficient of CO_2. At a given mass flux, the mean heat transfer coefficient increases as saturation temperature of CO_2 increases. And the heat transfer coefficient increases with varying heat flux. Namely, in all regions of mass flux, the mean heat transfer coefficient of CO_2 shows a tendency to increase evidently with heat flux and saturation temperature. Therefore, it is known that the mean evaporation heat transfer coefficient of CO_2 in a horizontal tube has a major effect on more heat flux and saturation temperature than mass flux.

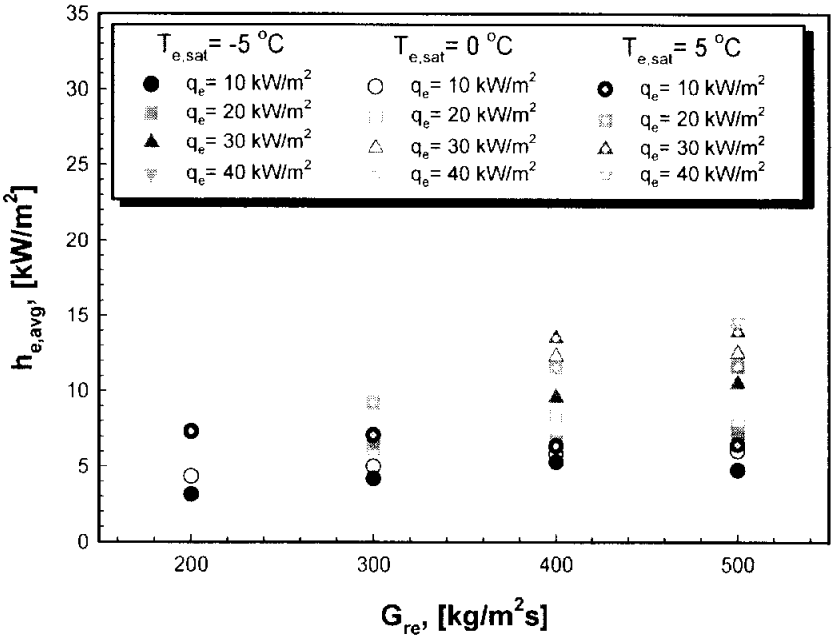

Fig. 3.10 Average heat transfer coefficients with respect to mass fluxes of CO_2 at varying heat flux and saturation temperature.

3.2.3 Comparison of CO_2, R-22 and R-134a

Fig. 3.10 presents the comparison between the heat transfer coefficients of R 744(CO_2) and those of R-22 and R-134a as Freon's refrigerant. The test conditions are the same. The inlet saturation temperature is 5℃ and the mass flux is kept at 300 kg/m^{2}s. Heat flux ranges from 10 to 20 kW/m^2. As can be seen in Fig. 3.10 (a), at low quality(0.12 <x <0.42), if a heat flux is 10 kW/m^2, the heat transfer coefficient of CO_2 is about 82% and 94.2% higher than that of R-22 and R-134a, respectively. And, as shown in Fig. 3.10 (b), at the quality region of 0.15 <x <0.66, if the heat flux is 20 kW/m^2, the heat transfer coefficient of CO_2 is about 87.2% and 93% higher than that of R-22 and R-134a, respectively. This phenomenon could be attributed to higher liquid and vapor conductivity of CO_2 than those of R-22 and R-134a. At low quality, the nucleate boiling of CO_2 is dominated more than that of R-134a and R-22. This is because the vapor velocity of CO_2 is higher than that of R-134a and R-22.

At high quality, the liquid film of CO_2 becomes thinner and easily drier. On the contrary, the flow pattern of R-134a and R-22 is a stable annular flow, and the liquid film of R-134a and R-22 is attached at inside tube wall for a long time. Also, the dropwise detach of CO_2 occurs at low quality. Therefore, the heat transfer coefficients of R-134a and R-22 increase with quality, and those of CO_2 decrease with vapor quality. Thus, CO_2 offers outstanding heat transfer characteristics compared to traditional refrigerants such as CFCs and HCFCs. These attractive characteristics are mainly due to the excellent thermal properties of CO_2.

Table 3.1 Thermophysical properties of refrigerants investigated

Refrigerant			R 744	R-22	R-134a
Saturation pressure, [MPa]		-5℃	3.042	0.4218	0.2433
		0℃	3.481	0.498	0.2928
		5℃	3.965	0.5841	0.3497
Saturation density, [kg/m^3]	Liquid	-5℃	956.7	1298	1311
		0℃	928.1	1282	1295
		5℃	896.7	1264	1278
	Vapor	-5℃	83.14	18.09	12.08
		0℃	97.32	21.23	14.43
		5℃	114.1	24.79	17.13
Saturation viscosity, [μPa · s]	Liquid	-5℃	115.2	230.4	289.1
		0℃	105.4	218.2	271.1
		5℃	95.84	206.7	254.4
	Vapor	5℃	13.85	11.28	10.53
		0℃	14.31	11.5	10.73
		5℃	14.83	11.73	10.94
Saturation thermal conductivity, [mW/m · K]	Liquid	5℃	116.7	97.09	94.24
		0℃	110.7	94.84	92.01
		5℃	104.5	92.61	89.8
	Vapor	-5℃	18.44	9.09	11.08
		0℃	19.93	9.42	11.51
		5℃	21.83	9.77	11.95

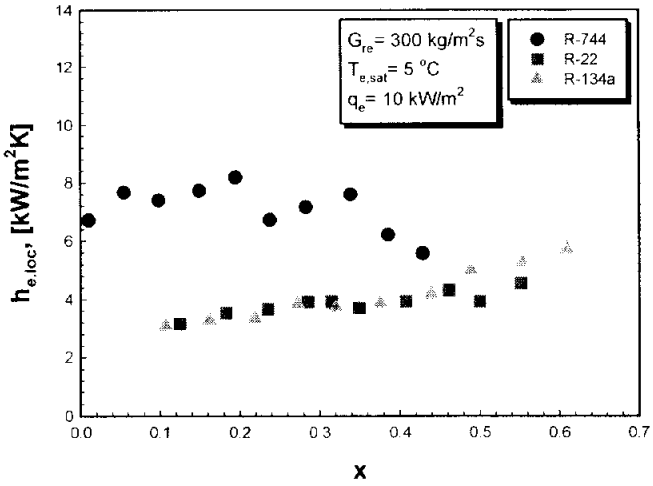

(a) G_{re}=300 kg/m^{2}s, $T_{e,sat}$=5 ℃, q_e=10 kW/m^2

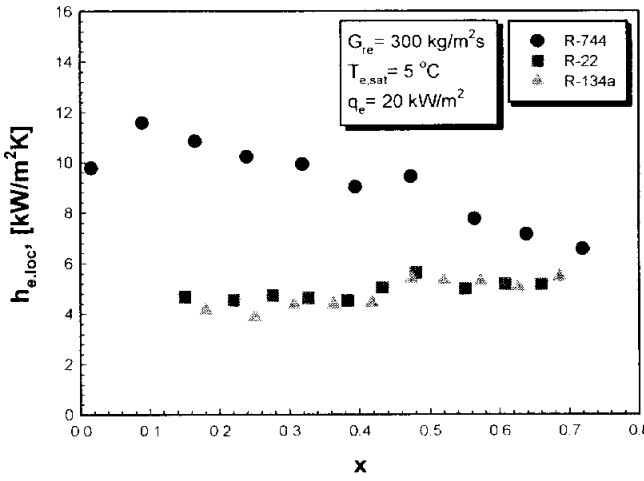

(b) G_{re}=300 kg/m^{2}s, $T_{e,sat}$=5 ℃, q_e=20 kW/m^2

Fig. 3.10 Comparison of the heat transfer coefficients of R-744 with those of some refrigerants (R-22 and R-134a).

3.3 PRESSURE DROP

3.3.1 Pressure drop during evaporation process

The accurate prediction of pressure drop in the evaporator is required to evaluate the substantial operating condition of air conditioning and refrigeration system, and to design for determining the main components such as compressor, fan and pump. Some investigator[30~33] conducted the study on pressure drop of two phase flow in a horizontal tube, and they proposed the theoretical and empirical correlations. It is very difficult to apply to the proposed correlations due to mathematical complex of their correlations.

Fig. 3.11 shows the measured pressure drop with respect to mass flux during the evaporation of CO_2 in a horizontal tube. For the given saturation temperature, the pressure drop of CO_2 in an evaporator increases with mass flux. For moderate mass flux, the pressure drop is lower as the saturation temperature of CO_2 is higher. This is not only because viscosity of CO_2 is lower as saturation temperature is higher but also because the vapor velocity decreases due to the decrease in density ratio of liquid to vapor, ρ_l/ρ_v.[24] The measured pressure drop of CO_2 in the evaporator with respect to varying heat flux is shown in Fig. 3.12. The measured pressure drop during evaporation process of CO_2 displays a tendency to increase as the heat flux is higher. It is concluded that this is because the vapor bubble formation from a heated surface is activated as the heat flux increases, and the flow disturbance of CO_2 is increased.

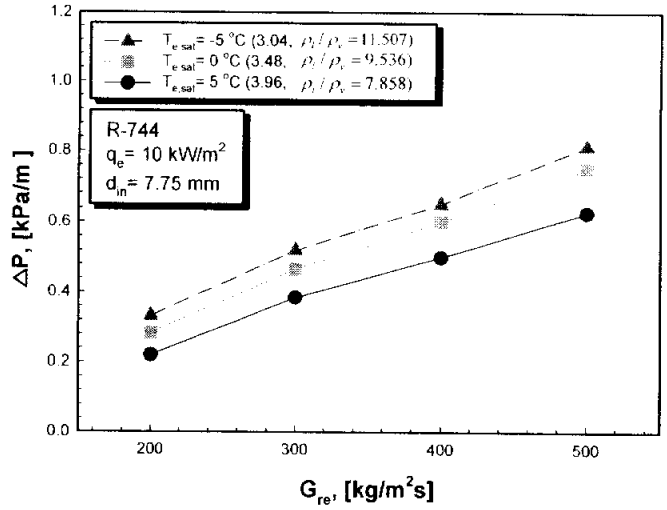

(a) q_e=10 kW/m^2

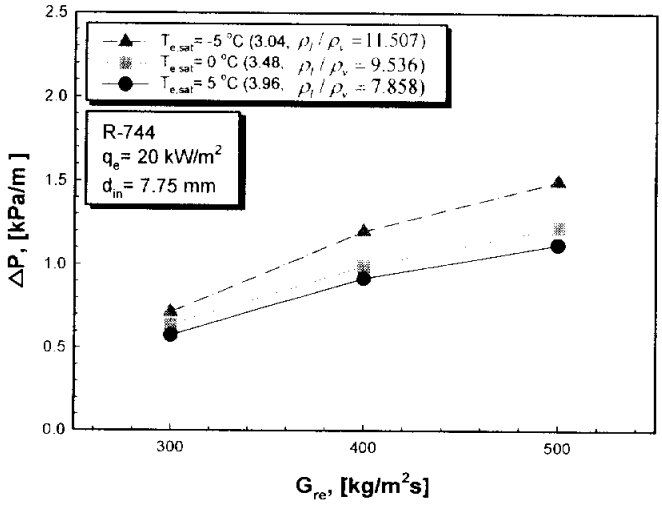

(b) q_e=20 kW/m^2

Fig. 3.11 Variation of the experimental pressure drop with respect to mass flux at different saturation temperature (continued).

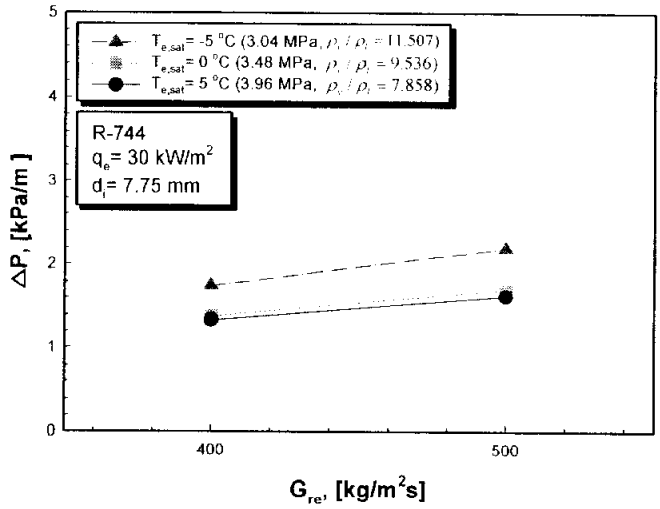

(c) q_e=30 kW/m^2

Fig. 3.11 Variation of the experimental pressure drop with respect to mass flux different saturation temperature.

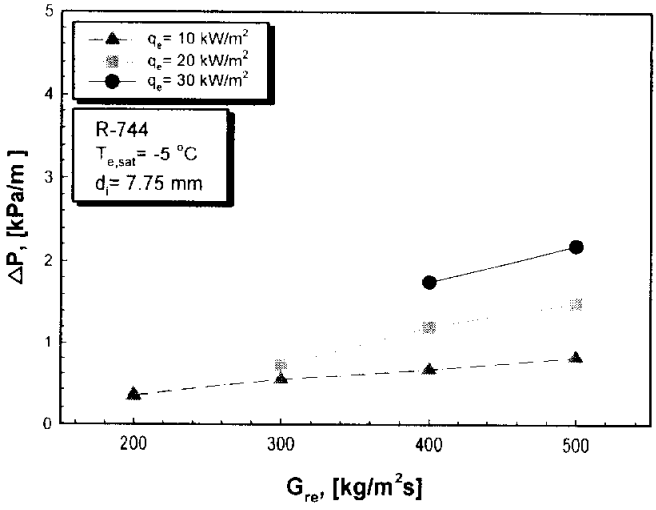

(a) $T_{e,sat}$= -5 ℃

Fig. 3.12 Variation of the experimental pressure drop with respect to mass flux at different heat flux (continued).

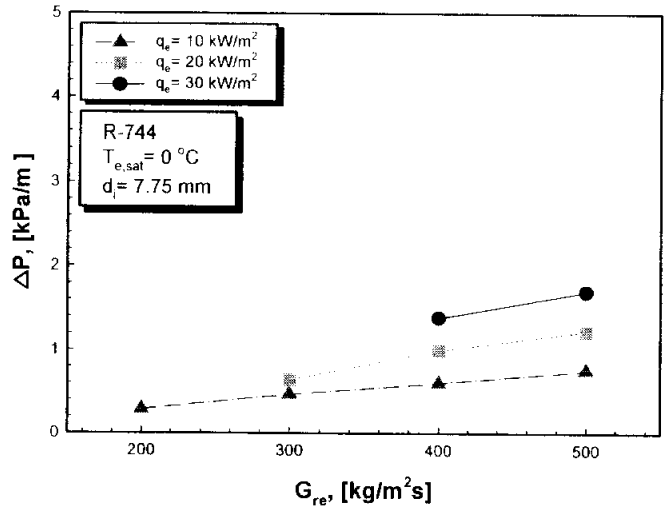

(b) $T_{e,sat}$=0 ℃

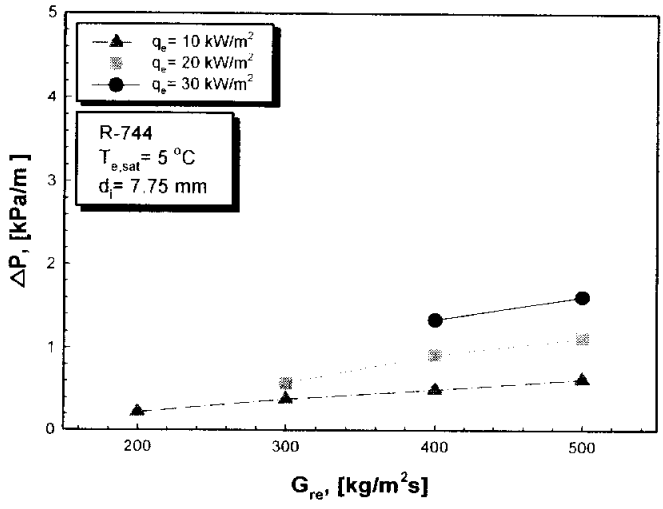

(c) $T_{e,sat}$=5 ℃

Fig. 3.12 Variation of the experimental pressure drop with respect to mass flux at different heat flux.

3.3.2 Comparison of CO_2 and R-22

Fig. 3.13 depicts the comparison of evaporation pressure drop between CO_2 and R 22 in a horizontal tube. The test conditions are the same. The saturation temperature of CO_2 is 5℃. The heat flux is 10 kW/m^2. As can be seen in Fig. 3.13, the pressure drop of CO_2 is much lower than that of R 22. The evaporation pressure drop of CO_2 is about 10 to 15% of R-22. These lower pressure drop of CO_2 is attributed to its unique thermal properties. The liquid viscosity of CO_2 at saturation temperature of 5℃ is 95.84 μPa · s, which is about 37.6% of R 22(254.4 μPa · s). Therefore, CO_2 has a lower pressure drop than of R 22.

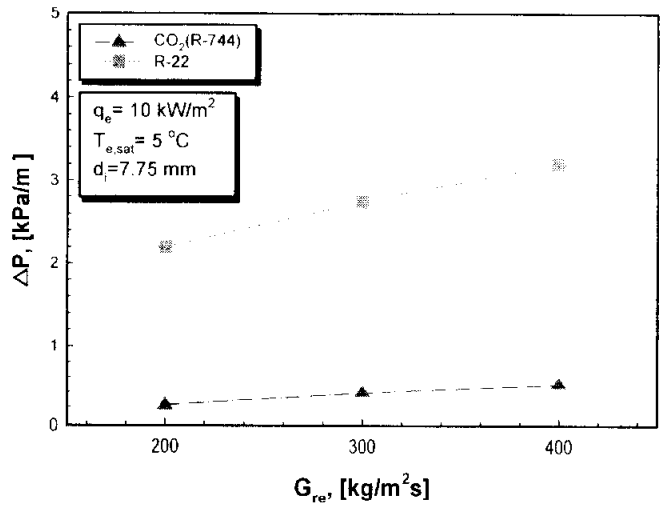

Fig. 3.13 Comparison of the pressure drop of CO_2(R-744) and R 22 at saturation temperature of 5℃ and heat flux of 10 kW/m^2.

3.3.3 Pressure drop correlations during evaporation process

The two phase pressure drops for flows inside tubes are the sum of frictional pressure drop and momentum pressure drop.

$$\left(\frac{dP}{dz}\right)_{tp}=\left(\frac{dP}{dz}\right)_{f}+\left(\frac{dP}{dz}\right)_{a} \tag{3.1}$$

In general, the frictional pressure drop results from the shear stress between the flowing fluid and the heating inside surface, and it constitutes the largest part of the total pressure drop. The momentum pressure drop is occurred by the change in momentum flux of the two phase. Soumerai[25] represents that the ratio of the frictional pressure drop to momentum pressure drop is about 2.5 to 5% if a aspect ratio, L/d_i, would be in the range of 500 to 1000. Consequently, the acceleration pressure drop is often negligible in comparison to the frictional pressure drop.

$$\left(\frac{dP}{dz}\right)_{tp}\approx\left(\frac{dP}{dz}\right)_{f} \tag{3.2}$$

In this study, since the length of evaporator is 5 m and inner diameter of inside tube is 7.75 mm, the dimensionless length, L/d_i, is 645. Therefore, it is valid for applying the assumption stated by Soumerai to experimental results of pressure drop during evaporation of CO_2.

The basic model for predicting the frictional pressure drop in a horizontal tube is divided into homogeneous model and separate model. In the homogeneous model for two phase flow, it is assumed that the two phases are traveling at the same velocities. There is Pierre[34]'s correlation in this model. In the separate model, the basic mode is that the two phases flow

in separate zones which may interact with each other. There are the correlations of Martinelli Nelson[35], Lockhart Martinelli[36], Baroczy[37], Chisholm[38](1968), Chisholm[39](1983), Reddy[40] and Jang et al.[41] in this model.

In the two phase flow, when it occurred the phase change such as evaporation and condensation, the pressure drop is calculated from separate model. Hence, in this section, the experimental frictional pressure drops of CO_2 in a horizontal tube have been compared to three correlations described earlier. The calculated frictional pressure drops were obtained by using the correlations predicted by Chisholm, Friedel[42], Jung et al. and Choi-Domanski[43], which is most widely used for the pressure drop of two phase flow in the separate model.

(1) Chisholm's correlation(1968)[38]

Chisholm(1968) proposed a detailed empirical method for a wide range of operating conditions. His two-phase frictional pressure drop gradient is given as

$$\left(\frac{dP}{dz}\right)_f \approx \left(\frac{dP}{dz}\right)_{lo} \Phi_{lo}^2 \tag{3.3}$$

here $(dP/dz)_{lo}$ is the pressure gradient of the liquid assuming that the entire mass of the fluid is flowing as liquid phase only through the channel. In this case, the gradient, $(dP/dz)_{lo}$, is defined by

$$\left(\frac{dP}{dz}\right)_{lo} = f_{lo} \frac{G_{re}^2}{2\rho_l d_i} \tag{3.4}$$

$$\left(\frac{dP}{dz}\right)_{vo} = f_{vo}\frac{G_{re}^2}{2\rho_g d_i} \tag{3.5}$$

where $(dP/dz)_{vo}$ is the pressure gradient of the vapor assuming that the entire mass of the fluid is flowing as vapor phase only through the channel. G_{re} is the mass flux of refrigerant in [kg/m^{2}s], d_i is inner diameter of the flow channel in [m], and ρ_l is the liquid density in [kg/m^3]. f_{lo} and f_{vo} are the friction factor, which is dependent upon the Reynolds number, and is to be calculated by using Eq. (3.6).

$$f_{lo,vo} = \begin{cases} 16/Re_{lo,vo} & \text{for} \quad Re \le 2\times10^3 \\ 0.316Re_{lo,vo}^{-1/4} & \text{for} \quad 2\times10^3 \le Re \le 2\times10^4 \\ 0.184Re_{lo,vo}^{-1/5} & \text{for} \quad Re \ge 2\times10^4 \end{cases} \tag{3.6}$$

in the above equation, Re_{lo} and Re_{vo} are the Reynolds number which is to be calculated with the assumption that the entire mass of fluid is flowing as liquid and vapor phase alone in the tube, respectively.

$$Re_{lo} = \frac{G_{re}\cdot d_i}{\mu_l}, \quad Re_{vo} = \frac{G_{re}\cdot d_i}{\mu_v} \tag{3.7}$$

Chisholm calculated the two phase frictional pressure drop using the dimensionless two phase multiplier for liquid and vapor phase.

$$Y^2 = \frac{\Phi_{vo}^2}{\Phi_{lo}^2} = \frac{(dP/dz)_{lo}}{(dP/dz)_{vo}} = \frac{f_{vo}\ \nu_v}{f_{lo}\ \nu_l} \tag{3.8}$$

where Y is the parameter used in the correlation of two-phase pressure drop. ν_v and ν_l are the specific volume of vapor and liquid phase, respectively. In Eq. (3.8), the dimensionless two phase multiplier, Φ_{lo}^2, is given by

Table 3.2 Criteria for selecting B

Y	G_{re}, kg/m^{2}s	B
<9.5	≤500	4.8
	500< G_{re} <1900	2400/ G_{re}
	>1900	55/ $G_{re}^{0.5}$
9.5< Y <28	≤600	520/(Y $G_{re}^{0.5}$)
	>600	21/Y
>28	-	15000/(Y^2 $G_{re}^{0.5}$)

$$\Phi_{lo}^2 = 1 + (Y^2 - 1)[Bx^{(2-n)/2}(1-x)^{(2-n)/2} + x^{(2-n)})] \tag{3.9}$$

where n is the exponent from the friction factor expression of Blasius (n 0.25), and Table 3.2 presents the parameter B depending on the mass flux and Chisholm parameter. The correlation of Chisholm does not adequately represent the effect on surface tension and inner diameter of tube, and is applicable to vapor qualities from $0 \le x \le 1$.

(2) Friedel's correlations(1979)[42]

Thome[44] recommends the Friedel's correlation for the frictional pressure gradient of supercritical CO_2 in a horizontal tube. Friedel's correlation is for vapor qualities from $0 \le x < 1$ and utilizes a two phase multiplier as :

$$\left(\frac{dP}{dz}\right)_f = \left(\frac{dP}{dz}\right)_{lo} \Phi_{lo}^2 = f_{lo} \frac{G_{re}^2}{2\rho_l d_i} \Phi_{lo}^2 \tag{3.10}$$

where Φ_{lo}^2 is a two phase multiplier, and f_{lo} is a friction factor calculated from Eq. (3.6). The two phase multiplier is defined as

$$\Phi_{lo}^2 = H_1 + \frac{3.24 \cdot H_2 \cdot H_3}{Fr_h^{0.0045} \cdot We_h^{0.035}} \tag{3.11}$$

with the Froude number, Fr_h, and Weber number, We_h, for a homogeneous flow without slip, and the factors

$$H_1 = (1-x)^2 + x^2 \frac{\rho_l \cdot f_{vo}}{\rho_v \cdot f_{lo}} \tag{3.12}$$

$$H_2 = x^{0.78} \cdot (1-x)^{0.224} \tag{3.13}$$

$$H_3 = \left(\frac{\rho_l}{\rho_v}\right)^{0.91} \cdot \left(\frac{\mu_v}{\mu_l}\right)^{0.19} \cdot \left(1 - \frac{\mu_v}{\mu_l}\right)^{0.7} \tag{3.14}$$

where f_{lo} and f_{vo} are given by Eq. (3.17). The Froude number and Weber number for a homogeneous flow are defined as

$$Fr_h = \frac{G_{re}^2}{g \cdot d_i \cdot \rho_h^2}, \quad We_h = \frac{G_{re}^2 \cdot d_i}{\sigma \cdot \rho_h} \tag{3.15}$$

where σ is the surface tension and ρ_h is the homogeneous density:

$$\frac{1}{\rho_h} = \left(\frac{x}{\rho_v} + \frac{1-x}{\rho_l}\right)^{-1} \tag{3.16}$$

The friction factor can be calculated according to Fanning:

$$f_{lo} = \frac{0.079}{Re_{lo}^{0.25}}, \quad f_{vo} = \frac{0.079}{Re_{vo}^{0.25}} \tag{3.17}$$

Friedel's correlation is typically that recommended when the ratio of (μ_l/μ_v) is less than 1000.

(3) Chisholm's correlation(1983)[39]

Chisholm represents the new pressure drop correlation correcting his

correlation proposed in 1963. The new correlation proposed by Chisholm can be depicted as a function of the parameter X_{tt}.

$$\Phi_{lo}^2 = 1 + \frac{C}{X_{tt}} + \frac{1}{X_{tt}^2} \tag{3.18}$$

where the constant C is determined according to the criteria given in Table 3.3. the quantity X_{tt} is usually characterized as Martinelli parameter. It assumes different values depending upon whether the type of flow in the two-phase is laminar or turbulent. In the two-phase flow in a horizontal tube, the vapor and liquid flow are all turbulent flow due to the high Reynolds number. Accordingly, Martinelli parameter, X_{tt}, follows according to Eq. (3.19).

Table 3.3 Criteria for selecting C for smooth tube

$(\mu_v/\mu_l)^{0.125}(\rho_l/\rho_v)^{0.5}$	C
>8.9	21
<8.9	$2.364Y^{-}(1/Y)$
=1.0	1.364

$$X_{tt} = \left(\frac{1-x}{x}\right)^{0.9}\left(\frac{\mu_l}{\mu_v}\right)^{0.1}\left(\frac{\rho_v}{\rho_l}\right)^{0.5} \tag{3.19}$$

(4) Jung et al.'s correlation(1989)[41]

Jung et al.(1989) performed the experiment on pressure drop during boiling flow of pure and mixture refrigerants in a horizontal tube. They developed a simple correlation adopting the thermodynamic corresponding

states. Their correlation is a type of Martinelli and Nelson's correlation and in developing the new correlation, they conducted the regression analysis with the experimental results. And then, they suggested the new correlation as shown Eq. (3.21).

$$\Phi_{lo}^{2} = \left(\frac{dP}{dz}\right)_{f} / \left(\frac{dP}{dz}\right)_{lo} \tag{3.20}$$

$$\Phi_{lo}^{2} = 3.58 X_{tt}^{-0.735} \tag{3.21}$$

where the dimensionless two-phase multiplier, Φ_{lo}, proposed by Martinelli and Nelson was applied to the evaporation process of refrigerant, and the correlation was summarized as follow Eq. (3.22).

$$\Phi_{lo}^{2} = \Phi_{lo}^{2}(1-x)^{1.8} = 12.82 X_{tt}^{-1.47}(1-x)^{1.8} \tag{3.22}$$

where X_{tt} is the Martinelli parameter defined as

$$X_{tt}^{2} = \frac{\Phi_{v}^{2}}{\Phi_{l}^{2}} = \frac{(dP/dz)_{l}}{(dP/dz)_{v}} \tag{3.23}$$

and $(dP/dz)_{v}$ and $(dP/dz)_{l}$ are the pressure gradient assuming the flow of the vapor and liquid phase alone in the tube, respectively. The monophase frictional pressure gradients are taken from the standard expressions for the liquid and vapor phases :

$$\left(\frac{dP}{dz}\right)_{l} = f_{l}\frac{G_{re}^{2}}{2\rho_{l} d_{i}} \tag{3.24}$$

$$\left(\frac{dP}{dz}\right)_{v} = f_{v}\frac{G_{re}^{2}}{2\rho_{v} d_{i}} \tag{3.25}$$

where f_{l} and f_{v} are the friction factors for laminar and turbulent flow and can be calculated by a Blasius's equation.

$$f_{l,v}=\begin{cases}16/Re_{l,v} & \text{for} \quad Re\leq 2\times 10^{3}\\ 0.316Re_{l,v}^{-1/4} & \text{for} \quad 2\times 10^{3}\leq Re\leq 2\times 10^{4}\\ 0.184Re_{l,v}^{-1/5} & \text{for} \quad Re\geq 2\times 10^{4}\end{cases} \tag{3.26}$$

In the equations, Re_l and Re_v are obtained with Eq. (3.26)

$$Re_l=\frac{G_{re}\cdot(1-x)\cdot d_i}{\mu_l},\quad Re_v=\frac{G_{re}\cdot x\cdot d_i}{\mu_v} \tag{3.27}$$

where x is the vapor quality and d_i is inner diameter tube. μ_l and μ_v are dynamic viscosity of the liquid and vapor, respectively.

(5) Choi and Domanski's correlation(1999)[43]

Choi and Domanski(1999) proposed the two phase frictional pressure drop during evaporation process in a horizontal tube. Their correlation is a form of Pierre's one using the different friction factor, f_n. In Eq. (3.29), the coefficient and exponent obtained from their experimental data.

$$\Delta P=\left[f_n+\frac{(x_{out}-x_{in})\cdot d_i}{x_m\cdot L}\right]\frac{G^2 L\nu_{tp}}{d_i} \tag{3.28}$$

where

$$f_n=0.05\,Re^{0.095}K_f^{0.155} \tag{3.29}$$

In Eq. (3.28), x_m is the mean quality evaluated at the inlet and outlet of subsection and L is a subsection length. f_n is the friction factor predicted by Pierre and K_f is the boiling number of Pierre.

$$K_f=\frac{(x_{out}-x_{in})\cdot i_{fg}}{L\cdot g} \tag{3.30}$$

where, i_{fg} is an evaporation latent heat and g is a gravity acceleration. In

Eq. (3.28), ν_{tp} is the two phase specific volume evaluated at liquid and vapor state.

$$\nu_{tp} = \frac{x_m}{\rho_v} + \frac{(1-x_m)}{\rho_l} \fallingdotseq x_m \cdot \nu_{m,v} \tag{3.31}$$

where, $\nu_{m,v}$ is the mean specific volume of vapor state calculated from the inlet and outlet of subsection.

3.3.4 Comparison of experimental data and correlations

Fig. 3.14 compares the measured pressure drop to those predicted by Chisholm's correlation(1968). As for this graph, the Chisholm's correlation (1968) predicts higher pressure drop than measured, especially at the higher heat flux and mass flux. The average deviation of the experimental data and Chisholm's correlation is 39.6%. Fig. 3.15 presents the comparison of the measured pressure drop and those predicted by Friedel's correlation (1979). As shown in Fig. 3.15, Friedel's correlation(1979) seems to significantly overpredict the experimental values, especially at the lower heat flux and mass flux. The average deviation of the experimental data and Friedel's correlation is 41.2%.

The comparison of pressure drop obtained from the experimental data and those predicted by Chisholm's correlation(1983) is displayed in Fig. 3.16. The Chisholm's correlation has a tendency to significantly overestimate the experimental values over a wide range of test conditions. The average deviation of the experimental data and Chisholm's correlation (1983) is 43.3%.

Fig. 3.17 presents the comparison of the measured pressure drop and those predicted by Jung et al.'s correlation(1989). As shown in Fig. 3.17, Jung et al.'s correlation(1989) seems to significantly overpredict the experimental values, especially at the lower heat flux and mass flux. The average deviation of the experimental data and Jung et al's correlation is 41.3%.

The comparison of pressure drop obtained from the experimental data

and those predicted by Choi and Domanski's correlation(1999) is displayed in Fig. 3.18. The Choi and Domanski's correlation agrees quite well with the experimental values over a wide range of test conditions. The average deviation of the experimental data and Choi and Domanski's correlation (1983) is 13.9%. Table 3.4 lists the results of comparison between the various correlations and the present results for CO_2.

A careful review of the frictional two phase flow pressure drop gave a conclusion that all those correlations have a tendency to significantly overpredict the experimental data. The main reason that the existing correlations fail to predict the pressure drop of CO_2 is related with the thermophysical properties of CO_2. Therefore, in order to accurately predict the pressure drop during evaporation process of CO_2, the new pressure drop correlation is needed.

Table 3.4 The errors between the calculated and experimental pressure drop

Deviation \ Authors	Chisholm (1968)	Friedel (1979)	Chisholm (1983)	Jung et al. (1989)	Choi and Domanski (1999)
Average deviation (%)	39.6	41.2	43.3	41.3	13.9
Mean deviation (%)	39.6	41.2	43.3	41.3	19.5

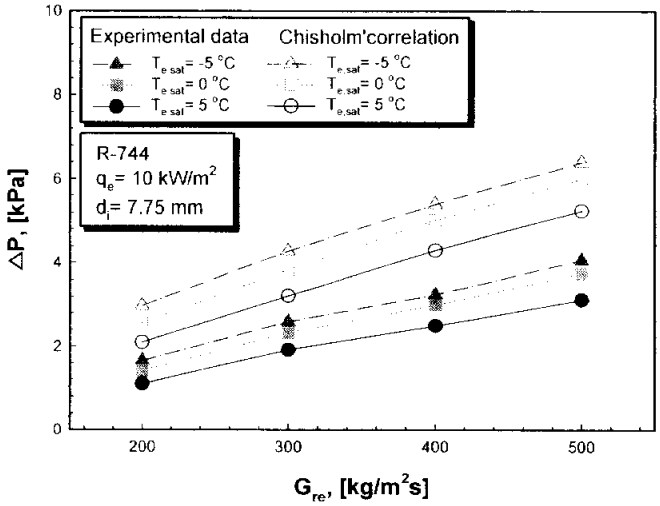

(a) q_e=10 kW/m^2

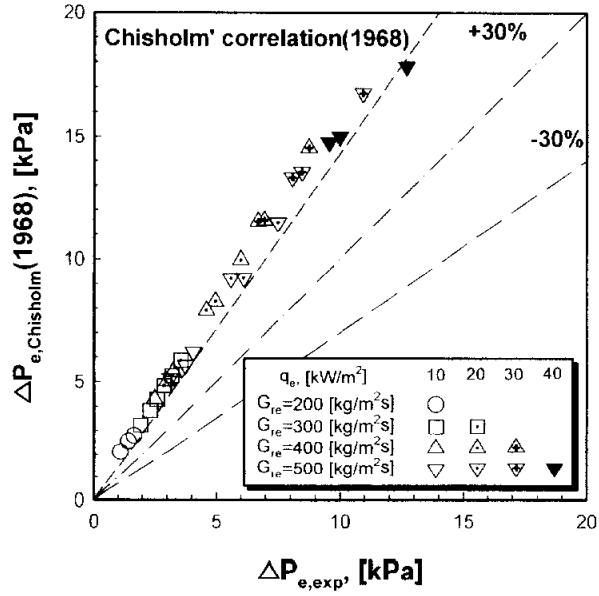

(b) q_e=10 kW/m^2~40 kW/m^2

Fig. 3.14 Comparison of the experimental pressure drop with those predicted by Chisholm's correlation (1968).

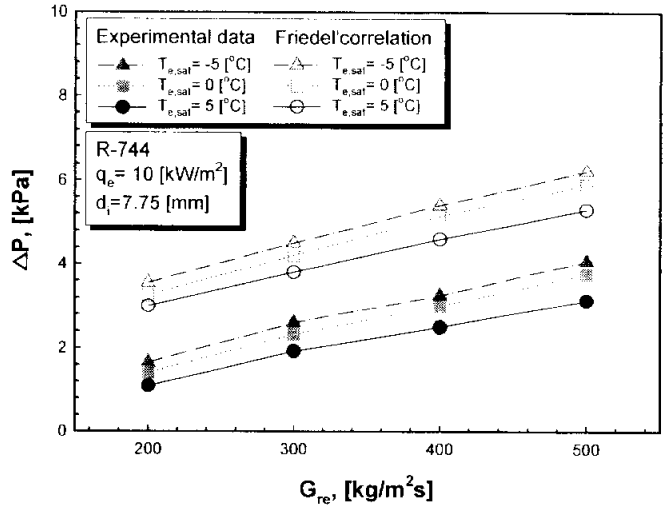

(a) q_e=10 kW/m^2

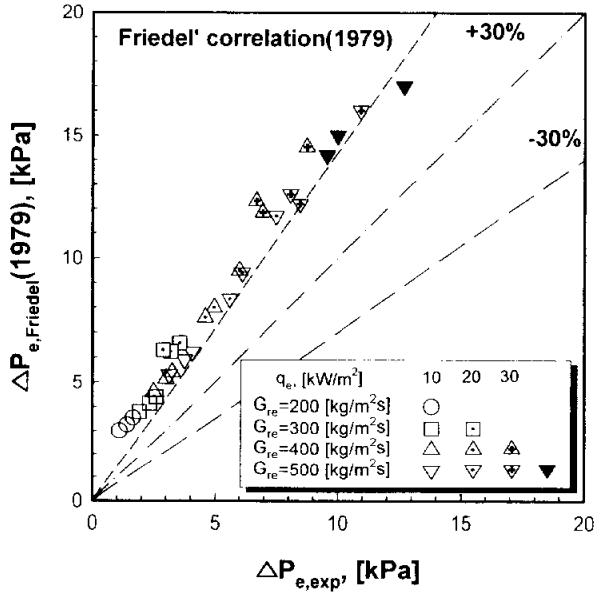

(b) q_e=10 kW/m^2~40 kW/m^2

Fig. 3.15 Comparison of the experimental pressure drop with those predicted by Friedel's correlation (1979).

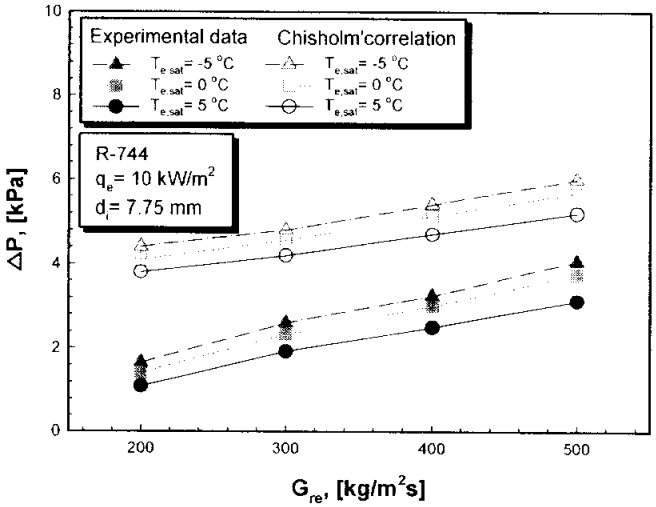

(a) q_e=10 kW/m^2

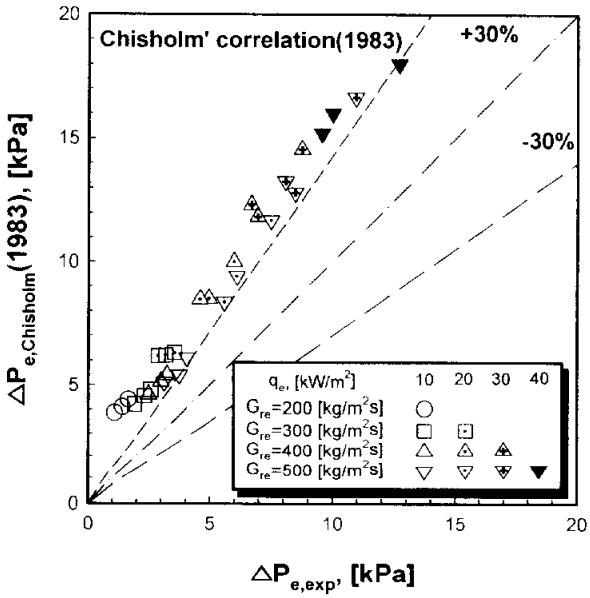

(b) q_e=10 kW/m^2~40 kW/m^2

Fig. 3.16 Comparison of the measured pressure drop data with those predicted by Chisholm's correlation (1983).

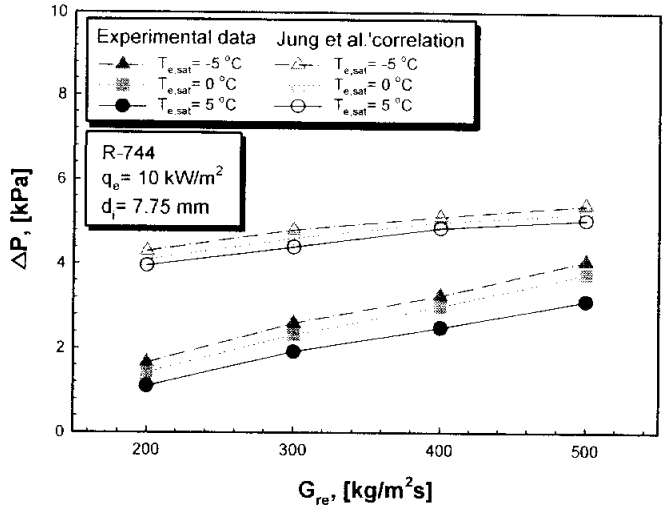

(a) q_e=10 kW/m^2

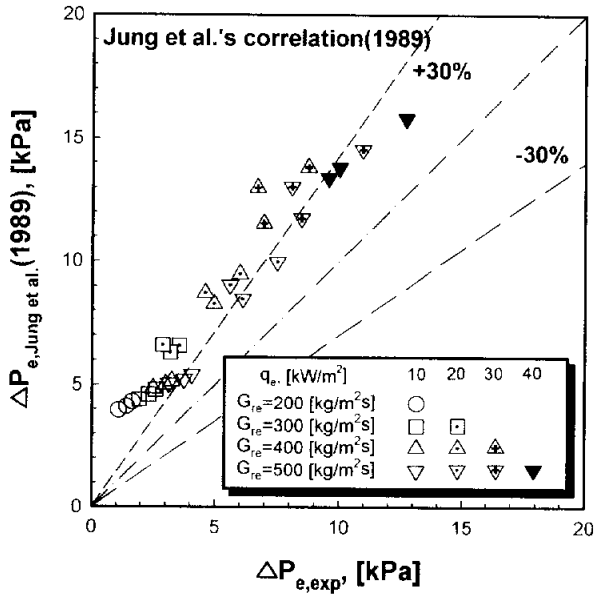

(b) q_e=10 kW/m^2~40 kW/m^2

Fig. 3.17 Comparison of the measured pressure drop data with those predicted by Jung et al.'s correlation(1989).

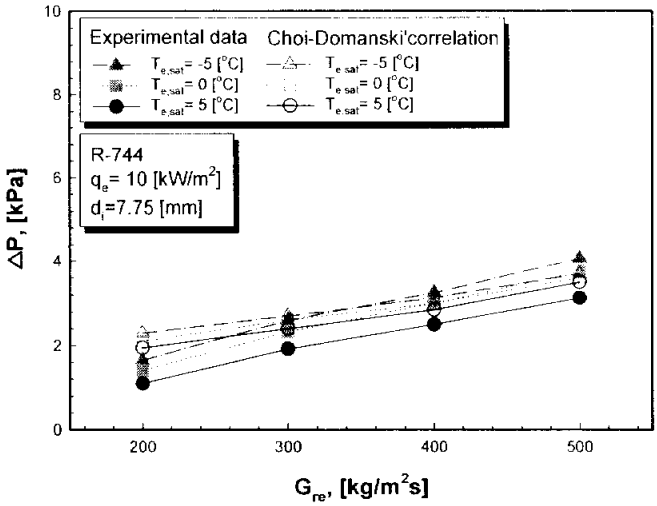

(a) q_e 10 kW/m^2

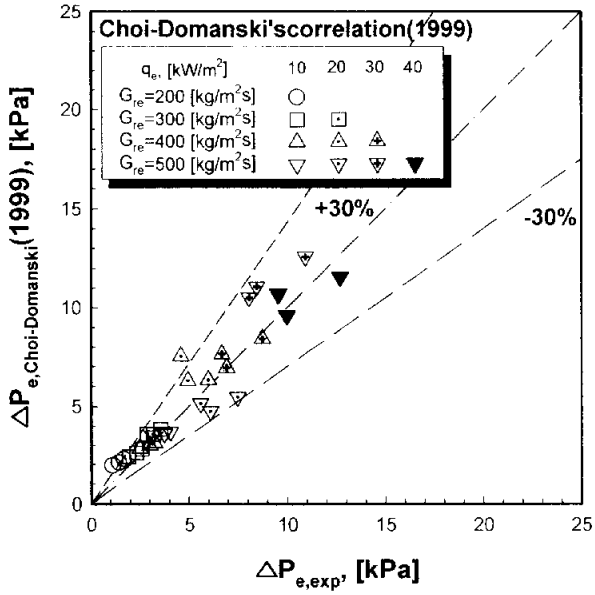

(b) q_e 10 kW/m^2~40 kW/m^2

Fig. 3.18 Comparison of the measured pressure drop data with those predicted by Choi-Domanski's correlation (1999).

3.4 COMPARISON OF EXPERIMENTAL DATA AND EXISTING CORRELATIONS

Since flow boiling is an important mode of heat transfer encountered in many heat exchangers, accurate estimation of heat transfer coefficient usually offers considerable economic savings in the design and operation of the system.

In order to predict the local evaporation heat transfer coefficient in a horizontal tube, some researchers proposed their correlations, and these correlations are presented by Shah[45], Gungor-Winterton[9], Kandlikar[46], Jung et al.[41] and Liu-Winterton[47]. In this chapter, some general correlations will be reviewed and compared to the experimental data, and confirmed this applicable possibility of their correlations.

3.4.1 Correlations for evaporation heat transfer

(1) Shah's correlation[45]

Shah has proposed the following correlation for flow boiling in vertical, horizontal tubes and annuli. He developed a correlation equation from an earlier chart based correlation. This correlation is applicable to nucleate, convection, and stratified boiling regions as evidences by its functional relationship with several dimensionless numbers including the boiling number, Froude number and convection number. As expected, nucleate boiling dominates at low qualities. while convective boiling dominates at higher qualities. For horizontal flow, Shah's correlation is

$$h_{TP} = \Psi \cdot h_l \tag{3.32}$$

where h_{TP} is the evaporation heat transfer coefficient in [kW/m^2·K] and h_l is the convection heat transfer coefficient based on a form of Dittus Boelter[48], as defined in Eq. (3.33).

$$h_l = 0.023\left[\frac{G\cdot(1-x)\cdot d_i}{\mu_l}\right]^{0.8}\mathrm{Pr}_l^{0.8}\frac{k_l}{d_i} \tag{3.33}$$

for vertical tubes at all values of Fr_l and for horizontal tubes when $Fr_l >$ 0.04,

$$N = Co \tag{3.34}$$

For horizontal tubes when $Fr_l < 0.04$,

$$N = 0.38\,Fr_l^{-0.3}\,Co \tag{3.35}$$

The convection number, Co, and Froude number, Fr_l, used in the preceeding expressions can be calculated as follows.

$$Fr_l = \frac{G_{re}^2}{\rho_l^2\cdot g\cdot d_i} \tag{3.36}$$

$$Co = \left(\frac{1-x}{x}\right)^{0.8}\left(\frac{\rho_v}{\rho_l}\right)^{0.5} \tag{3.37}$$

where the convection number, Co, is similar to the Martinelli parameter, Eq. (3.37), except that the vapor viscosity effect is excluded.

The Shah's correlation in terms of these dimensionless parameters was originally presented in graphical form and was evaluated by taking the largest of the three heat transfer coefficients calculated for the nucleate boiling, convective boiling, and boiling suppression region. Thus, the term Ψ is evaluated by the following procedure

For $N > 1$,

$$\Psi_{nb} = 230 Bo^{0.5} \quad \text{for} \quad Bo \geq 3.0\times10^{-5} \tag{3.38}$$

$$\Psi_{nb} = 1 + 46 Bo^{0.5} \quad \text{for} \quad Bo < 3.0\times10^{-5} \tag{3.39}$$

$$\Psi_{cb} = \frac{1.8}{N^{0.8}} \tag{3.40}$$

where the parameter Ψ is the larger of Ψ_{nb} and Ψ_{cb}, and applies to all the case, irrespective of the value N.

For $0.1 < N \leq 1.0$,

$$\Psi_{bs} = F \cdot Bo^{0.5} \exp^{2.74 N^{-0.1}} \tag{3.41}$$

For $N < 0.1$,

$$\Psi_{bs} = F \cdot Bo^{0.5} \exp^{2.74 N^{-0.15}} \tag{3.42}$$

where the parameter Ψ is the larger of Ψ_{nb} and Ψ_{bs}. The constant F in the preceding expression depends on the boiling number, Bo, which is interpreted as the mass of vapor generated at the tube surface relative to the total mass velocity parallel to the tube surface,

$$F = 14.7 \quad \text{for} \quad Bo \geq 11\times10^{-4} \tag{3.43}$$

$$F = 15.43 \quad \text{for} \quad Bo < 11\times10^{-4} \tag{3.44}$$

and the boiling number Bo can be calculated as

$$Bo = \frac{q}{G_{re} \cdot i_{fg}} \tag{3.45}$$

where q is the heat flux in [kW/m^2] and G_{re} is the mass velocity in [kg/m^2·s]. And i_{fg} is the latent heat of vaporization in [kJ/kg].

(2) Gungor and Winterton's correlation[9]

A new correlation of the Chen form has been developed by Gungor and Winterton(1986). For vertical upward and downward flows and horizontal flows, a large data base(3696 points) was used covering both the nucleate and convection dominated boiling regimes for water, refrigerants(R 11, R-12, R 22, R-113 and R114) and ethylene glycol. The basic equation for saturated boiling is

$$h_{TP} = E \cdot h_l + S \cdot h_{pool} \tag{3.46}$$

with h_l calculated from the Dittus-Boelter correlation, using the local liquid fraction of the flow, i.e., $G(1-x)$. The new convection enhancement factor E is given by the expression

$$E = 1 + 2.4 \times 10^4 Bo^{1.16} + 1.37 \left(\frac{1}{X_{tt}} \right)^{0.86} \tag{3.47}$$

where X_{tt} is the Martinelli parameter defined by Eq. (3.19) and the new completely empirical boiling suppression factor S is

$$S = \frac{1}{1 + 1.15 \times 10^{-6} E^2 Re_l^{1.17}} \tag{3.48}$$

with Re_l based on $G(1-x)$. The nucleate pool boiling coefficient is calculated from the Cooper(1984a) reduced pressure correlation:

$$h_{pool} = 55 P_{rp}^{0.12} (-\log_{10} P_{rp})^{-0.55} W^{-0.5} q^{0.67} \tag{3.49}$$

which gives the heat transfer coefficients in [kW/m^2·K]. where W is the molecular weight in [kg/kmol]. P_{rp} is the reduced pressure and q is the heat flux in [kW/m^2]. If the tube is horizontal and the Froude number is

below 0.05, stratified flow occurs and E must be multiplied by

$$E_2 = Fr_l^{(0.1 - 2Fr_l)} \tag{3.50}$$

and S must be multiplied by

$$S_2 = \sqrt{Fr_l} \tag{3.51}$$

(3) Kandlikar's correlation[46]

The correlation proposed by Kandlikar also considers nucleate, convection and stratified boiling flow. He introduced a general correlation for flow boiling in vertical and horizontal tubes. The correlation for vertical tubes and for horizontal tubes with $Fr_l > 0.04$ is given as

$$h_{NBD} = (0.6683\, Co^{-0.2} + 1058.0\, Bo^{0.7} F_{fl})\, h_l \tag{3.52}$$

$$h_{CBD} = (1.1360\, Co^{-0.9} + 667.2\, Bo^{0.7} F_{fl})\, h_l \tag{3.53}$$

where the two-phase flow heat transfer coefficient, h_{TP}, is the larger of h_{NBD} and h_{CBD}. h_{NBD} is contribution due to nucleate boiling and h_{CBD} is contribution due to convective boiling. h_l is a liquid only convective heat transfer coefficient based on a form of the Dittus Boelter equation, Eq. (3.65). The convective number, Co, and boiling number, Bo, can be defined as Eq. (3.37) and Eq. (3.45), respectively. The quantity F_{fl} is a fluid-dependent parameter whose values are listed for water, CFC11, CFC12, CFC13B1, HCFC22, CFC113, CFC114, CFC152, nitrogen and neon by Kandlikar. For fluids not listed, Kandlikar recommends that F_{fl} be estimated as the multiplier S, needed in the Froster Zuber[49]'s correlation

Table 3.5 Fluid dependent parameter F_{fl} in the proposed correlation

Fluid	F_{fl}	Fluid	F_{fl}
Water	1.00	R-113	1.30
R-11	1.30	R-114	1.24
R-12	1.50	R-152B	1.10
R-13B1	1.31	Nitrogen	4.70
R-22	2.20	Neon	3.50

to correlate the pool boiling data for the experimental fluid. The factor S is defined in Eq. (3.54) and is called the suppression factor, which reflects the fact that as the forced convection effect increases, the nucleate boiling contribution is more strongly suppressed because of a reduction in the thermal boundary layer thickness. The value of S is less than unity and is assumed to be a function of the equivalent Reynolds number. It was originally available in graphical form developed by Chen[14]'s correlation, but later Collier and Thome[50].

$$S = \frac{1}{1 + 2.56 \times 10^{-6} Re_{eq}^{1.17}} \tag{3.54}$$

where the equivalent Reynolds number, Re_{eq}, and the equivalent mass flux, G_{eq}, are defined by

$$Re_{eq} = G_{eq} \cdot d_i / \mu_l \tag{3.55}$$

$$G_{eq} = G_{re} \cdot [(1-x) + x(\rho_l/\rho_v)^{1/2}] \tag{3.56}$$

where μ_l, μ_v, ρ_l and ρ_v are the viscosity and density of vapor and liquid

phase, respectively.

(4) Jung et al.'s correlation[41]

Based on the analysis of experimental data for the forced convection, Jung et al.(1989) proposed the evaporation correlation for pure refrigerants using the original form of Chen(1966).

$$h_{TP} = h_{nb} + h_{cb} = N \times h_{SA} + F_p \times h_l \tag{3.57}$$

in above equation, h_{TP} is the heat transfer coefficient of two phase flow and h_{nb} is the heat transfer coefficient in nucleate boiling, and h_{cb} is the heat transfer coefficient during forced convective boiling. h_{SA} is a pool boiling heat transfer coefficient obtained by Stephan and Abdelsalam's correlation(1980)[51] and h_l is a single phase heat transfer coefficient obtained by Dittus Boelter's correlation, assuming the total flow to be liquid.

$$h_{SA} = 207 \frac{k_f}{b-d} \left(\frac{q\ b_d}{k_f T_{sat}} \right)^{0.745} \left(\frac{\rho_v}{\rho_f} \right)^{0.581} \mathrm{Pr}_f^{0.533} \tag{3.58}$$

where bubble departure diameter, b_d, is defined by Eq. (3.59) predicted by Fritz[52].

$$b_d = 0.0146\theta \left(\frac{2\sigma}{g(\rho_f - \rho_v)} \right)^{0.5}, \quad \theta = 35^\circ \tag{3.59}$$

the non-dimensional parameter, F_p, is

$$F_p = 2.37 \left(0.29 + \frac{1}{X_{tt}} \right)^{0.85} \tag{3.60}$$

and the quantity X_{tt} is the Martinelli parameter defined as

$$X_{tt}=\left(\frac{1-x}{x}\right)^{0.9}\left(\frac{\mu_l}{\mu_v}\right)^{0.1}\left(\frac{\rho_v}{\rho_l}\right)^{0.5} \tag{3.61}$$

In Eq. (3.57), N is a variable depending upon boiling number, Bo, and Martinelli parameter, X_{tt}, and calculated from follow conditions.

$$N=4048\times(X_{tt})^{1.22}(Bo)^{1.13},\quad X_{tt}<1 \tag{3.62}$$

$$N=2.0-0.1\times(X_{tt})^{-0.28}(Bo)^{-0.33},\quad 1\le X_{tt}\le 5 \tag{3.63}$$

(5) Liu and Winterton's correlation[47]

Liu and Winterton(1991) analyzed experimental data for many refrigerants and compared the measured evaporation heat transfer coefficient with the existing correlation. They introduced the following correlation for flow boiling in tubes based on Kutateladze's power-type addition model. Their correlation constitutes the sum of forced convective boiling and nucleate boiling.

$$h_{tp}=[(E\cdot h_l)+(S\cdot h_{nb})]^2 \tag{3.64}$$

In Eq. (3.64), $(E\cdot h_l)$ is a term of boiling in forced convective flow and $(S\cdot h_{nb})$ is a term of nucleate boiling. h_l is a single phase heat transfer coefficient calculated by Dittus-Boelter, assuming the total flow to be liquid.

$$h_l=0.023Re_l^{0.8}\mathrm{Pr}_l^{0.4}\left(\frac{\kappa_l}{d_i}\right) \tag{3.65}$$

where h_l is the evaporation heat transfer coefficient calculated by

Cooper's correlation[25].

$$h_{nb} = 55 P_{rp}^{0.12} q^{2/3} (-\log_{10} P_{rp})^{-0.55} W^{-0.5} \tag{3.66}$$

where P_{rp} is a reduced pressure, which is the ratio of critical pressure to system pressure. W is a molecular weight in [kg/kmol]. In Eq. (3.64), S and E are a boiling suppression and forced convection heat transfer enhancement factor, respectively.

$$E = \left[1 + x \cdot \mathrm{Pr}_l \cdot \left(\frac{\rho_l}{\rho_v} - 1 \right) \right]^{0.35} \tag{3.67}$$

$$S = \left(1 + 0.055 \cdot E^{0.1} \cdot Re_l^{0.16} \right)^{-1} \tag{3.68}$$

where Re_l is a liquid Reynolds number and Pr_l is a liquid Prandtl number.

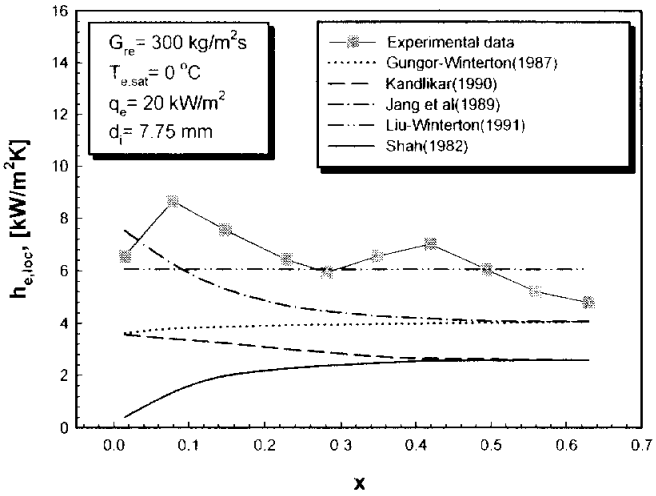

(a) q_e=20 kW/m^2, G_{re}=300 kg/m^{2}s, $T_{e,sat}$= 0 ℃

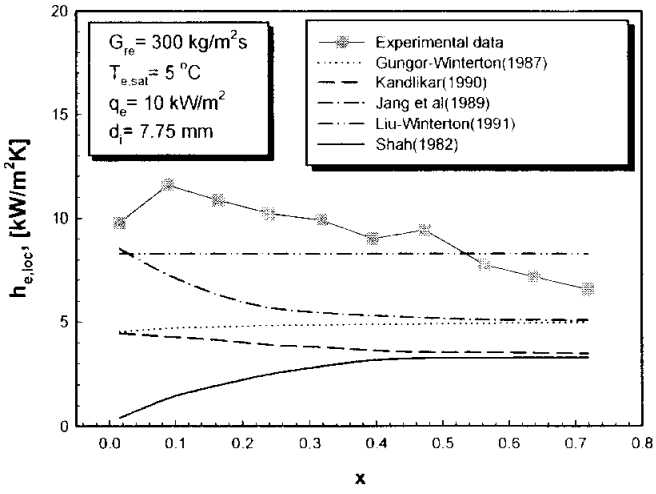

(b) q_e=10 kW/m^2, G_{re}=300 kg/m^{2}s, $T_{e,sat}$= 5 ℃

Fig. 3.19 Comparison of the experimental data with the calculated heat transfer coefficients using existing correlations as a function of quality.

3.4.2 Comparison of experimental data and correlations

In order to get a correct comparison between measured and correlated data, the mean heat transfer coefficient for the range of quality in the test section had to be calculated for each experiment. Based on the measured inlet and outlet quality to the test section, the heat transfer coefficient was calculated as the mean value for "subsections" using the above method of correlating heat transfer in each subsection.

Fig. 3.19 displays comparison between the evaporation heat transfer coefficients obtained from the experiment and the correlations predicted by Shah, Gungor Winterton, Jung et al., Kandlikar and Liu Winterton. All the correlations tend to underestimate the experimental heat transfer coefficients. Among the correlations, the best fit of the present test data is obtained with the correlation of Jung et al., Kandlikar and Jung et al.'s correlation shows a similar tendency to decrease with respect to quality. But, for the same conditions, the correlations of Gungor Winterton, Shah and Kandlikar show a increasing tendency of heat transfer coefficient with respect to quality. Liu and Winterton's correlation remains constant with quality.

Fig. 3.20 depicts the comparison of measured heat transfer coefficient with that predicted by the existing correlations. In all of the experimental conditions, all the correlations underpredicted the experimental data. For the same conditions, the deviation of experimental and calculated data is higher as mass flux and heat flux of CO_2 are higher.

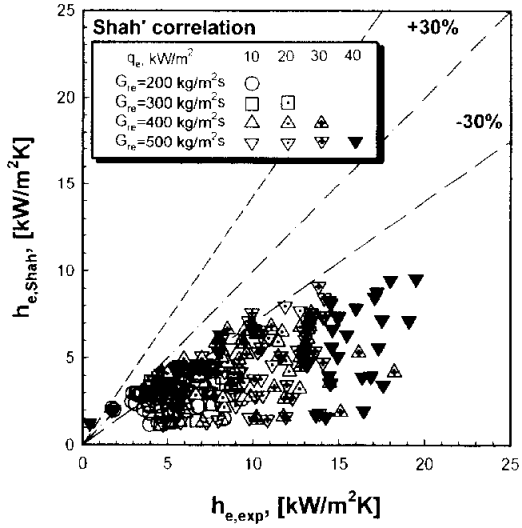

(a) Shah's correlation

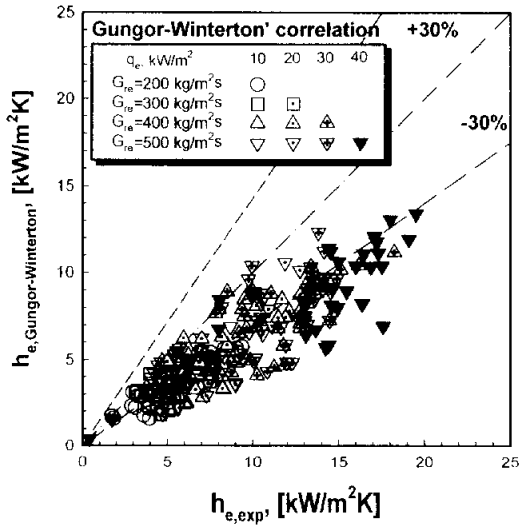

(b) Gungor Winterton's correlation

Fig. 3.20 Comparison between calculated and measured heat transfer coefficient at varying experimental conditions (continued).

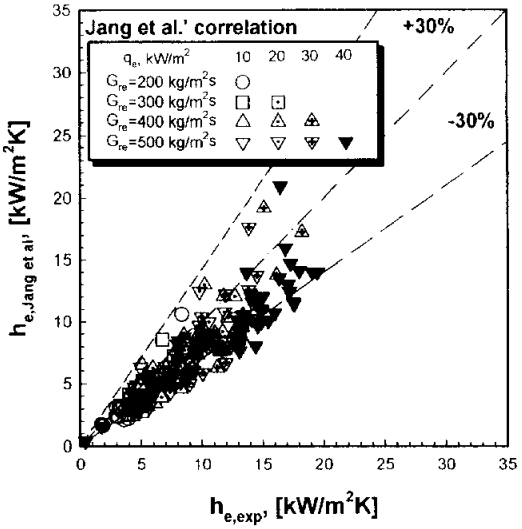

(c) Jung et al.'s correlation

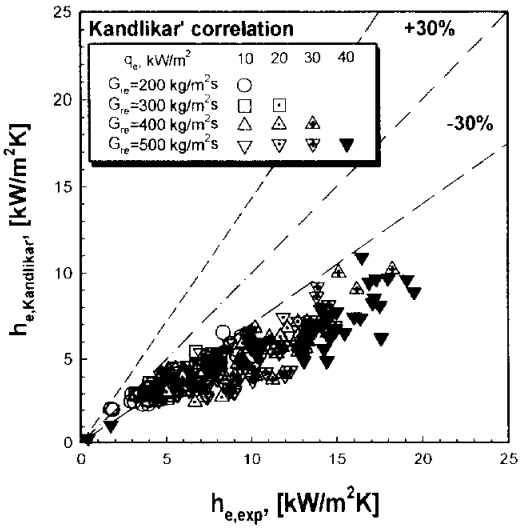

(d) Kandlikar's correlation

Fig. 3.20 Comparison between calculated and measured heat transfer coefficient at varying experimental conditions (continued).

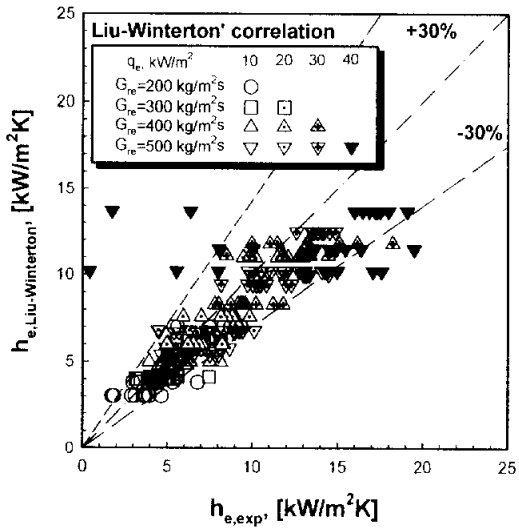

(e) Liu Winterton's correlation

Fig. 3.20 Comparison between calculated and measured heat transfer coefficient at varying experimental conditions.

Table 3.6 lists the results of comparison between the various correlations and the present results for CO_2. In table 3.6, the average deviation, σ_{avg}, and mean deviation, σ_{abs}, are defined as

$$\sigma_{avg} = \frac{1}{N}\left[\sum_{i=1}^{N}\left(\frac{h_{cal,i}-h_{\exp,i}}{h_{\exp,i}}\right)\right]\times 100 \tag{3.61}$$

$$\sigma_{abs} = \frac{1}{N}\left[\sum_{i=1}^{N}\left|\frac{h_{cal,i}-h_{\exp,i}}{h_{\exp,i}}\right|\right]\times 100 \tag{3.62}$$

where N is the number of experimental data. $h_{\exp}$ is the measured heat transfer coefficient obtained experimental data and h_{cal} is the local heat transfer coefficient predicted by correlations. Fig. 3.20 (a) shows the comparison of experimental heat transfer coefficients with those predicted by Shah's correlation. For the wide range of mass velocity, average deviation is 47.3% and mean deviation is 49.1%. Comparison of the measured heat transfer coefficients with those predicted by Gungor-Winterton's correlation is depicted in Fig. 3.20 (b). In the entire range of mass velocity, average deviation is 32.4% and mean deviation is 32.7%. Fig. 3.20 (c) displays the comparison of experimental heat transfer coefficients with those predicted by Jung et al.'s correlation. In case of all mass velocities, average deviation is 14.3% and mean deviation is 21.6%. Comparison of the measured heat transfer coefficients with those predicted by Kandlikar's correlation is presented in Fig. 3.20 (d). In all range of mass velocity, average and mean deviation is 38.9% and 39.2%, respectively. Fig. 3.20 (e) shows the comparison of experimental heat transfer coefficients with those predicted by Liu-Winterton's correlation. In

Table 3.6 The errors between the calculated and experimental heat transfer coefficients

Deviation \ Authors	Shah (1982)	Gungor and Winterton (1986)	Jung et al. (1989)	Kandlikar (1989)	Liu and Winterton (1991)
Average deviation (%)	47.3	32.4	14.3	38.9	12.6
Mean deviation (%)	49.1	32.7	21.6	39.2	32.6

a wide range of mass flux, average deviation is 12.6% and mean deviation is 32.6%. As mentioned earlier, when comparison of calculated and experimental heat transfer coefficients, Jung et al.'s correlation shows the best agreement to experimental data.

3.5 SUMMARY

In this chapter, for optimum design of refrigeration and air conditioning evaporator using CO_2 as working fluid, the heat transfer coefficients and pressure drop during the evaporation process of CO_2 in a horizontal tube have been investigated and the followings are the findings of this study.

(1) At low quality, the evaporation heat transfer coefficient increases as vapor quality increases due to domination of nucleate boiling. But, at high quality, the heat transfer coefficient has a tendency to decrease with quality. It is because surface tension and viscosity of CO_2 is far smaller than those of conventional refrigerants so that the liquid film covering inside tube breaks down easily.

(2) The characteristics of convective boiling of CO_2 are different from those of conventional refrigerants in many aspects. The heat transfer coefficients of CO_2 are greater than those of CFCs and HCFCs refrigerants by 2~3 times. Generally, the evaporation heat transfer coefficient of conventional refrigerants increases with vapor quality, but the heat transfer coefficient of CO_2 decreases with vapor quality. Besides, the liquid film dryout of CO_2 occurs at moderate quality, which was not observed in the evaporation process of conventional refrigerants. Smaller surface tension of CO_2 makes nucleate boiling more active, and the value of ρ_v/ρ_l significantly affects on liquid film thickness and liquid film dryout. High thermal conductivity and low viscosity of CO_2 also yield a higher

evaporation heat transfer coefficient.

(3) The measured pressure drop during evaporation process of CO_2 increases with increased mass flux, and decreases as saturation temperature increases. When comparison between the pressure drop obtained with experimental data and the various existing correlations, the average deviation of Chisholm's correlation(1968), Chisholm's correlation (1983), Jung et al.'s correlation(1989) and Choi Domanski's correlation (1999) are 65.9%, 83.1%, 79.4% and 12.3%, respectively.

(4) In a horizontal tube, the evaporation heat transfer coefficient obtained in the experimental data of CO_2 was compared with the several existing pressure drop correlations. The existing correlations for heat transfer coefficient underestimated the experimental data because of the different flow pattern of CO_2. Jung et al.'s correlation shows an agreement to experimental data.

(5) As mentioned in earlier, a comprehensive studies related to evaporation heat transfer were carried out experimentally, including heat transfer and pressure drop during evaporation process of CO_2. The local heat transfer coefficients and pressure drop of CO_2 during evaporation process are greatly dependent on both the local mean temperature, heat flux and saturation temperature because of the thermophysical properties of CO_2 changing drastically during this process. The great variation in

thermophysical properties exists not only along but also perpendicular to fluid flow direction. The effect of the former can be eliminated with small enough dimensional increments in calculating, but that of the latter cannot. In these circumstances, conventional models of the local heat transfer coefficient and pressure drop do not apply. Thus, the new evaporation heat transfer and pressure drop correlation of CO_2 in a horizontal tube should be developed throughout the comprehensively experimental data.

CHAPTER 4
EXPERIMENTAL RESULTS FOR COOLING PROCESS OF CO_2

In the heat rejection of a conventional refrigeration cycle, refrigerant changes from the gas state to the liquid state in the high pressure side heat exchanger so that condensing phenomenon takes place and heat exchanger is called a condenser. During the supercritical heat rejection, refrigerant of CO_2 stays in the gas state without phase changing so that the heat exchanger is called a gas cooler instead of a condenser. Although phase change dose not take place at the supercritical pressures, the thermophysical properties of CO_2 change drastically during the process. In these circumstances, this gas cooling process of a supercritical cycle is of particular interest as it is significantly different from the condensation process in a convention vapor compression cycle. For the design of gas cooler, relatively few investigations have been performed to examine closely local heat transfer coefficients and pressure drop characteristics during heat rejection or heat absorption, and available information is both sparse and scattered. And recent research on CO_2 as a potential alternative refrigerant of HCFCs and CFCs is limited.

The objective of this chapter is to investigate the heat transfer characteristics and pressure drop during the in tube supercritical gas cooling process of CO_2 as a potential alternative refrigerant of R 22 and

R 134a. The gas cooling heat transfer coefficients and pressure drop are measured experimentally, and the main results for the design of gas cooler of CO_2 are presented by analyzing the experimental data.

4.1 HEAT BALANCE OF GAS COOLER

In order to make an accurate measurement of heat exchanger capacity, heat balance between refrigerant and secondary source flow in the gas cooler is examined. In the Fig. 4.1, experimental capacity, Q_{cw}, which was calculated with source water flow rate and enthalpy difference in the inlet and outlet of the gas cooler, was presented in the axis of ordinate and calculated heating capacity, Q_{re}, which was acquired from refrigerant flow rate and enthalpy difference in the inlet and outlet of the gas cooler, was represented in the axis of abscissa.

The symbol, ○, □, △ and ◇ display the mass velocity of CO_2 for 200, 300, 400 and 500 kg/m^{2}s, respectively. As can be seen in Fig. 4.1, Q_{cw} of Eq. (2.2) and Q_{re} of Eq. (2.3) generally match within ±10%, irrespective of mass velocity changes. Energy balance in this study was maintained, thus this energy balance indicated the accuracy of the experiment. All raw data acquired in the experimental apparatus showed a high level of reliability to validate the experimental results.

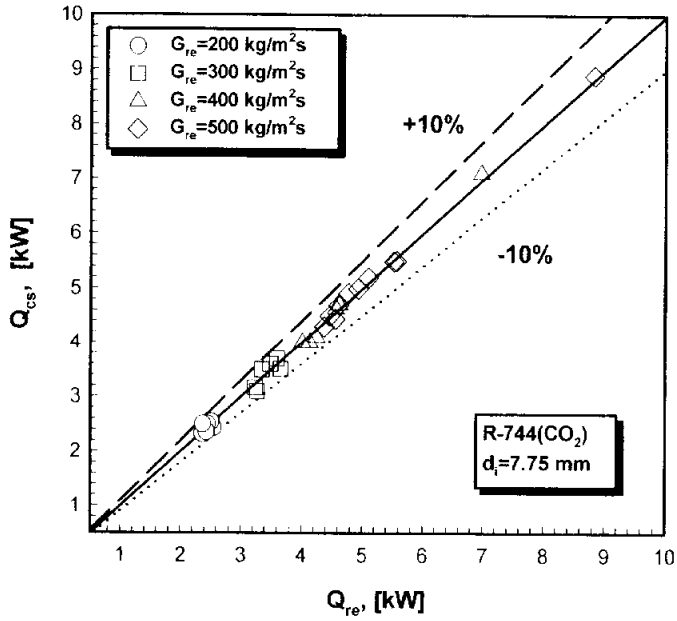

Fig. 4.1 Heat balance between the capacity of CO_2 refrigerant side, Q_{cs}, and that of cooling water, Q_{re}, with respect to varying mass flux.

4.2 COOLING HEAT TRANSFER CHARACTERISTICS

4.2.1 Temperature profile

Fig. 4.2 shows refrigerant temperature, mean wall temperature of inner tube and specific heat measured at the gas cooler of inner diameter of 7.75 mm. The abscissa and ordinate in Fig. 4.2 present dimensionless length and temperature distribution along the gas cooler, respectively. The symbols ●, ○ and ■ in Fig. 4.2 represent refrigerant temperature, T_{re}, mean wall temperature, $T_{w,in}$, and specific heat, c_p, respectively.

As may be observed in Fig. 4.2, CO_2 refrigerant and wall temperature of inner tube shows a tendency to largely decrease, especially at the entrance and exit of gas cooling process. The temperatures of CO_2 refrigerant and inner wall remain almost constant in the middle stage of gas cooler. Because the heat transfer between CO_2 refrigerant and cooling water is activated near the pseudocritical temperature, T_{pc}, at which the specific heat reaches its maximum value, the CO_2 refrigerant and wall temperature does not almost change at the middle stage of gas cooler. The sudden drop in CO_2 refrigerant and wall temperature at the final stage of gas cooling process is most likely caused by the variation of CO_2 state which changes from supercritical CO_2 to liquid state. During cooling process of CO_2, temperature difference between CO_2 refrigerant and inside tube wall has a minimum value at the pseudocritical temperature. This indicates that the heat transfer coefficient of CO_2 is the highest value at the pseudocritical temperature.

As for moderate inlet cooling pressure, the specific heat of CO_2 has a lower value in the early and final stage of gas cooler, and has a higher value in the middle stage of cooling process, like near dimensionless length of 300 to 400. As the CO_2 refrigerant is cooled down in the gas cooler, the maximum specific heat for constant cooling pressure exists in the pseudocritical temperature. As cooling pressure decreases, this maximum specific heat, $c_{p,\max}$, increases and pseudocritical temperature, T_{pc}, decreases. And as mass flux of CO_2 increases at the given pressure of gas cooler, CO_2 temperature rapidly approaches at the pseudocritical point. Therefore, the maximum specific heat presents more in the early stage than in the middle stage of gas cooler. Specific heat has a major effect on heat transfer characteristics for cooling process of CO_2, and it is important factor having a dependant upon cooling heat transfer of CO_2.

Fig. 4.3 depicts the variation of pseudocritical temperature with inlet cooling pressure and corresponding maximum values of specific heat for CO_2 in a supercritical region. The abscissa and ordinate in Fig. 4.3 represent inlet cooling pressure and temperature distribution along the gas cooler, respectively. The symbols ● and ○ represent pseudocritical temperature, T_{pc}, with respect to pressure and corresponding maximum values of specific heat for CO_2 in the supercritical region, respectively.

Based on NIST Refrigerants Database (REFPROP Version 6.01)[2], the pseudocritical temperature is a function of gas cooling pressure and is expressed by algebraic equation as shown in Eq. (4.1)

$$T_{pc} = -122.6 + 6.124P - 0.1657P^2 + 0.017739P^{2.5} - 0.000560P^3 \quad (4.1)$$

Pseudocritical temperature, T_{pc}, is a temperature at which the specific heat shows its maximum value. Pseudocritical temperature increases with system pressure. Fig. 4.3 depicts that pseudocritical temperature corresponds to the temperature at which measured heat transfer coefficient reaches maximum value for constant pressure. Since the heat transfer coefficient reaches a maximum at the pseudocritical temperature, the maximum will change depending on the operating pressure.

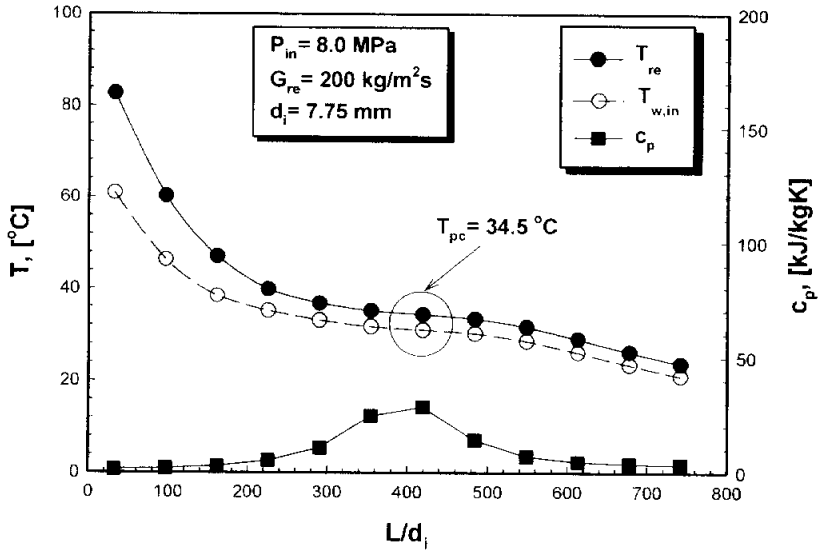

(a) P_{in}-8.0 MPa

Fig. 4.2 Temperature profiles with respect to dimensionless ratio of length to inner diameter tube in the gas cooler (continued).

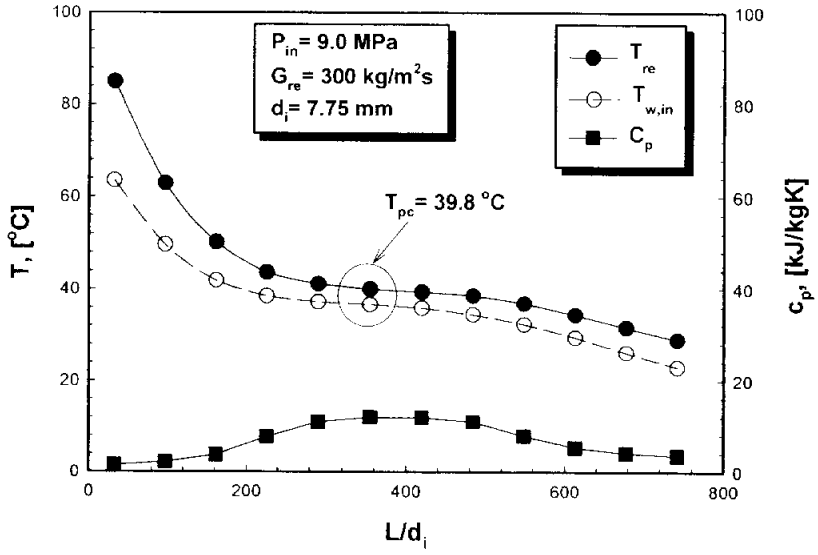

(b) P_{in}=9.0 MPa

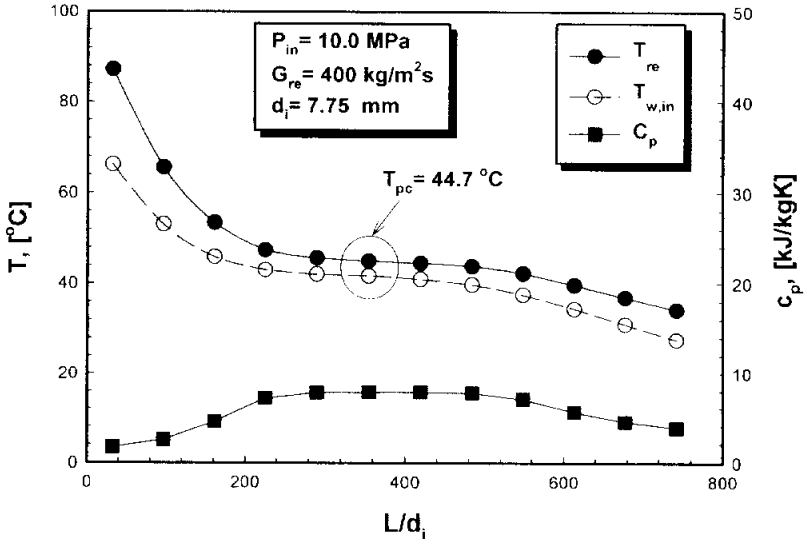

(c) P_{in}=10.0 MPa

Fig. 4.2 Temperature profiles with respect to dimensionless ratio of length to inner diameter tube in the gas cooler.

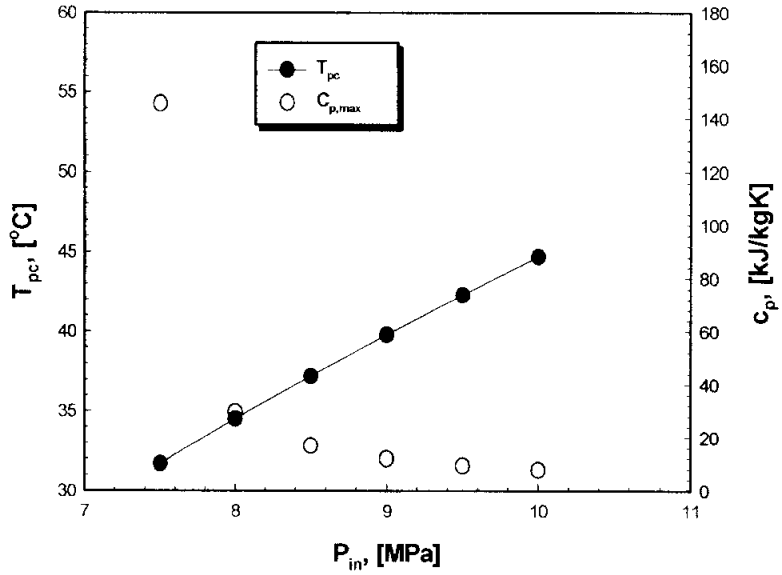

Fig. 4.3 Variation of the pseudocritical temperature with inlet cooling pressure and corresponding maximum values of specific heat for CO_2 in the supercritical region.

4.2.2 Local cooling heat transfer

The local heat transfer coefficients of CO_2 are influenced by refrigerant temperature, inlet pressure of gas cooler and mass velocity of CO_2 during gas cooling process. This gas cooling process of supercritical region is of particular interest as it is significantly different from the condensation process of two phase flow, like vapor and liquid state. For the well planned design of gas cooler in a supercritical cycle, the understanding of heat transfer characteristics of CO_2 during gas cooling process is required.

(1) Influences of refrigerant temperature

During cooling process of CO_2 under moderate system pressure, local heat transfer coefficients with respect to CO_2 refrigerant temperature are shown in Fig. 4.4. As can be seen in Fig. 4.4, the local heat transfer coefficient depends strongly on the CO_2 temperature. This is caused by the significant change of the Prandtl number near the pseudocritical temperature. Local heat transfer coefficients for cooling process show a tendency to increase slowly, have its maximum values near the pseudocritical point, and decrease again.

Because the variation of thermophysical properties with respect to CO_2 temperature is very small in the early and final region of gas cooler, local heat transfer coefficients increase slowly. The local cooling heat transfer coefficients of CO_2 have its peak values in the middle stage of gas cooler, which is mainly due to the higher specific heat of CO_2 in the test section.

Accordingly, during cooling process of supercritical CO_2, it is shown that the thermophysical properties of CO_2, especially like specific heat, have an increasing effect on local heat transfer coefficients.

The thermal conductivity and viscosity also change dramatically near the pseudocritical temperature. However, these effects of transport properties on the heat transfer coefficient of CO_2 are small. When CO_2 temperature is close to the pseudocritical point, the specific heat of CO_2 increases largely, and the Prandtl number, which represents the ratio of diffusion of momentum to the diffusion of heat, has a maximum at the pseudocritical temperature. Hence, the local heat transfer coefficients of supercritical CO_2 increase greatly close to the pseudocritical temperature, and have the maximum at the pseudocritical temperature.

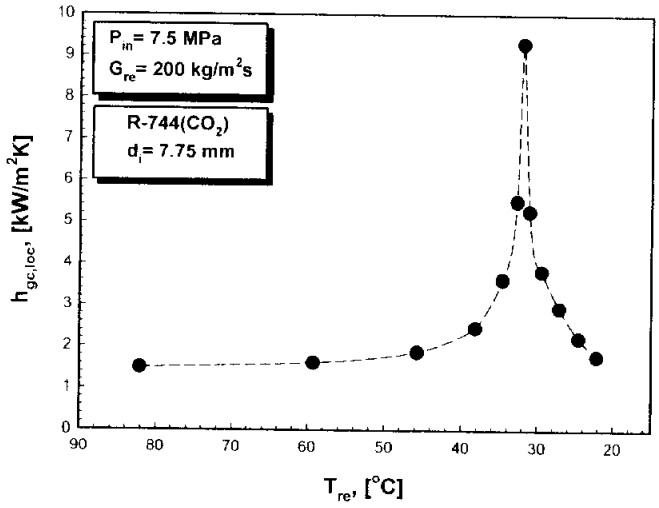

(a) P_{in}=7.5 MPa

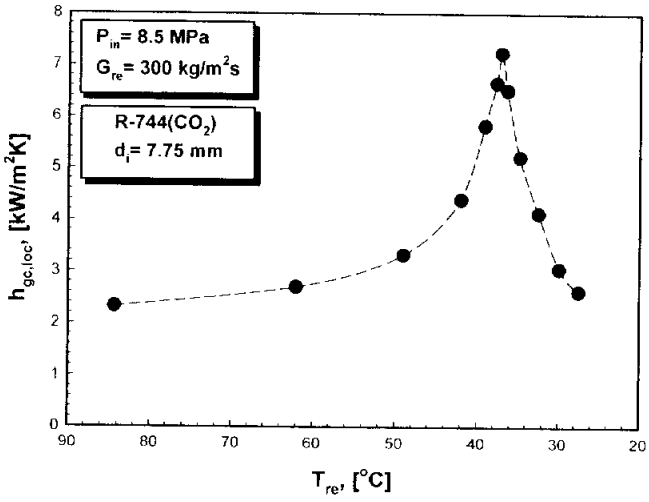

(b) P_{in}=8.5 MPa

Fig. 4.4 Local cooling heat transfer coefficients with respect to CO_2 refrigerant temperature at moderate mass flux and inlet pressure (continued).

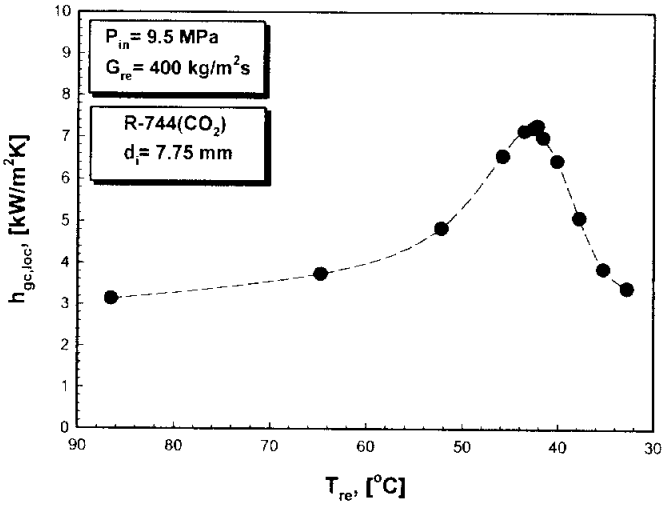

(c) P_{in}=9.5 MPa

Fig. 4.4 Local cooling heat transfer coefficients with respect to CO_2 refrigerant temperature at moderate mass flux and inlet pressure.

(2) Influences of gas cooling pressure

The effect of various cooling pressures on the heat transfer coefficient of CO_2 during gas cooling process should be considered. Fig. 4.5 shows the local heat transfer coefficient of CO_2 for varying pressures as CO_2 temperature changes along the gas cooler for a fixed mass flux. As seen in Fig. 4.5, thermophysical properties don't change very much at the early stage of gas cooling, where the CO_2 temperature are high, and the change of heat transfer coefficient is very small at this stage. It has a tendency to decrease as gas cooling pressure increases at this stage.

However, in the middle stage of cooling process, where the CO_2 temperature is close to the critical temperature. The heat transfer coefficient changes very much for the pressure variation when the refrigerant temperature of CO_2 is at the pseudocritical one. As the CO_2 gas is cooled down and varies from supercritical state to liquid state in the final stage of gas cooler. A variety of inlet pressures have little effect on the variation of thermophysical properties. Accordingly, the change in heat transfer coefficients of CO_2 is also very small, and it has a tendency to increase as gas cooling pressure increases at this stage.

As can be seen in Fig. 4.5, as for the same mass flux of CO_2, when cooling pressure in the gas cooler tube is 7.5 MPa, the maximum of local heat transfer coefficient comes out in the final stage of gas cooler, and when gas cooling pressure is 10.0 MPa, the maximum presents in the middle stage of cooling pressure. This is because pseudocritical temperature of CO_2 becomes lower as decreasing inlet pressure of gas

cooler, CO_2 temperature approaches quickly at the pseudocritical temperature. And because pseudocritical temperature is high as increasing inlet pressure of gas cooler, CO_2 temperature reaches slowly at the pseudocritical one. For the same mass velocity of CO_2, when cooling pressure is 7.5 MPa, the maximum of the local heat transfer coefficient for pressure variations is highest, and when gas cooling pressure is 10.0 MPa, the maximum for pressure variations is lowest. As shown in Fig. 4.4, when cooling pressure is 7.5 MPa, pseudocritical temperature is 31.7℃, and the maximum specific heat is 145.7 kJ/kgK. When gas cooling pressure is 10.0 MPa, pseudocritical temperature is 44.7℃, and the maximum specific heat is 7.9 kJ/kgK. Therefore, as the CO_2 refrigerant temperature approaches the pseudocritical value, the heat transfer coefficient increases strongly. And this maximum will change depending on inlet pressure of CO_2. Namely, For the same mass flow rate, the maximum of the heat transfer coefficient becomes considerably smaller at higher pressures.

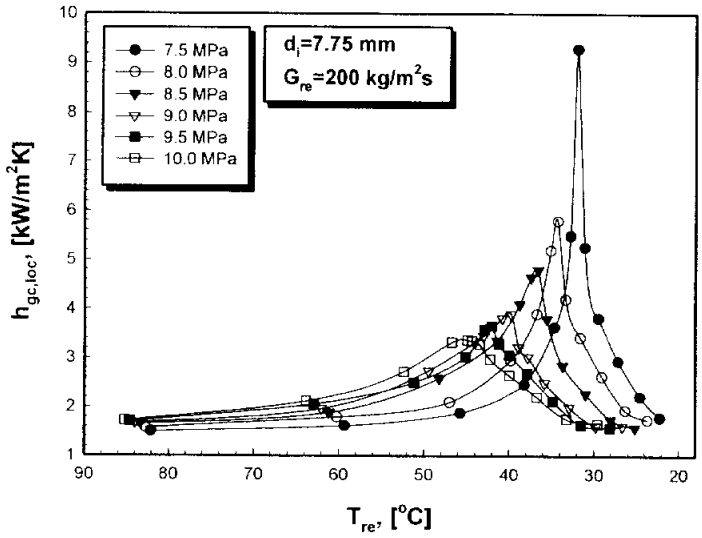

(a) G_{re}=200 kg/m^{2}s

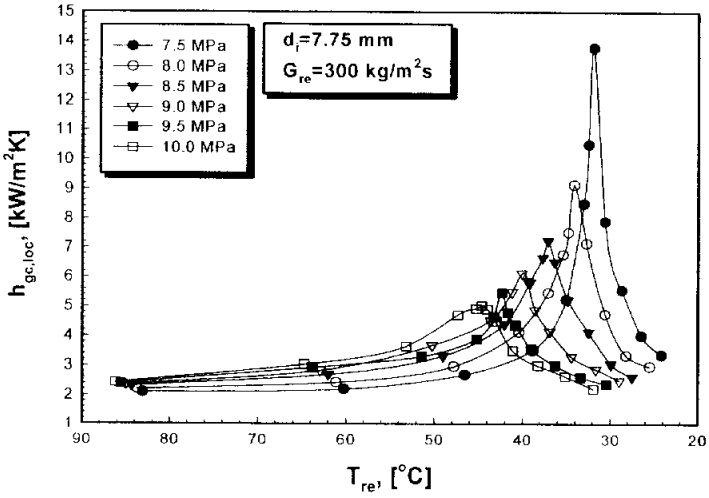

(b) G_{re}=300 kg/m^{2}s

Fig. 4.5 Heat transfer coefficients versus bulk temperature distribution along the gas cooler for different inlet pressures at a constant mass flux condition (continued).

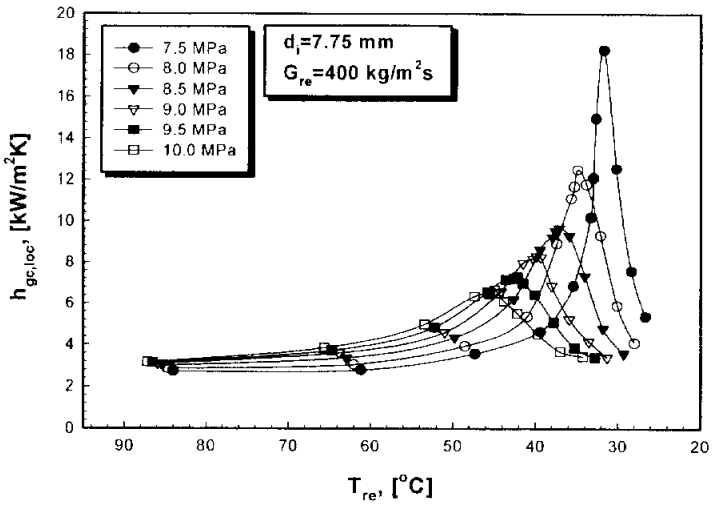

(c) G_{re}=400 kg/m^{2}s

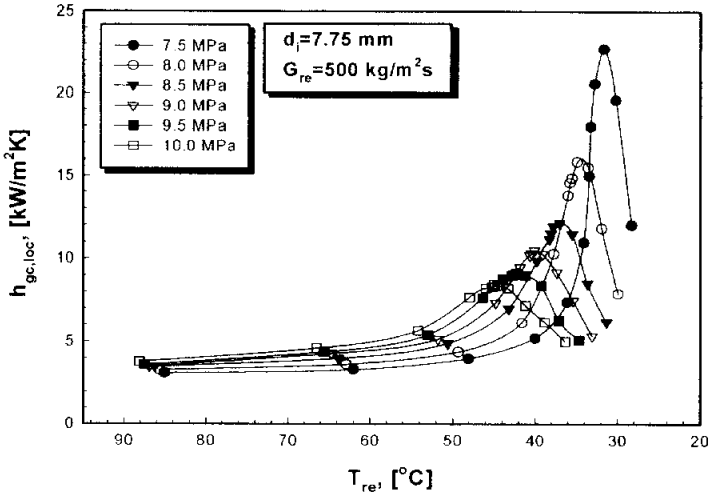

(d) G_{re}=500 kg/m^{2}s

Fig. 4.5 Heat transfer coefficients versus bulk temperature distribution along the gas cooler for different inlet pressures at a constant mass flux condition.

(3) Influences of mass flux

For constant pressure of gas cooler, the local heat transfer coefficients with respect to the variation of mass flux are shown in Fig. 4.6. For all pressures, the increase in the heat transfer coefficient of CO_2 is obtained for increased mass flux, which corresponds to higher Reynolds number. For the moderate pressure of gas cooler, the increase of heat transfer coefficient with the mass flux obviously appears at the pseudocritical temperature. Because of large variation of thermophysical properties near the pseudocritical temperature, the heat transfer coefficient as increasing mass flux is highest at the inlet pressure of 7.5 MPa, and presents the lowest value at the cooling pressure of 10.0 MPa.

As presents in Fig. 4.6, for the given pressure of supercritical gas cooler, the local heat transfer coefficients of CO_2 with respect to mass velocity show the peak values at the pseudocritical temperature of 34.5℃, 39.8℃ and 44.7℃, respectively. The heat transfer coefficient above this temperature has a tendency to increase, and decreases below the pseudocritical temperature. In the early stage of gas cooling, mass flux difference has less effect on the variation of heat transfer coefficients near the upstream, however it has a great influence on the variation of heat transfer coefficient at the downstream.

Under this circumstances, according to Mori et al.[23]'s results, at higher than pseudocritical temperature, the thermal conductivity in liquid film varies much more than the thickness of the viscous sublayer. Therefore, the decrease in the thermal conductivity dominates and the heat transfer

coefficient of CO_2 decreases. Below this temperature, the thickness of the viscous sublayer varies much more than the thermal conductivity in liquid film. Hence, the observed increase in the heat transfer coefficient in this temperature range will largely be due to the decrease in heat resistance that occurs with a decrease in the thickness of viscous sublayer.

Mori et al. conducted the experimental study to examinate the cooling heat transfer characteristics of CO_2 at a supercritical pressure. As the CO_2 flow was turbulent under most conditions examined in their study, the flow in the tube wall was divided into two concentric layers ; a viscous sublayer near the tube wall and a turbulent layer in the core of the tube. The flow is sufficiently turbulent in the core region to consider the temperature to be uniform. Heat transfer in the system is then associated with heat conduction in the viscous sublayer.

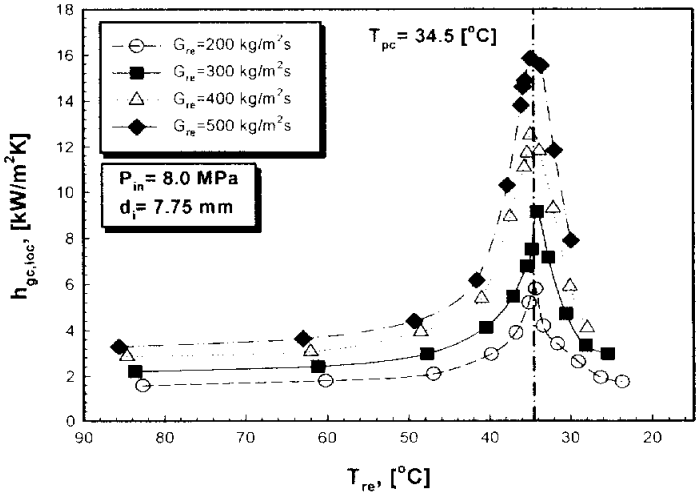

(a) P_{in}=8.0 MPa

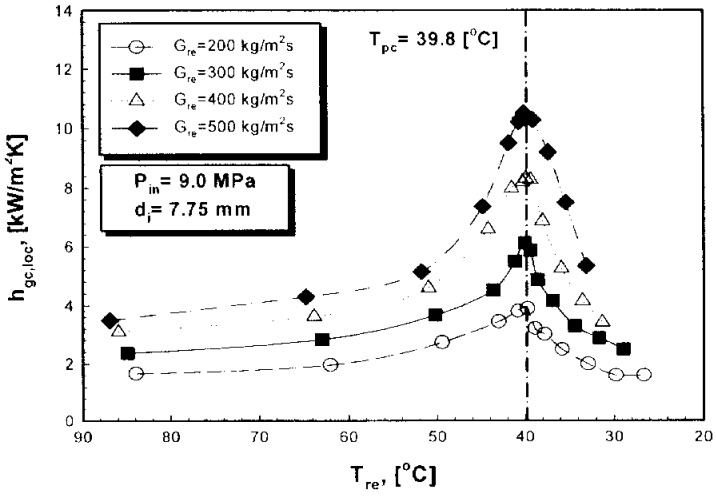

(b) P_{in}=9.0 MPa

Fig. 4.6 Heat transfer coefficients versus bulk temperature distribution along the gas cooler for different mass fluxes at a constant inlet pressure condition (continued).

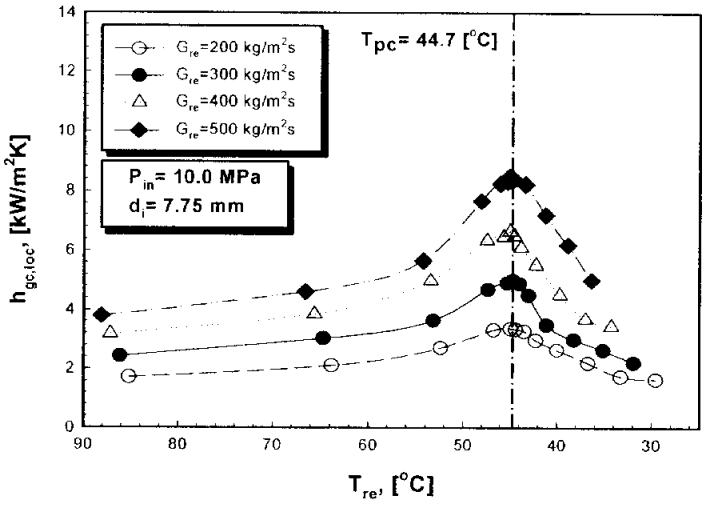

(c) P_{in}=10.0 MPa

Fig. 4.6 Heat transfer coefficients versus bulk temperature distribution along the gas cooler for different mass fluxes at a constant inlet pressure condition.

4.2.3 Mean cooling heat transfer

Fig. 4.7 presents the mean heat transfer coefficient, $h_{gc,avg}$, of supercritical CO_2 in the gas cooler as a function of mass flux, G_{re}, for a fixed pressure. In the Fig. 4.7, for the entire mass flux ranges, the heat transfer coefficient of CO_2 increases linearly with mass flux. This is mainly due to increasing Reynolds number caused by the increasing mass flux of CO_2.

As CO_2 mass flux increases, the mean heat transfer coefficient increases about 338% at 7.5 MPa, and it increases about 262% at 10.0 MPa. As the mass flux varies from 200 to 500 kg/m^{2}s, the total mean heat transfer coefficient of CO_2 increases about 298% for the total mass velocity ranges.

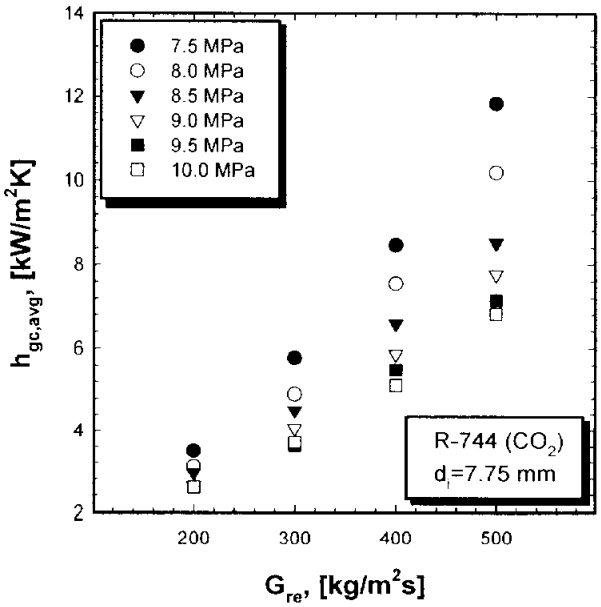

Fig. 4.7 Average heat transfer coefficients with respect to CO_2 mass fluxes at inlet pressure of P_{in}=8.0 to 10.0 MPa.

4.3 PRESSURE DROP

4.3.1 Pressure drop during gas cooling process

The measured pressure drop between the inlet and outlet of the gas cooler was observed less than 1 kPa/m throughout the tests. Fig. 4.8 shows the measured pressure drop with respect to mass flux at the test conditions of the mass velocity of 200 to 500 kg/m^{2}s and the inlet pressure of 7.5 to 10.0 MPa. As can be seen in the Figure, the pressure drop of CO_2 for moderate inlet pressure increases with CO_2 mass flux, and the pressure drop of supercritical CO_2 has a tendency to decrease if the system pressure increases at given mass flux. As the mass flux increases, pressure drop is increased at a high rate in the lower pressure of cooling process. This is because CO_2 density is increased if the system pressure is higher. The measured pressure drop decreases if the density increases at a given mass flux as shown in Eq. (4.3). In general, the pressure drop of CO_2 has a tendency to decrease from inlet of gas cooler to outlet. Especially, because the CO_2 state in gas cooler varies from supercritical CO_2 to liquid state, the pressure drop hardly change hardly in the final stage of gas cooler.

The frictional pressure drop for fully developed turbulent single phase flow in a smooth tube is shown in Eq. (4.2) ;

$$\Delta P = f \cdot \frac{L}{d_i} \cdot \frac{\rho_{re}\, u_m^2}{2} \tag{4.2}$$

where u_m is the mean velocity of the CO_2 flow, and it changes a lot as the CO_2 is cooled, it is better to rewrite this equation as

$$\Delta P = f \cdot \frac{L}{d_i} \cdot \frac{G_{re}^2}{2\,\rho_{re}} \tag{4.3}$$

In Eq. (4.3), L is the total length of test section and d_i is the inner diameter of gas cooler tube. ρ_{re} is the CO_2 density, G_{re} is the mass flux of CO_2 and ΔP is the measured pressure drop in this study.

4.3.2 Pressure drop correlations of cooling process

Strictly speaking, the flow pattern of CO_2 in a supercritical region is not only two phase flow of vapor and liquid state but also single phase of vapor state. But, since the flow pattern of CO_2 in the supercritical region is somewhat similar to conventional single phase flow, the transcritical region also belongs to the single vapor phase region. Thus, it is reasonable that the supercritical CO_2 pressure drop has to be compared with single phase pressure drop correlations.

Therefore, Blasius[53]'s equation(1911) is most widely used for the turbulent flow in smooth tubes, Petrov and Popov[19]'s equation is most recently proposed for cooling process of supercritical CO_2. The experimental data in this study was compared with the prediction by their correlations and confirmed this applicable possibility of their correlations.

(1) Blasius's correlation[43]

Blasius's correlation(1911) is most widely used for the turbulent and laminar flow in a smooth tube as shown in Eq. (4.4).

$$f=\begin{cases}0.316Re^{-1/4} & \text{for} \quad Re\leq 2\times 10^{4}\\ 0.184Re^{-1/5} & \text{for} \quad Re>2\times 10^{4}\end{cases} \tag{4.4}$$

Fig. 4.9 displays the comparison of measured pressure drop data with those predicted by Blasius's equation. As can be seen in Figure, the pressure drop predicted by Blasius's correlation is underestimated with experimental data, and most of the experimental data predicted well within the accuracy of 10%. The mean deviation of the measured pressure drop and predicted pressure drop by correlation is 4.6%.

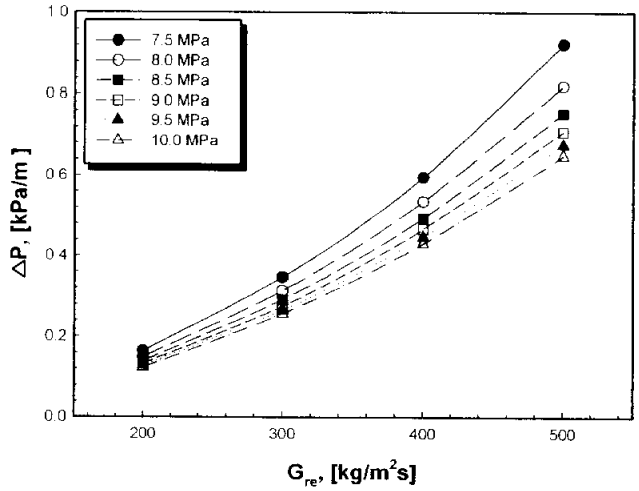

Fig. 4.8 Variation of the pressure drop with respect to varying mass flux at different inlet pressures during gas cooling process.

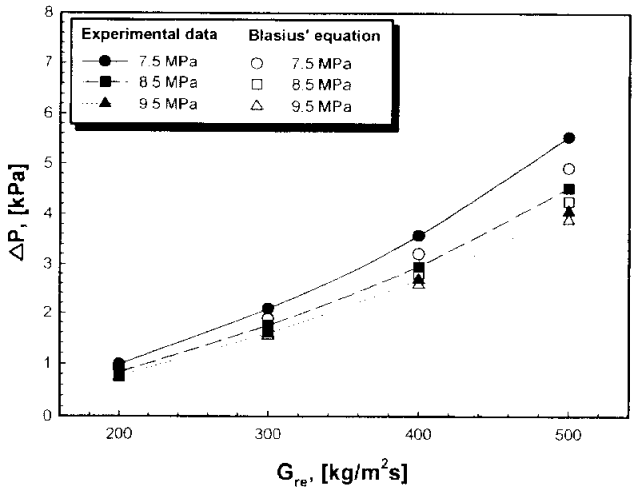

Fig. 4.9 Comparison of the measured pressure drop data with those predicted by Blasius's correlation (1911).

(2) Petrov and Popov's correlation[19]

Petrov and Popov(1985) proposed for the correlation of friction factor of CO_2 cooled in supercritical conditions in the range of $1.4\times10^4 \leq Re_w \leq 7.9\times10^5$. They obtained an interpolation equation of the friction factor.

$$f = f_{ow}\frac{\rho_w}{\rho_b}\left(\frac{\mu_w}{\mu_b}\right)^s \tag{4.5}$$

where f_{ow}, which is the friction factor at constant thermophysical properties, is calculated by Eq. (4.6) at tube wall temperature, T_w, and s is a function of heat flux and mass velocity calculated by Eq. (4.7).

$$f_{ow} = (1.82\ \log Re_w - 1.64)^{-2} \tag{4.6}$$

$$s = 0.023\left(\frac{|q|}{G_{re}}\right)^{0.42} \tag{4.7}$$

where ρ_w, ρ_b, μ_w and μ_b are the density and viscosity at tube wall temperature, T_w, and bulk temperature of CO_2, respectively. Re_w is the Reynolds number at tube wall temperature, T_w.

Fig. 4.10 presents the comparison of the measured pressure drop data with those predicted by Petrov and Popov(1985)'s correlation. As shown in the Figure, the pressure drop predicted by their correlation is higher than the measure pressure drop. The average deviation between the measured pressure drop and Petrov and Popov(1985)'s correlation is -64%, and mean deviation is 64%. This is because their numerical suggestion is not based on the sufficient set of experimental data.

As summarized above mentioned results, the pressure drop during cooling process of supercritical CO_2 in a horizontal tube shows relatively

good agreement with that predicted by Blasius's equation. Hence, based on the above comparison, Blasius's correlation is recommended for use in the supercritical CO_2 state.

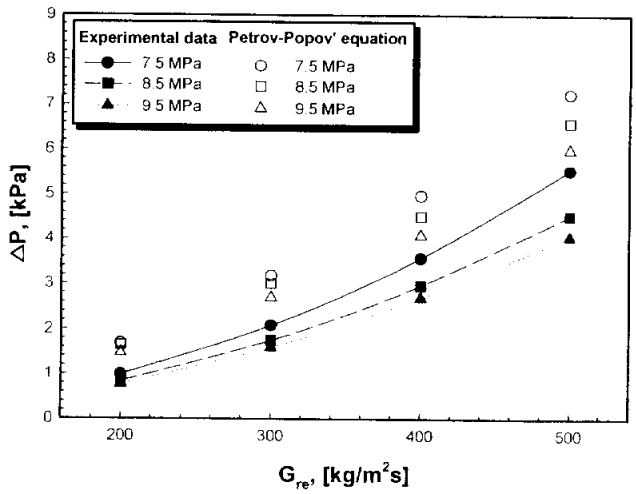

Fig. 4.10 Comparison of the measured pressure drop data with those predicted by Petrov-Popov's correlation (1985).

4.4 COMPARISON OF EXPERIMENTAL DATA AND EXISTING CORRELATIONS

An accurate correlation is required to examinate cooling heat transfer characteristics of CO_2 in the supercritical region. Various correlations which are based on the results of investigator[18,19,54,55,56] have been proposed. Some researchers developed correlations in the heating condition, and the others developed correlations in the cooling condition. In spite of the different conditions, the forms of developed correlations are very similar. To perform a comparative study for the experimental data and proposed correlations, this chapter presents the heat transfer correlations of CO_2 for both heating and cooling conditions near the critical region in a smooth tube.

4.4.1 Correlations for cooling heat transfer

(1) Bringer and Smith's correlation[55]

For cooling process of CO_2 in the supercritical region, various correlations based on the results of each investigator have been produced. Among them, Bringer and Smith(1957) proposed a correlation for forced convection near the critical region based on their experimental results. Their correlation is a form of Dittus Boelter's single phase heat transfer correlation as shown in Eq. (4.8), and a function of Reynolds number and Prandtl number that is calculated based on thermophysical properties of wall temperature.

$$Nu_b = 0.0375\, Re_x^{0.77} \mathrm{Pr}_w^{0.55} \tag{4.8}$$

where Re_x is Reynolds number at the reference temperature, and Pr_w is Prandtl number at the wall temperature.

$$Pr_w = \frac{\mu_w \cdot c_{pw}}{k_w}, \quad Re_x = \frac{\rho_x \cdot u_m \cdot d_i}{\mu_x} \tag{4.9}$$

as stated in above, T_x is determinated according to the following conditions :

$$T_x = \begin{cases} T_b & \text{for } (T_{pc} - T_b)/(T_w - T_b) < 0 \\ T_{pc} & \text{for } 0 \le (T_{pc} - T_b)/(T_w - T_b) < 0 \\ T_w & \text{for } (T_{pc} - T_b)/(T_w - T_b) > 0 \end{cases} \tag{4.10}$$

where T_{pc}, T_b and T_w are pseudocritical temperature, bulk temperature and wall temperature, respectively.

(2) Petukhov et al.'s correlation[57]

Based on their experimental results for the heating of supercritical CO_2 in tube flows, Petukhov et al.(1961) developed a correlation for determining the Nusselt number. To account for the variation of thermophysical properties, they introduced the enhancement parameter which is the ratio of thermophysical property estimated by bulk and wall temperature. They considered the variation of conductivity and viscosity ratio as transport properties, and the variation of specific heat ratio as thermodynamics properties. Based on their experimental data(307 points), they determinated the coefficients of Eq. (4.11).

$$Nu_b = Nu_b' \left(\frac{\mu_b}{\mu_w}\right)^{0.11} \left(\frac{k_b}{k_w}\right)^{-0.33} \left(\frac{\overline{c_p}}{c_{p,b}}\right)^{0.35} \tag{4.11}$$

where μ_b, μ_w, k_b and k_w are the viscosity and conductivity calculated from bulk and wall temperature, respectively. $c_{p,b}$ is the isobar specific heat evaluated by bulk temperature of CO_2. Nu_b' is calculated using the Petukhov and Kirillov's correlation[58].

$$Nu_b' = \frac{f_b/8 Re_b \mathrm{Pr}_b}{12.7\sqrt{(f_b/8)} \cdot (\mathrm{Pr}_b^{2/3} - 1) + 1.07} \tag{4.12}$$

where the friction factor, f_b, is calculated with the correlation proposed by Eq. (4.13) and $\overline{c_p}$ is the integrated mean specific heat calculated from Eq. (4.14).

$$f_b = [1.82 \log(Re_b) - 1.64]^{-2} \tag{4.13}$$

$$\overline{c_p} = \frac{i_b - i_w}{T_b - T_w} \tag{4.14}$$

where Re_b and Pr_b are calculated by using the properties evaluated by bulk and wall temperature, respectively. i_b and i_w are the enthalpy of bulk and wall temperature in [kJ/kg], and T_b and T_w are the bulk and wall temperature in [K], respectively.

$$Re_b = \frac{\rho_b \cdot u_m \cdot d_i}{\mu_b}, \quad Pr_b = \frac{\mu_b \cdot c_{p,b}}{k_b} \tag{4.15}$$

where ρ_b is the density estimated by bulk temperature and u_m is the mean velocity of CO_2 in [m/s].

(3) Krasnoshchekov and Protopopov's correlation[30]

Kransnoshchekov and Protopopov(1966) conducted an experimental study

Table 4.1 Coefficients A_1 and A_2 in Petuhkov Kirillov's equation

Authors	$Nu=\frac{(f/8)\cdot Re\cdot \mathrm{Pr}}{A_1+A_2\sqrt{(f/8)}(\mathrm{Pr}^{2/3}-1)}$			
Petuhkov-Kirillov(1958)	A_1	A_2	Re	Pr
	1.07	12.7	$10^4\sim5\times10^6$	0.5~200
Petuhkov-Popov(1963)	A_1	A_2	Re	Pr
	$1+3.4f$	$11.7+\frac{1.8}{\mathrm{Pr}^{1/3}}$	$10^4\sim5\times10^6$	0.5~200
Petuhkov-Kurganov-Gladuntsov (1973)	A_1	A_2	Re	Pr
	$10.7+\frac{900}{Re}-\frac{0.63}{1+10\mathrm{Pr}}$	12.7	Fully developed turbulent flow	$0.7\sim5\times10^6$

to investigate the heat transfer coefficient of supercritical CO_2 in a horizontal tube during heating, as did Petukhov et al.(1961). These authors observed that the changes in the thermophysical properties over the cross section of the tube are great and hence Eq. (4.17), which does not consider any variations in the thermophysical properties in the cross section of the tube, cannot be used. they assumed that, in the supercritical region, the Nusselt number is a function of the Reynolds number and Prandtl number, just as it is in single phase region. The variation of the thermophysical properties in the cross section of the tube were taken into account by introducing correlation factors for density and specific heat ratio. They proposed the correlations :

$$Nu_b=Nu_b'\left(\frac{\rho_w}{\rho_b}\right)^{0.3}\left(\frac{\overline{c_p}}{c_{p,b}}\right)^n \tag{4.16}$$

where Nu_b' is the Nusselt number which is calculated by using Eq. (4.17)

and $\overline{c_p}$ is the mean specific heat calculated with Eq. (4.18). f is the friction factor calculated from Eq. (4.19).

$$Nu_b' = \frac{f/8 Re_b \mathrm{Pr}_b}{12.7\sqrt{(f/8)} \cdot (\mathrm{Pr}_b^{2/3} - 1) + 1.07} \tag{4.17}$$

$$\overline{c_p} = \frac{i_b - i_w}{T_b - T_w} \tag{4.18}$$

$$f_b = [1.82 \log(Re_b) - 1.64]^{-2} \tag{4.19}$$

The exponent n is prescribed as follows :

$$n = \begin{cases} 0.4 & \text{for } T_w/T_{pc} \le 1 \text{ or } T_b/T_{pc} \ge 1.2 \\ b_1 = 0.22 + 0.18(T_w/T_{pc}) & \text{for } 1 \le T_w/T_{pc} \le 2.5 \\ b_1 + (5b_1 - 2)(1 - T_b/T_{pc}) & \text{for } 1 \le T_b/T_{pc} \le 1.2 \\ 0.7 & \text{for } T_b/T_{pc} \le 1 \text{ and } T_b/T_w < 1 \end{cases} \tag{4.20}$$

where T_{pc}, T_b and T_w are the pseudocritical temperature, bulk temperature and wall temperature, respectively.

(4) Krasnoshchekov et al.'s correlation[60]

Krasnoshchekov et al.(1970) carried out an experimental study of the heat transfer characteristics during turbulent flow in a round tube with CO_2 at supercritical pressures under cooling conditions. They proposed the following correlation :

$$Nu_w = Nu_w' \left(\frac{\rho_w}{\rho_b}\right)^n \left(\frac{\overline{c_p}}{c_{p,w}}\right)^m \tag{4.21}$$

where in Eq. (4.20), Nu_w' is calculated by using the Petukhov and Kirillov's correlation. The exponent m and $\overline{c_p}$ are calculated by using Eq.

(4.23), respectively.

$$Nu_w = \frac{f_w/8 Re_b \mathrm{Pr}_b}{12.7\sqrt{(f_w/8)} \cdot (\mathrm{Pr}_b^{2/3} - 1) + 1.07} \tag{4.22}$$

$$\overline{c_p} = \frac{i_b - i_w}{T_b - T_w}, \quad m = B\left(\frac{\overline{c_p}}{c_{p,w}}\right)^J \tag{4.23}$$

where f_w is the Blasius[53]'s and Filonenko[61]'s correlation calculated with Eq. (4.24) and (4.25).

$$f_w = 0.316 Re_w^{-1/4} \qquad \text{for} \quad (Re_w \leq 10^5) \tag{4.24}$$

$$f_w = [0.79 \ln(Re_w) - 1.64]^{-2} \qquad \text{for} \quad (1\times10^4 \leq Re_w \leq 5\times10^5) \tag{4.25}$$

where n, B and J are the constants determinated by the pressure ratio in P_b/P_{cp} and specific heat ratio in $c_{p,i}/c_{p,w}$.

$$n = \frac{-48.3865106}{(P_b/P_{cp})} - 184.4985 \log(P_b/P_{cp}) + 48.5062915(P_b/P_{cp}) \tag{4.26}$$

$$B = \frac{-9.0586}{(P_b/P_{cp})} - 27.2799 \log(P_b/P_{cp}) + 9.670075\sqrt{(P_b/P_{cp})} \tag{4.27}$$

$$J = -9.4638845\times10^{-6}(P_b/P_{cp})^{15} + \frac{0.24072314}{(P_b/P_{cp})^6} + \frac{0.098613245}{(P_b/P_{cp})^{15}} \tag{4.28}$$

where P_b represents the gas cooling pressure in [MPa] and P_{cp} is the critical pressure in 7.38 [MPa]. Table 4.2 shows the value for n, B and J. Fig. 4.11 displays Exponents and coefficients in supercritical heat transfer correlations formulas developed by Protopopov research group.

(5) Baskov et al.'s correlation[56]

Baskov et al.(1977) experimentally investigated the variation of local heat

Table 4.2 Values for n, B and J in Krasnoshchekov et al.'s equation

Pressure, [MPa]	8.0	10.0	12.0
n	0.38	0.38	0.80
B	0.75	0.97	1.00
J	0.18	0.04	0

transfer coefficients at high Reynolds numbers in cooling conditions and found no appreciable influence of free convective heat transfer. They compared the value of Nu_w using the correlation shown in Eq. (4.21) and found that their experimental value of Nu_w was lower. They concluded that the correlation proposed by Krasnoshchekov et al.(1966) was for horizontal tubes and that it was not valid for their experiment that used a vertical tube. Therefore, they proposed the following new correlation for vertical tubes :

$$Nu_w = Nu_w' \left(\frac{\overline{c_p}}{c_{p,w}} \right)^m \left(\frac{\rho_b}{\rho_w} \right)^n \tag{4.29}$$

where $c_{p,w}$ is the isobar specific heat at the wall temperature. ρ_b and ρ_w are the density of CO_2 at the bulk and wall temperature, respectively. Nu_w' is the Nusselt number that is evaluated, based on the thermophysical properties at the wall temperature. The Petukhov Kurganov Gladuntsov[62], as shown in Eq. (4.30), is used to calculate the Nusselt number.

$$Nu_w' = \frac{(f_w/8) Re_w \mathrm{Pr}_w}{1.07 + \frac{900}{Re_w} - \frac{0.63}{1+10\mathrm{Pr}_w} + 12.7\sqrt{(f_w/8)} \cdot (\mathrm{Pr}_w^{2/3} - 1)} \tag{4.30}$$

where

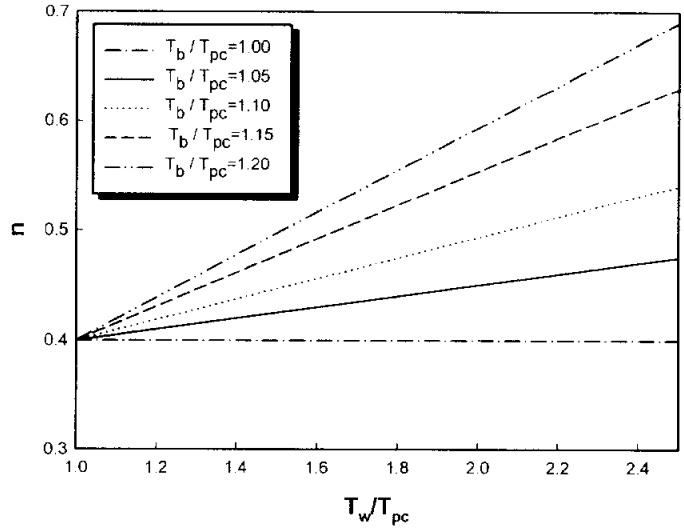

(a) The exponent n in Eq. (4.22)

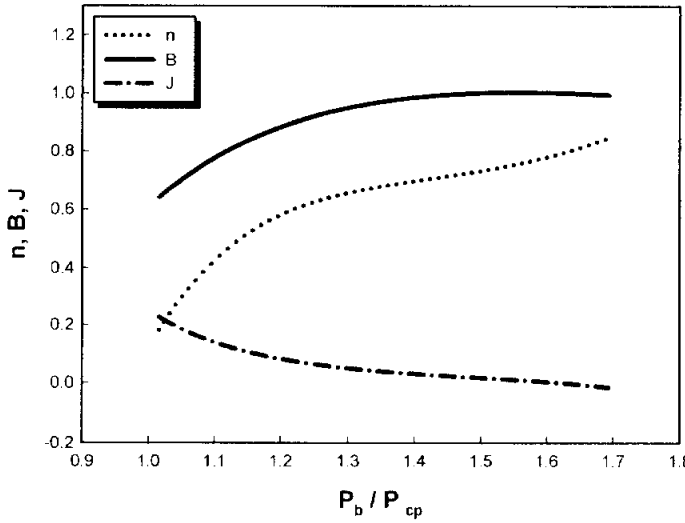

(b) Exponent and coefficient in Eq. (4.26) ~ Eq. (4.28)

Fig. 4.11 Exponents and coefficients in supercritical heat transfer correlations formulas developed by Protopopov research group.

$$Re_w = \frac{\rho_w \cdot u_m \cdot d_{in}}{\mu_w}, \quad Pr_w = \frac{\mu_w \cdot c_{p,w}}{k_w}, \quad \overline{c_p} = \frac{i_b - i_w}{T_b - T_w} \tag{4.31}$$

in Eq. (4.31), k_w is the conductivity at the wall temperature, $c_{p,w}$ is the isobar specific heat at the wall temperature and u_m is the mean mass flux of CO_2. Re_w and Pr_w are the Reynolds and Prandtl number that are evaluated based on the thermophysical properties of wall temperature, respectively.

$$f_w = [1.82 \log(Re_w) - 1.64]^{-2} \tag{4.32}$$

For $T_b/T_{pc} > 1$, the values of m and n are determinated from Table 4.3 and for $T_b/T_{pc} < 1$, the values are calculated according to the following ones. However, Baskov et al. provided the values of m and n only at pressure P=8.0, 10.0 and 12.0 [MPa]. Therefore, this correlation is difficult to apply in other pressure ranges. The applicable ranges of their correlation are $4 \times 10^3 \leq Re_w \leq 6 \times 10^5$ and $0.7 \leq Pr_w \leq 5 \times 10^5$.

$$m = 1.4, \quad n = 0.15 \qquad \text{for} \quad T_b/T_{pc} \leq 1 \tag{4.33}$$

Table 4.3 Values for m and n in Baskov et al.'s Equation

Parameters	$\overline{c_p}/c_{p,w} > 1$			$\overline{c_p}/c_{p,w} < 1$		
P_b, [MPa]	8.0	10.0	12.0	8.0	10.0	12.0
m	1.2	1.6	1.6	0.45	0.45	0.45
n	0.15	0.10	0	0.15	0.10	0

(6) Petrov and Popov's correlation[19]

Petrov and Popov(1985) numerically solved the governing conservation equation for cooling process of CO_2 in the supercritical region, and

developed the following new correlation :

$$Nu_w = Nu_w' \cdot \left(1 - 0.001\frac{q_w}{G_{re}}\right)\left(\frac{\overline{c_p}}{c_{p,w}}\right)^n \tag{4.34}$$

where Nu_w' is the Nusselt number that is evaluated, based on the thermophysical properties at the wall temperature. The Petukhov and Popov correlation, as shown in Eq. (4.35), is used to calculate the Nusselt number.

$$Nu_w' = \frac{(f_w/8)Re_w \mathrm{Pr}_w}{(1+3.4f_w)+\left(11.7+\frac{1.8}{\mathrm{Pr}^{1/3}}\right)\sqrt{(f_w/8)}\cdot(\mathrm{Pr}_w^{2/3}-1)} \tag{4.35}$$

where f_w is the friction factor that is calculated according to Eq. (4.18), and the exponent n can be calculated from the follow conditions.

$$n = \begin{cases} 0.66 - k(q_w/G_{re}) & \text{for } \overline{c_p}/c_{p,w} \le 1 \\ 0.9 - k(q_w/G_{re}) & \text{for } \overline{c_p}/c_{p,w} > 1 \end{cases} \tag{4.36}$$

where q_w is the heat flux in [kW/m^2], G_{re} is the mean mass flux of CO_2 and k is conductivity ($\sim 4\times10^{-4}$). The correlation can be valid for $1.4\times10^4 \le Re_w \le 7.9\times10^5$, and used within $3.1\times10^4 \le Re_b \le 8\times10^5$.

(7) Ghajar and Asadi's correlation[63]

Ghajar and Asadi(1986) studied some of the correlations that were developed for forced convective heat transfer in the supercritical region. Based on their studied, they proposed the new correlation that combined Petuhkov's correlation with Krasnoshchekov and Protopopov's correlation. Their correlation is a Jackson and Fewster type heat transfer ones. Ghajar

and Asadi came to conclude that the convective heat transfer in the supercritical region can be predicted by a Dittus Boelter type heat transfer correlation that has property ratios to account for the large variations in the physical properties in this region.

$$Nu_b = 0.025\, Re_b^{0.8}\ \mathrm{Pr}_b^{0.417} \left(\frac{\rho_w}{\rho_b}\right)^{0.32} \left(\frac{c_{p,i}}{c_{p,b}}\right)^n \tag{4.37}$$

where $c_{p,i}$ is the integrated mean specific heat and the exponent n can be calculated from the follow conditions.

$$n = \begin{cases} 0.4 & \text{for } T_b < T_w \le T_{cp} \text{ and } 1.2T_{cp} \le T_b < T_w \\ 0.4 + 0.2\left(\frac{T_w}{T_{cp}} - 1\right) & \text{for } T_b \le T_{cp} < T_w \\ 0.4 + 0.2\left(\frac{T_w}{T_{cp}} - 1\right)\left[1 - 5\left(\frac{T_b}{T_{cp}} - 1\right)\right] & \text{for } T_{cp} \le \frac{T_b}{1.2T_{cp}} \text{ and } T_b < 1.2T_w \end{cases}$$

where the applicable range of this correlation is suggested to be in $2\times10^4 \le Re_b \le 12\times10^5$.

(8) Gnielinski's correlation[64]

Gnielinski(1994) has hard studied the heat transfer of CO_2 in the supercritical region. He proposed a new correlation to determine the heat transfer coefficients of supercritical CO_2.

$$Nu_b = \frac{f_w/8 Re_b \mathrm{Pr}_b}{12.7\sqrt{(f_w/8)}\cdot(\mathrm{Pr}_b^{2/3} - 1) + 1.07} \cdot \left[1 + \left(\frac{d_i}{L}\right)^{2/3}\right] \tag{4.38}$$

where L is the length of gas cooler and d_i is the inner diameter tube. f_b is the friction factor according to

$$f_b = [1.82\log(Re_b) - 1.64]^{-2} \tag{4.39}$$

If fluid is the liquid phase, Nusselt number considers the influence of the temperature on the thermodynamic properties. The influence of the temperature on the properties can be taken into account by

$$Nu_b = Nu_b \cdot \left(\frac{\mathrm{Pr}_b}{\mathrm{Pr}_w}\right)^{0.11} \quad \text{for} \quad \text{liquids} \tag{4.40}$$

where Pr_b is the Prandtl number at the average fluid temperature and Pr_w is the Prandtl number of fluid at wall temperature (range of validity $0.1 < \mathrm{Pr}_b/\mathrm{Pr}_w < 10$). Since there is no noticeable influence of temperature on the Prandtl number in the case of gaseous fluids, the influence is taken into account by

$$Nu_b = Nu_b \cdot \left(\frac{T_b}{T_w}\right)^{0.11} \quad \text{for} \quad \text{gases} \tag{4.41}$$

where T_b is the average fluid temperature in [K] and T_w is the wall temperature in [K]. For cooling ($T_b/T_w > 1$), the exponent n is zero, for heating ($1 > T_b/T_w > 0.5$), n depends on the fluid ; for CO_2, n=0.12.

(9) Pitla et al.'s correlation[22]

Pitla et al.(1998) was concerned with developing a suitable heat transfer correlation for CO_2 flow in the supercritical region during in tube cooling. The correlation was developed, based on the numerical and experimental work. Based on the numerical predictions of heat exchanger problem, it was attempted to develop a new correlation for the Nusselt number in terms of other dimensionless parameters. For this purpose, the numerically

predicted Nusselt number was correlated. The final outcome was a new correlation that is based on the " mean Nusselt number" and is defined as shown in equation (4.43).

$$Nu = \left(\frac{Nu_b + Nu_w}{2} \right) \frac{k_w}{k_b} \tag{4.42}$$

where Nu_b is the Nusselt number that is evaluated based on the thermophysical properties at the bulk temperature. The Gnielinski correlation, as shown in Eq. (4.42), is used to calculate the Nusselt number.

$$Nu_b = \frac{f_b/8 Re_b \mathrm{Pr}_b}{12.7\sqrt{(f_b/8)} \cdot (\mathrm{Pr}_b^{2/3} - 1) + 1.07} \tag{4.43}$$

in Eq. (4.43), f_b is the friction factor at the bulk temperature, and is defined as shown in Eq. (4.44).

$$f_b = [1.82 \log(Re_b) - 1.64]^{-2} \tag{4.44}$$

where Nu_w is the Nusselt number that is evaluated, based on the thermophysical properties at the wall temperature. The Gnielinski correlation, as shown in Eq. (4.45), is used to calculate the Nusselt number.

$$Nu_w = \frac{f_w/8 Re_w \mathrm{Pr}_w}{12.7\sqrt{(f_w/8)} \cdot (\mathrm{Pr}_w^{2/3} - 1) + 1.07} \tag{4.45}$$

f_b is the friction factor at the bulk temperature and f_w is defined as shown in Eq. (4.46).

$$f_w = [1.82 \log(Re_w) - 1.64]^{-2} \tag{4.46}$$

Once the mean Nusselt number is obtained, the heat transfer coefficient can be computed as shown in Eq. (4.47).

$$h = \frac{Nu}{d_i} k_b \tag{4.47}$$

(10) Fang's correlation[20]

Based on Gnielinski's correlation and Petrov-Popov's correlation, Fang (1999) obtained the following in-tube heat transfer model of gas cooler throughout the numerical analysis :

$$Nu_w = \frac{(f_w/8)(Re_w - 1000)\,\mathrm{Pr}_w}{A + 12.7(f_w/8)^{1/2}(\mathrm{Pr}_w^{2/3} - 1)} \left(1 - 0.001\frac{q_w}{G}\right)\left(\frac{\overline{c_p}}{c_{p,w}}\right)^n \tag{4.48}$$

where

$$A = \begin{cases} 1 + 7\times 10^{-8} Re_w & \text{for} \quad Re_w < 10^6 \\ 1.07 & \text{for} \quad Re_w \geq 10^6 \end{cases} \tag{4.49}$$

in Eq. (4.49), f_w is the friction factor evaluated at T_w by the following Churchill's equation (4.50) and c_p is calculated by Eq (4.23). n is calculated by Eq. (4.36).

$$f_w = 8\left\{\left(\frac{8}{Re_w}\right)^{12} + \left[\left(2.457\ln\frac{1}{(7/Re_w)^{0.9} + 0.27R_{rt}}\right) + \left(\frac{37530}{Re_w}\right)^{16}\right]^{-3/2}\right\}^{1/12} \tag{4.50}$$

where R_{rt} is the relative roughness of tubes. The experimental range of the Fang's correlation is $3500 \leq Re_w \leq 2.5\times 10^4$ and $115 \leq q_w/G \leq 3$ J/kg.

4.4.2 Comparison of experimental data and correlations

In order to get the correct comparison between measured and correlated data, the mean heat transfer coefficient in the test section had to be calculated for each experiment. Based on the measured inlet and outlet bulk temperature to the test section, the heat transfer coefficient was calculated as the mean value for twelve "subsections" using the above method of correlating heat transfer in each subsection. The local heat transfer coefficients of CO_2 obtained in this study are compared with those generated by Bringer and Smith, Petuhkov et al., Krasnoshchekov et al., Baskov et al., Petrov and Popov, Ghajar and Asadi, Gnielinski, Krasnoshchekov and Protopopov, Pitla et al. and Fang's correlations.

Fig. 4.12 shows the comparison of the experimental heat transfer coefficients with those predicted by the existing correlations for the supercritical CO_2 heat transfer coefficient under cooling conditions. In the early stage of gas cooling, the heat transfer coefficient gradually increases and drastically increases near the critical point. After reaching the maximum peak, the heat transfer coefficient decreases as CO_2 is cooled down. Most of the existing correlations showed a large difference with the experimental data, and the supercritical cooling correlations generally underpredicted the experimental data. In the early and final stage of gas cooling, the deviation of experimental data with predicted data is not larger. However, especially near the critical point, the deviation between experimental data and those predicted by existing correlations is much larger. Because it is the large variations of the viscosity, density and thermal conductivity near the pseudo critical point.

As seen in Fig. 4.12, among the proposed correlations in the supercritical region, Pitla et al.'s correlation(1994) predicted a different peak location. Their correlation is very simple, but failed to consider the change of thermophysical properties of CO_2. This is because they simply averaged the Gnielinski's equation at bulk and wall temperature. Actually, heat transfer coefficient is not equally influenced by the thermophysical properties of the bulk and wall conditions.

The correlations predicted by Petrov-Popov(1985) and Fang(1999) mostly underpredicted the experimental data. Since their correlation is only numerically developed, formula itself is very simple and clear. But their correlation cannot reasonably reflect experimental data, because of the rack of the correlation's connection with experimental data. The correlation by Baskov et al.(1977) generally underpredicted the experimental data. Their correlation has a demerit of its applicably only for the pressure of P=8.0, 10.0, and 12.0 MPa. Bring Smith's correlation(1957) indicates fairly good agreement to the experimental data. Because this correlation is a form of Dittus-Boelter's correlation, the correlation is very simple and clear. But their correlation cannot remarkably reflect the experimental data, because of the rack of the equation to account for the variation of the density and specific heat. The correlations by Krasnoshchekov Protopopov(1966) and Ghajar Asadi(1986) reflect well the effect of thermophysical properties and critical enhancement. But their correlations are very complex and the correlation's conditions do not agree with the experimental data.

The method that compares the heat transfer coefficients obtained

experimental data with those predicted by correlations is the quantitative and qualitative one. The quantitative one is average and mean deviation calculated by Eq. (4.51) and (4.52), respectively. Therefore, based on the present results of CO_2, the deviation between the heat transfer coefficients obtained experimental data and those predicted by correlation is calculated from the following Equations.

$$\sigma_{avg} = \frac{1}{N}\left(\sum_{1}^{N} \frac{h_{\exp} - h_{cal}}{h_{\exp}}\right) \times 100 \tag{4.51}$$

$$\sigma_{abs} = \frac{1}{N}\left(\sum_{1}^{N} \left|\frac{h_{\exp} - h_{cal}}{h_{\exp}}\right|\right) \times 100 \tag{4.52}$$

where N is the total number of measurement. h_{exp} is the measured heat transfer coefficient obtained experimental data and h_{cal} is the local heat transfer coefficient predicted by correlations.

Fig. 4.13 (a) represents the comparison of experimental heat transfer coefficients with those predicted by Bringer and Smith's correlation. For the total range of mass velocity, mean deviation is 29%. Mean deviation is 23.6%, 27.5%, 31% and 33.7% for 200, 300, 400 and 500 kg/m^{2}s, respectively. Fig. 4.13 (b) shows the comparison of experimental heat transfer coefficients with those predicted by Petuhkov et al.'s correlation. For the total range of mass velocity, mean deviation is 45.7%. Mean deviation is 41%, 45%, 52.7% and 54.4% for 200, 300, 400 and 500 kg/m^{2}s, respectively. Fig. 4.13 (c) presents the comparison of experimental heat transfer coefficients with those predicted by Krasnoshchekov and Protopopov's correlation. For the total range of mass velocity, mean

deviation is 49.9%. Mean deviation is 44.3%, 49.5%, 52% and 53.7% for 200, 300, 400 and 500 kg/m^{2}s, respectively. Fig. 4.13 (d) shows the comparison of experimental heat transfer coefficients with those predicted by Krasnoshchekov et al.'s correlation. For the wide range of mass flux, mean deviation is 51.6%. Mean deviation is 47.7%, 51.6%, 52.7% and 54.4% for 200, 300, 400 and 500 kg/m^{2}s, respectively. Fig. 4.13 (e) presents the comparison of experimental heat transfer coefficients with those predicted by Baskov et al.'s correlation. In the total range of mass velocity, mean deviation is 54.6%. Mean deviation is 50.6%, 54.2%, 56% and 57.8% for 200, 300, 400 and 500 kg/m^{2}s, respectively. Fig. 4.13 (f) displays the comparison of experimental heat transfer coefficients with those predicted by Petrov and Popov's correlation. For the total range of mass velocity, mean deviation is 50.9%. Mean deviation is 46.3%, 50.2%, 52.5% and 54.7% for 200, 300, 400 and 500 kg/m^{2}s, respectively. Fig. 4.13 (g) depicts the comparison of experimental heat transfer coefficients with those predicted by Gnielinski's correlation. For the total range of mass velocity, average deviation is 42% and mean deviation is 43.7%. Mean deviation is 34.2%, 44.5%, 47.1% and 49.2% for 200, 300, 400 and 500 kg/m^{2}s, respectively. Fig. 4.13 (h) show the comparison of experimental heat transfer coefficients with those predicted by Pitla et al.'s correlation. For the total range of mass velocity, mean deviation is 36.4%. Mean deviation is 30.3%, 37.7%, 39.3% and 38.5% for 200, 300, 400 and 500 kg/m^{2}s, respectively. Fig. 4.13 (i) presents the comparison of experimental heat transfer coefficients with those predicted by Fang's correlation. For the total range of mass velocity,

mean deviation is 48.7%.

As mentioned in above, when comparing the measured values obtained with experimental data and the predicted values proposed by correlations, the correlation proposed by Bring and Smith agrees quite well with the experimental data within the mean deviation of 23.6%. Table 4.4 shows the average and mean deviation between measured heat transfer coefficients and calculation correlations.

Table 4.4 Deviations between the measured and calculated heat transfer coefficients

Correlations	σ_{avg} and σ_{abs} **(%)**
Bringer and Smith. (1957)	29
Petuhkov et al. (1961)	45.7
Krasnoshchekov and Protopopov. (1996)	49.9
Krasnoshchekov et al. (1970)	51.6
Baskov et al. (1977)	54.6
Petrov and Popov. (1985)	50.9
Gnielinski. (1994)	42, 43.7
Pitla et al. (1998)	36.4
Fang (1999)	48.9

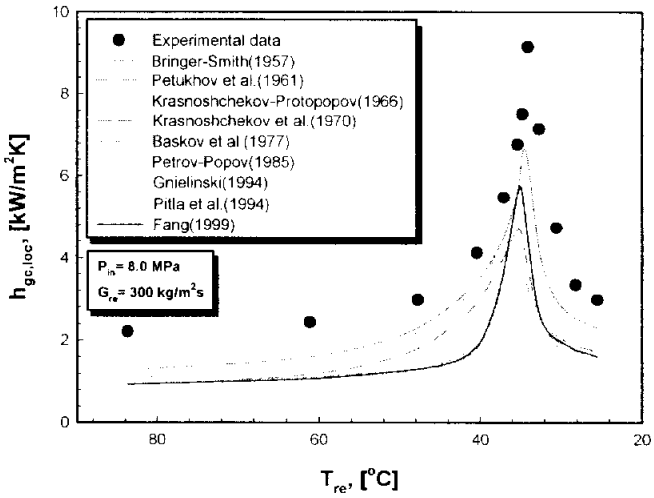

(a) P_{in}=8.0 MPa, G_{re}=300 kg/m^{2}s

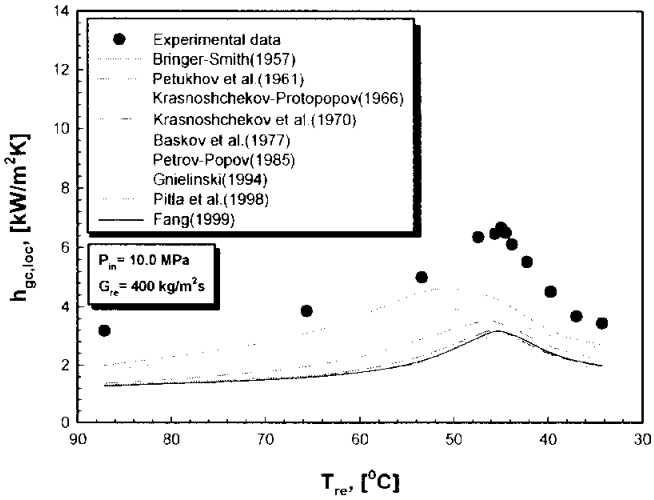

(b) P_{in}=10.0 MPa, G_{re}=400 kg/m^{2}s

Fig. 4.12 Comparison of the experimental data with the calculated heat transfer coefficients using existing correlations as a function of refrigerant temperature.

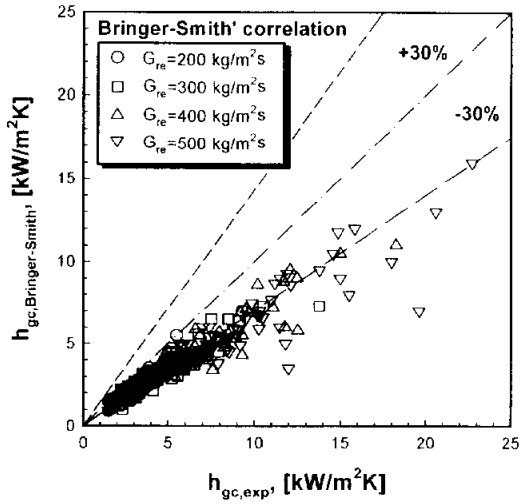

(a) Bringer Smith's correlation(1957)

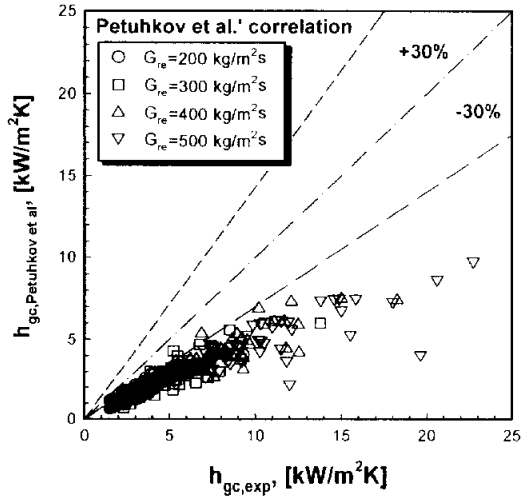

(b) Petuhkov et al.'s correlation(1961)

Fig. 4.13 Comparison between the calculated and measured heat transfer coefficient at varying mass fluxes (continued).

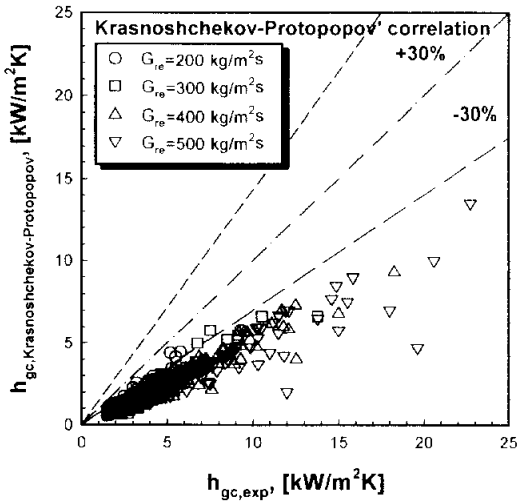

(c) Krasnoshchekov Protopopov's correlation(1966)

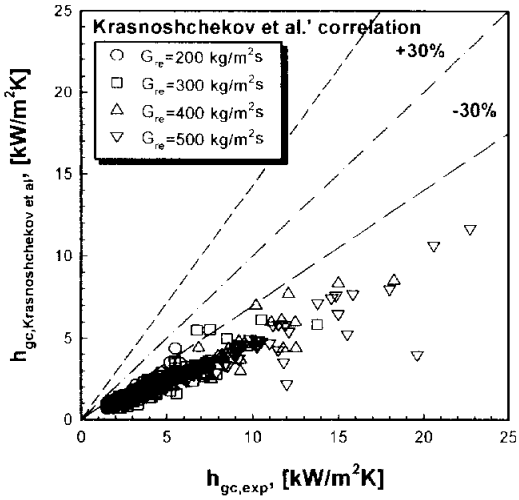

(d) Krasnoshchekov et al.'s correlation(1970)

Fig. 4.13 Comparison between the calculated and measured heat transfer coefficient at varying mass fluxes (continued).

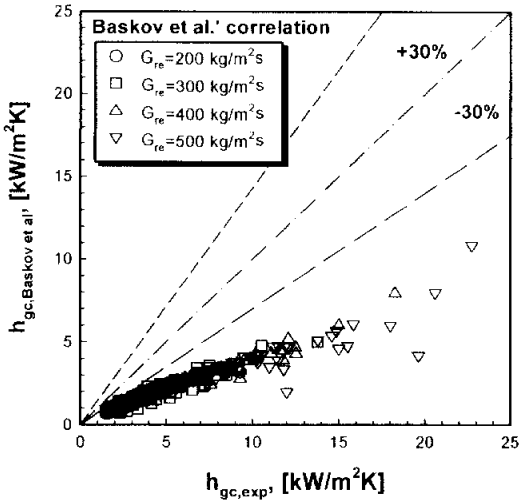

(e) Baskov et al.'s correlation(1977)

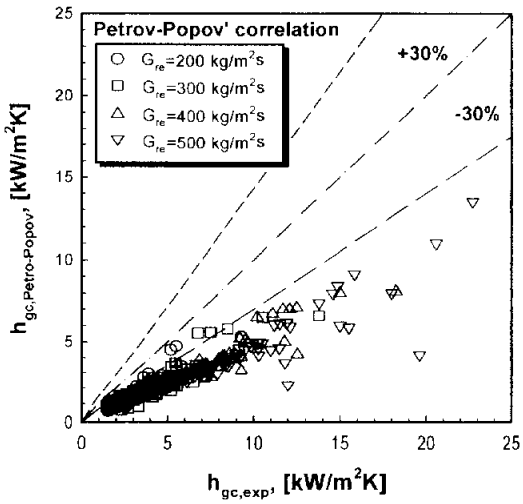

(f) Petrov Popov's correlation(1985)

Fig. 4.13 Comparison between the calculated and measured heat transfer coefficient at varying mass fluxes (continued).

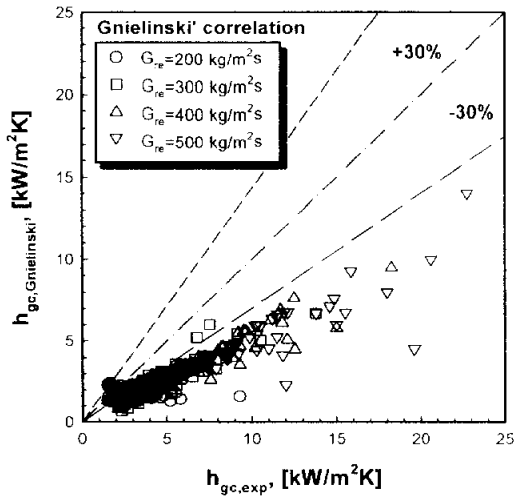

(g) Gnielinski's correlation(1994)

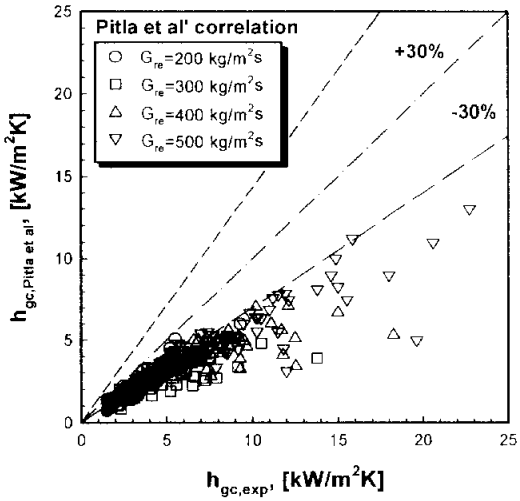

(h) Pitla et al.'s correlation(1998)

Fig. 4.13 Comparison between the calculated and measured heat transfer coefficient at varying mass fluxes (continued).

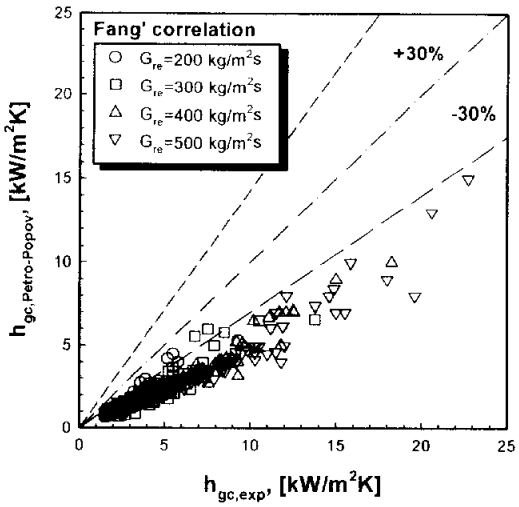

(i) Fang's correlation(1999)

Fig. 4.13 Comparison between the calculated and measured heat transfer coefficient at varying mass fluxes.

4.4.3 Correlation development

As the results of comparison of various correlations with heat transfer coefficients for cooling of supercritical CO_2, it is clear that the deviation between experimental data and the existing correlations is quite large. So there is a need for a new correlation based on experimental data, and a new correlation proposes in present study. The new proposed correlation is a form of Dittus Boelter's one. Because the change of thermophysical properties in the supercritical region is great, it introduces the specific heat and density into the new proposed correlation.

Therefore, the following forced convective heat transfer correlations are proposed for turbulent flows of CO_2 during supercritical gas cooling process.

$$Nu_b = a' Re_b^{b'} \ \mathrm{Pr}_b^{c'} \left(\frac{c_{p,b}}{c_{p,w}} \right)^{d'} \tag{4.53}$$

$$Nu_b = a' Re_b^{b'} \ \mathrm{Pr}_b^{c'} \left(\frac{\rho_b}{\rho_w} \right)^{d'} \tag{4.54}$$

As can be seen in above equations, Eq. (4.53) introduces the term, $c_{p,b}/c_{p,w}$, for considering the influence of large property variations in the heat transfer, and also Eq. (4.54) uses the term, ρ_b/ρ_w, to account for the change of thermophysical properties near the critical region.

As mentioned in earlier chapter, the heat transfer coefficients during cooling process of CO_2 dramatically increases for the temperature range above the pseudocritical point, and then decreases for the temperature range below the pseudocritical point. Therefore, since the new proposed

correlation cannot predict the heat transfer coefficients near the pseudocritical temperature, it is good to separate the region above and below the pseudocritical temperature ($T_b/T_{pc} > 1$ and $T_b/T_{pc} \leq 1$).

In the range of $T_b/T_{pc} > 1$, the constants in the proposed heat transfer correlations shown in Eq. (4.55) and (4.56) were obtained by least square curve fitting[64]. The exponents a′, b′, c′ and d′ obtained from the least square curve-fitting are shown as following Equations

$$Nu_b = Re_b^{0.55}\ \mathrm{Pr}_b^{0.23}\left(\frac{c_{p,b}}{c_{p,w}}\right)^{0.15} \quad \text{for} \quad T_b/T_{pc} > 1 \tag{4.55}$$

$$Nu_b = Re_b^{0.54}\ \mathrm{Pr}_b^{0.28}\left(\frac{\rho_b}{\rho_w}\right)^{-0.38} \quad \text{for} \quad T_b/T_{pc} > 1 \tag{4.56}$$

where $c_{p,b}$ is the mean isobar specific heat at T_b and $c_{p,w}$ is the isobar specific heat at T_w. ρ_b and ρ_w are the density at T_b and T_w, respectively. Most of the experimental data can be predicted by the correlation of Eq. (4.55) within the average deviation of 4.2% and mean deviation of 16.9%. The predicted correlation by Eq. (4.56) is the average deviation of 10.6% and mean deviation of 19.8%. Hence, the average and mean deviation of Eq. (4.55) which includes the term, $c_{p,b}/c_{p,w}$, is smaller than those of Eq. (4.56).

In case of $T_b/T_{pc} \leq 1$ which includes the region between pseudocritical and critical temperature, the change of the CO_2 properties is much bigger. In order to reflect the property change, an attempt is made to insert thermophysical properties to the correlation. As the density and specific

heat evaluated at T_b and T_w have a great effect on heat transfer coefficients, the density and specific heat normalized by the property at the pseudocritical temperature are introduced as shown in Eq. (4.57), (4.58) and (4.59). The exponents in the proposed heat transfer correlations shown in Eq. (4.57), (4.58) and (4.59) were obtained by the same method.

$$Nu_b = Re_b^{0.36}\ \mathrm{Pr}_b^{1.9}\left(\frac{c_{p,b}}{c_{p,w}}\right)^{-2.9} \quad \text{for} \quad T_b/T_{pc} \le 1 \qquad (4.57)$$

$$Nu_b = Re_b^{0.44}\ \mathrm{Pr}_b^{0.96}\left(\frac{\rho_b}{\rho_w}\right)^{0.29} \quad \text{for} \quad T_b/T_{pc} \le 1 \qquad (4.58)$$

$$Nu_b = Re_b^{0.35}\ \mathrm{Pr}_b^{1.9}\left(\frac{\rho_b}{\rho_w}\right)^{-1.6}\left(\frac{c_{p,b}}{c_{p,w}}\right)^{-3.4} \quad \text{for} \quad T_b/T_{pc} \le 1 \qquad (4.59)$$

Most of the experimental data can be predicted by the correlation of Equation (4.57) within the average deviation of -5.8% and mean deviation of 16.6%. The average and mean one of the predicted correlation by Equation (4.58) is 11.2% and 18%, respectively. And also the correlation predicted by Eq. (4.59) is the average deviation of 9.7% and mean deviation of 17.6%. Consequently, in the range of $T_b/T_{pc} \le 1$, the average and mean deviation of Eq. (4.57) which includes the term of $c_{p,b}/c_{p,w}$ is smaller than those of Eq. (4.58) and (4.59).

Fig. 4.14 depicts the comparison of the Nusselt numbers, Nu_{exp}, obtained by experimental data and that, Nu_{cal}, calculated by the new proposed correlations. As can be seen in Fig. 4.14, the deviation of Nu_{exp} and Nu_{cal} is the greatest near the value of $T_b/T_{pc}=1$. As stated in earlier chapter,

because the thermophysical properties of the density and specific heat near $T_b/T_{pc}=1$ change dramatically, the deviation of the proposed correlation for considering the effect of critical enhancement near the value of $T_b/T_{pc}=1$ is large.

Finally, the simple correlations for considering the effect of critical enhancement are suggested. The new proposed correlation in this study is a form of Dittus-Boelter's equation multiplying the density and specific heat ratio for considering the effect of it. The correlations proposed for this study are used for predicting heat transfer coefficients of supercritical CO_2. But, among them, the new correlation with the smallest deviation is suggested.

$$Nu_b = a' Re_b^{b'} \Pr_b^{c'} \left(\frac{\rho_b}{\rho_w}\right)^{d'} \left(\frac{c_{p,b}}{c_{p,w}}\right)^{e'} \tag{4.60}$$

$a'=1,\ b'=0.55,\ c'=0.23,\ d'=0,\ e'=0.15$ for $T_b > T_{pc}$

$a'=1,\ b'=0.36,\ c'=1.9,\ d'=0,\ e'=-2.9$ for $T_b \leq T_{pc}$

Table 4.5 Coefficients and exponents in the new proposed correlations

Parameters	$Nu_b = a' Re_b^{b'} \Pr_b^{c'} \left(\frac{\rho_b}{\rho_w}\right)^{d'} \left(\frac{c_{p,b}}{c_{p,w}}\right)^{e'}$		σ_{avg}, σ_{abs} (%)
$T_b/T_{pc} > 1$	Eq. (4.55)	a′ 1, b′ =0.55, c′ =0.23, d′ =0, e′ -0.15	4.2, 16.9
	Eq. (4.56)	a′ =1, b′ =0.54, c′ =0.28, d′ =-0.38, e′ =0	-10.6, 19.8
$T_b/T_{pc} > \leq 1$	Eq. (4.57)	a′ =1, b′ =0.36, c′ =1.9, d′ =0, e′ = 2.9	-5.8, 16.6
	Eq. (4.58)	a′ =1, b′ =0.44, c′ =0.96, d′ -0.29, e′ =0	-11.2, 17.9
	Eq. (4.59)	a′ =1, b′ =0.35, c′ =1.9, d′ = -1.6, e′ = 3.4	-9.7, 17.6

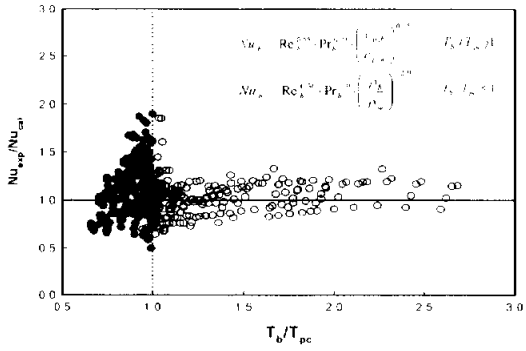

(a) Eq. (4.55)+ Eq. (4.57)

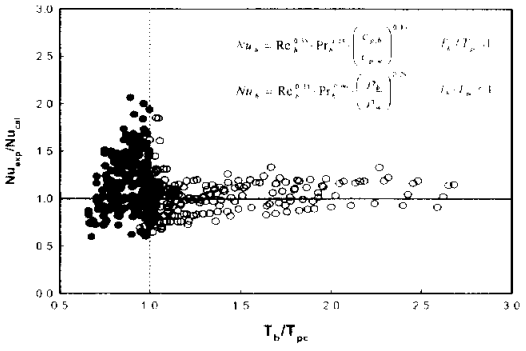

(b) Eq. (4.55)+ Eq. (4.58)

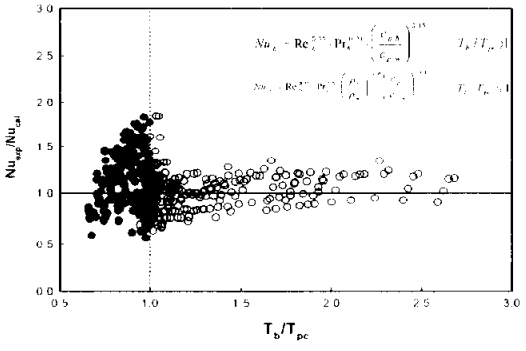

(c) Eq. (4.55)+ Eq. (4.59)

Fig. 4.14 Experimental values of the Nusselt numbers compared with those given by the proposed correlation (continued).

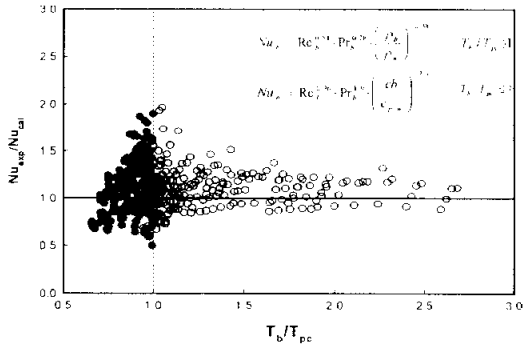

(d) Eq. (4.56)+ Eq. (4.57)

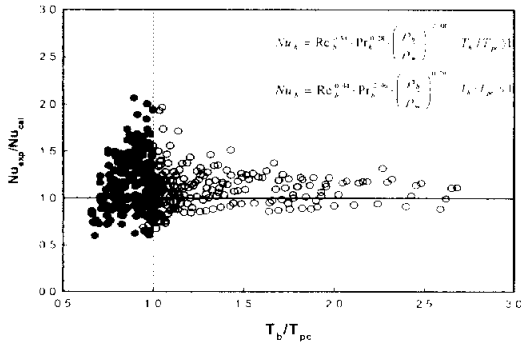

(e) Eq. (4.56)+ Eq. (4.58)

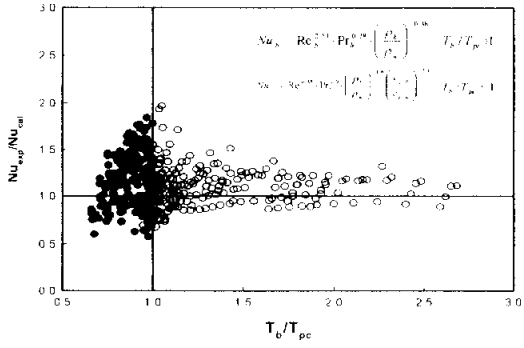

(f) Eq. (4.56)+ Eq. (4.59)

Fig. 4.14 Experimental values of the Nusselt numbers compared with those given by the proposed correlation.

4.5 SUMMARY

In this chapter, the heat transfer coefficients and pressure drop during the gas cooling process of CO_2 have been measured and the findings of this study are summarized as follows.

(1) During cooling process of CO_2, the heat transfer coefficient of CO_2 slowly increases in the entrance of gas cooler and again decreases in the exit of gas cooler. Because the specific heat of CO_2 has its maximum near pseudocritical temperature, $T_b/T_{pc}=1$, the heat transfer coefficient has its peak value in the middle stage of gas cooler. Because thermophysical properties of CO_2 for pressure variation is small, The heat transfer coefficient variation tends to decrease as cooling pressure of CO_2 increases. The heat transfer coefficient with respect to mass flux increases as mass flux increases, because the Reynolds number of CO_2 increases with mass flux, and increases the effect of heat transfer.

(2) Because of the large variation of specific heat of CO_2 near the pseudocritical region, the pressure drop during cooling process of supercritical CO_2 decreases as the inlet pressure of gas cooler increases. When compared of the pressure drop obtained with experimental data and that of predicted by Blasius's equation, the correlation which is proposed by Blasius agrees quite well with the experimental data. Therefore, during gas cooling process of CO_2 in the supercritical region, Blsius's correlation is recommended for the prediction of pressure drop.

(3) The existing supercritical correlations underpredicted the measured heat transfer coefficients of gas cooling process. Because of the large variation of specific heat, density and thermal conductivity near the critical point, the deviation of the measured heat transfer coefficients and the existing correlations becomes larger close to the pseudocritical temperature. And among the existing correlations which is proposed for cooling process of supercritical CO_2, the correlation predicted by Bring and Smith shows the best agreement to experimental data. To predict more accurate heat transfer coefficient, a new correlation which includes the density and specific heat ratio evaluated at mean wall and bulk temperature has been proposed.

CHAPTER 5

CONCLUSIONS

Because CO_2 naturally exists in the atmosphere and has a lower Global Warming Potential(GWP), in order to apply CO_2 as the working fluid of refrigeration and air conditioner, the study on the heat transfer and pressure drop characteristics of CO_2 in a horizontal tube is required.

Therefore, in this study, it is investigated that the heat transfer coefficient during evaporation and cooling process of CO_2 in a stainless steel tube with an inner diameter of 7.75 mm. The main results were summarized as follows :

(1) For low quality, the evaporation heat transfer coefficients of CO_2 in a horizontal tube increase with vapor quality. This results from the increased void fraction and the thinner liquid film with quality. At higher quality, the heat transfer coefficient has a peak value at the pseudocritical temperature, and decreases with quality. This is because the surface tension and viscosity of CO_2 are higher than those of fluorocarbon refrigerants.

(2) The measured pressure drop during evaporation process of CO_2 increases with the increased mass flux and the decreased saturation temperature. This has something to do with thermophysical property like density. When comparing the evaporation pressure drop obtained from

experimental data with the correlations proposed by some researchers, the deviation between the measured values and the calculated values by Chisholm's correlation(1968), Chisholm's correlation(1983), Jung et al.'s correlation and Choi Domanski's correlation(1999) is 65.9%, 83.1%, 74.9% and 12.3%, respectively.

(3) In order to predict the evaporation heat transfer coefficient in a horizontal tube, several investigators proposed the their correlation through experimental and theoretical analysis. Among these correlations, the proposed correlations by Shah, Gungor Winterton, Kandlikar and Jung et al. have been widely used for predicting the evaporation heat transfer coefficient in a horizontal tube. In this study, these correlations were compared to experimental data. Jung et al.'s correlation has relatively agreement to experimental data. Kandlikar's correlation shows a tendency to decrease with the increased vapor quality, while the proposed correlations by Gungor-Winterton, Kandlikar and Shah increase with quality.

(4) At low quality, the local heat transfer coefficient of CO_2 during gas cooling process increases slowly. For higher vapor quality, it has a maximum value at the pseudocritical temperature and decreases with quality. One of the reason that the cooling heat transfer coefficient has a peak value near the pseudocritical temperature is the large variation of thermophysical properties at this temperature. But, because CO_2 is

subcooled in the exit range of gas cooler, the change in thermophysical property of CO_2 is small and CO_2 heat transfer coefficient decreases dramatically.

(5) For the different cooling pressure and same mass flux conditions, due to comparatively few variation of thermophysical properties in the inlet and outlet range of gas cooler, the variation in the heat transfer coefficient with respect to the inlet pressure of gas cooler is small. But, in the vicinity of pseudocritical region, the heat transfer coefficient of CO_2 decreases largely as the inlet pressure of gas cooler increases.

(6) For the constant inlet pressure, the local cooling heat transfer coefficient of CO_2 increases with mass flux. This results from the high Reynolds number as increased mass velocity. The change in the heat transfer coefficient with respect to mass flux is distinct at the critical point. The heat transfer coefficient of CO_2 has the highest value at the inlet pressure of 7.5 MPa and has the lowest value at the inlet pressure of 11.0 MPa. This is because the change of thermophysical properties is large at the pseudocritical point.

(7) At the constant inlet pressure of gas cooler, the pressure drop of CO_2 has a tendency to increases with the increased mass flux and the decreased inlet pressure. And, for the higher mass flux, the measured pressure drop is increased at a high rate in the lower pressure of cooling

process. This is because CO_2 density is higher as the system pressure is higher.

(8) In order to examine the cooling heat transfer coefficient of supercritical CO_2, the experimental data in this study was compared to the correlations proposed by Bringer-Smith, Petuhkov et al., Krasnoshchekov et al., Baskov et al., Petrov Popov, Ghajar Asadi, Gnielinski, Krasnoshchekov-Protopopov and Pitla et al. Among these correlations, the Bringer-Smith's correlation agrees quite well with the experimental data within 23.6%. Therefore, based on the experimental results, the new correlation, which is including a density and specific heat ratio evaluated at mean wall and bulk temperature, was proposed in this study.

REFERENCES

(1) Lorentzen, G. and Pettersen, J., 1993, A new, efficient and environmentally benign system for car air-conditioning, International Journal of Refrigeration, Vol. 16, No. 1, pp. 4~12.

(2) McLinden, M. O., Klein, S. A., Lemmon, E. W., and Peskin, A. P., 1998, NIST Thermodynamic Properties and Refrigerant Mixtures Database (REFPROP), Version 6.01, National Institute of Standards and Technology, Gaithersburg, MD, U.S.A.

(3) Hwang, Y., 1997, Comprehensive Investigation of Carbon Dioxide Refrigeration Cycle, Univ. of Maryland, Ph.D. Thesis.

(4) Hwang, Y., and Radermacher, R., 1998, Theoretical evaluation of carbon dioxide refrigeration cycle, HAVC & Research, Vol. 4, No. 3, 245~263.

(5) Vesovic, V., Wakeham, W. A., Olchowy, G. A., Sergers, J. V., Watson, J. T. R., and Millat J., 1990, The transport properties of carbon dioxide, J. Phy. Chem. Ref. Data, Vol. 19, No. 3, pp. 763~810.

(6) Rieberer, R., 1998, CO_2 as Working Fluid for Heat Pumps, Institute of Thermal Engineering Graz University of Technology, Inffeldgasse 25, A 8010 Graz, Austria, Doctoral thesis.

(23) Pettersen, J., Rieberer, R., and Munkejord, S. T., 2000, Heat transfer and pressure drop for flow of supercritical and subcritical CO_2 in microchannel tubes, SINTEF Energy Research.

(7) Kuo, C. S. and Wang, C. C., 1996, In tube evaporation of HCFC 22 in

a 9.52 mm micro fin/smooth tube, Int. J. Heat Mass Transfer, Vol. 39, No. 12, pp. 2559~2569.

(8) Yuan, Z., Michael, M., and Jafer, D., 1999, Forced Convection Boiling Heat Transfer of CO_2 in Horizontal Tubes, Xth ASME/JSME Joint Thermal Engineering Conference.

(9) Gungor, K. E. and Winterton, R. H. S., 1987, Simplified General Correlation for Flow Saturated Boiling and Comparisons of Correlations with Data, Chem. Eng. Res, Des., Vol. 65, pp. 148~156.

(10) Hihara, E. and Tanaka, S., 2000, Boiling Heat Transfer of Carbon dioxide in Horizontal Tubes, Proc. 4th IIR-Gustav Lorentzen Conf. On Natural Working Fluids, Purdue University, USA, pp. 279~284.

(11) Choi, Jun Y., Kedzierski, A. Mark, and Domanski A. Piotr, 1999, A Generalized pressure drop correlation for evaporation and condensation of alternative refrigerants in smooth tube and micro-fin tube, NISTIR 6333, pp. 7~15

(24) Yun, R., 2002, Convective Boiling of Carbon Dioxide in Mini Tubes and Microchannels, Korea University, Department of Mechanical Engineering, Thesis for the Degree of Doctor.

(45) Shah, M. M., 1979, A general correlation for heat transfer during film condensation inside pipes, International Journal of Heat and Mass Transfer, Vol. 22, pp. 157~165.

(47) Liu, Z. and Winterton, R. H. S., 1991, A General Correlation for Saturated and Subcooled Flow Boiling in Tubes and Annuli, Based on a Nucleate Pool Boiling Equation, Int. J. Heat and Mass Transfer, Vol. 34,

No. 1, pp. 2759 2766.

(13) Bredesen, A. M., K. Aflekt, J., Pettersen, A., Hafner, P., Neksà, G., Skaugen, 1997, Studies on CO_2 heat exchangers and heat transfer, IEA/IIR workshop on CO_2 technologies in refrigeration, heat pump, and air-conditioning systems, Trondheim, Norway, May 13~14.

(14) Chen, J. C., 1966, "A correlation for boiling heat transfer to saturated fluids in vertical flow", Heat Transfer Engineering, Vol. 1, No. 4, pp. 32 ~ 37.

(15) Bennett, D. L. and Chen, J. C., 1980, Forced convective boiling in vertical tubes for saturated pure components and binary mixtures, AIChE Journal, Vol. 26, No.3, pp. 454~461

(16) Schrock, V. E., and L. M. Grossman, 1959, Forced convective boiling studies, Rept. No. 73308-UCX 2182, University of California, Berkeley.

(17) Hashimoto, K., Saikawa, M., and Iwatsubo, T., 2000, Experimental study about heat transfer coefficient of CO_2 on supercritical condition, 37th Heat Transfer Symposium, Japan, pp. 401~402.

(54) Olson, D. A., 2000, Heat transfer of supercritical carbon dioxide flowing in a cooled horizontal tube, Preliminary Proceedings of the 4th IIR-Gustav Lorentzen Conference on Natural Working Fluids at Purdue, July 25~28, pp. 251~258.

(59) Krasonshchekov, E. A. and Protopopov. V. S., 1966, Experimental Study of Heat Exchange in Carbon Dioxide in the Supercritical Range at High Temperature Drops, Teplofizika Vysokikh Temperatur, 4(3), pp. 389~398.

(64) Gnielinski, V., 1976, New Equation for Heat and Mass Transfer in Turbulent Pipe and Channel Flow, Int. Chem. Eng., 16 : pp. 359~368.

(18) Gao, L. and Honda, T., 2002, Experimental on heat transfer characteristics of heat exchanger for CO_2 heat pump system, Proceedings of the Asian Conference on Refrigeration and Air Conditioning, December 4, Kobe, Japan, pp. 75~80.

(19) Petrov, N. E. and V. N. Popov., 1985, Heat Transfer and Resistance of Carbon Being Cooled in the Supercritical Region, Thermal Engineering., 32(3), 131~134.

(20) Fang, X., Bullard, C. W., and Hrnjak, P. S., Heat Transfer and Pressure Drop of Gas Coolers, ASHRAE Transaction, Vol. 107, Part 1, pp. 255~266.

(21) Fang, X. D., 1999, Modeling and analysis of gas coolers. ACRC CR 16, Air Conditioning and Refrigeration Center, Department of Mechanical and Industrial Engineering, University of Illinois at Urbana Champaign, USA.

(22) Pitla, S. S., Robinson, D. M., Groll, E. A. and Ramadhyani, S., 1998, Heat Transfer from Supercritical Carbon Dioxide in Tube Flow: A Critical Review, 1998, HVAC&R research, Vol. 4, No. 4, 281~301.

(23) Mori, K., Onishi, J., Shimaoka, H., Nakanishi, S., and Kimoto, H., 2002, Cooling heat transfer characteristics of CO_2 Oil mixture at supercritical pressure conditions, Proceedings of the Asian Conference on Refrigeration and Air Conditioning, December 4, Kobe, Japan, pp. 81~86.

(25) Yoon, S. H., 2002, Studies on the Characteristics of Evaporative and

Supercritical Gas Cooling Heat Transfer of Carbon Dioxide, Seoul National University, School of Mechanical and Aerospace Engineering, Thesis for the Degree of Doctor of Philosophy.

(26) Yun, L., Kim, Y. C., and Kim, M. S., Two-phase flow patterns of CO_2 in a narrow rectangular channel, International Congress of Refrigeration 2003, Washington D. C., pp. 1~7.

(27) Zhao, Y., Ohadi, M. M., Dessiatoun, S. V., Molki, M., Darabi, J., 1999. Forced convection boiling heat transfer of CO_2 in horizontal tube, in : AJTE99-6249, Proc. 5th ASME/JSME Joint Thermal Engineering Conference, San Diego, California.

(28) Cho, E. S., Yoon, S. H., and Kim, M. S., 2000, A study on the characteristics of evaporative heat transfer for carbon dioxide in a horizontal tube, in: Proceedings of the KSME Spring Annual Meeting, pp. 104~107.

(29) Cooper, M. G., 1984, Heat Flow Rates in Saturated Nucleate Pool Boiling a Wide ranging Examination Using Reduced Properties, Advances in Heat Transfer, Vol. 16, pp. 157~239.

(30) Oh, H. K., and Hong, J. W., 1999, Condensing heat transfer characteristics of alternative refrigerants in small diameter tubes, SAREK, Vol. 28, No. 5, pp. 396~402.

(31) Son, C. H., Choi, Y. S., Kim, G. S., and Oh, H. K., 2001, The Condensation Pressure Drop of Alternative Refrigerants for R-22 in Small diameter Tubes, KSME International Journal B, Vol. 25, No. 9, pp. 1245~1252.

(32) Kim, J. S., and Katsuta, M., 1995, Development of High Performance Heat Exchanger For CFC Alternative Refrigerants (1st Report : Condensing Heat Transfer and Pressure Drop of HFC 134a in Multi-pass Tubes, Journal of Refrigeration & Air Conditioning Engineering, Vol. 14, No. 5, pp. 273~283.

(33) Kim, G. S., 1999, Study on condensing heat transfer characteristics of horizontal double pipe heat exchangers using small diameter tube, Pukyong National University, Department of Refrigeration Engineering, Thesis for the Degree of Master.

(34) Pierre, B., 1964, Flow resistance with boiling refrigerants part I, ASHRAE Journal, September, pp. 58~65.

(35) Martinelli, R. C. and Nelson, D. B., 1948, Prediction of pressure drop forced circulation boiling of water, Trans. Am. Soc. Mech. Eng., 70, pp. 695~702.

(36) Lockhart, R. W. and Martinelli, R. C., 1949, Proposed correlation of data for isothermal, two phase, two component flow in pipes, Chemical Engineering Progress, Vol. 45, pp. 39~48.

(37) Baroczy, C. J., 1966, A systematic correlation for two-phase pressure drop, Chemical Engineering Progress Symposium Series, Vol. 62, No. 64, pp. 232~249.

(38) Chisholm, D., 1968, The influence of mass velocity on friction pressure gradients during steam water flow, Presented at 1968 Thermodynamics and Fluid Mechanics Convection of the Institute of Mechanical Engineer, Bristol, UK.

(39) Chisholm, D., 1983, Two Phase Flow in Pipelines and Heat Exchangers, Longman.

(40) Reddy, D. G., Fighetti, C. F., and Merilo, M., 1983. Evaluation of two-phase pressure drop correlations for high pressure steam water systems, ASME JSME Thermal Engineering Joint Conference Proceedings, Honolulu, HI, Vol. 1, pp. 251~259.

(41) Jung, D. S, McLinden, M., Randermacher, R., and Didion, D., 1989, "A study of flow boiling heat transfer with refrigerant mixtures", International Journal of Heat and Mass Transfer, Vol. 32, No. 9, pp. 1751~1764.

(42) Friedel, L., 1979, Improved friction pressure drop correlation for horizontal and vertical two phase pipe flow, European Two-Phase Flow Group Meeting, Ispra, Italy, Paper E2, June,

(43) Choi, Jun Y., A. Mark Kedzierski and P. A. Domanski, 1999, A generalized pressure drop correlation for evaporation and condensation of alternative refrigerants in smooth tube and micro-fin tube, NISTIR 6333, 7~15.

(44) Collier, J. C., and Thome, J. R., 1994, Convective Boiling and Condensation, Oxford University Press, pp. 24~25, 67~68.

(46) Kandlikar, S. G., 1990, "A general correlation for saturated two phase flow boiling horizontal and vertical tubes", Trans. ASME, Vol. 112, pp. 219 ~ 228.

(48) Dittus, F. W. and Boelter, L. M. K., 1930, University of California, Berkeley, Publications on Engineering, Vol. 2, p. 443.

(49) Froster, H. K. and Zuber, N., 1955, Dynamics of vapor bubbles and boiling heat transfer, AIChE J., Vol. 1, 531~535.

(50) Collier, J. G. and Thome, J. R., 1994, "Convective boiling and condensation", Oxford Science Pub.

(51) Stephan, K. and Abdelsalam, M., 1980, "Heat transfer correlations for natural convection boiling", Int. J. Heat Mass Transfer 29, pp. 73~87.

(52) Fritz, W., 1935, "Berechnung des maximalvolumens von dampfblasen", Phys. Z. 36, pp. 379~384.

(53) Incropera, F. P. and DeWitt, D. P., 1996, Introduction to Heat Transfer, 3rd Edition, John Wiley & Sons.

(55) Bringer, R. P. and Smith, J. M., 1957, AIChE. Journal, Vol. 3, No. 1, pp. 49~55.

(56) Baskov, V. L., Kuraeva, I. V., and Protopopov., V. S., 1977, Heat Transfer with the Turbulent Flow of a Liquid at Supercritical Pressure in Tubes under Cooling Conditions., Teplofizika Vysokikh Temperatur 15(1): pp. 96~102

(57) Petukhov, B. S., E. A. Krasnoshchekov, and V. S. Protopopov., 1961, An Investigation of Heat Transfer to Fluids Flowing in Pipes under Supercritical Conditions, ASME International Developments in Heat Transfer Part. 3, pp. 569~578.

(58) Petukhov, B. S. and Kirillov, V. V., 1958, On heat exchange at turbulent flow of liquid in pipes, Teploenergetika, No. 4, pp. 63~68.

(60) Krasonshchekov, E. A., Kuraeva, I. V., and Protopopov., V. S., 1970, Local Heat transfer of Carbon Dioxide at Supercritical Pressure Under

Cooling Conditions, Teplofizika Vysokikh Temperatur, 7(5), pp. 922~930.

(61) Filonenko, G. K., 1954, Hydraulic Resistance in Pipe(in Russian), Teploenergetiks, Vol. 1, No. 4, pp. 40~44.

(62) Petukhov, B. S., Kurganov, V. A., and Gladuntsov, A. I., 1973, Heat transfer in turbulent pipe flow of gases with variable properties, Heat Transfer Soviet Research 5(4), pp. 109~116.

(63) Ghahar, A. J. and A. Asadi. 1986, Improved Forced Convective Heat Transfer Correlations for Liquids in the Near Critical Region, AIAA. Journal, 24(12), pp. 2030~2037.

(64) Yu, H. Y., and Lee, K. S., 1994, Numerical Methods for Engineers, Hee Jung Dang, pp. 391~394, 492~494.

ACKNOWLEDGEMENTS

7년 동안의 냉동공학 실험실 생활을 마무리하면서 아쉬운 점도 많고 즐거웠던 점도 많았지만, 무엇보다도 내 인생에서 되돌릴 수 없는 소중한 시간이었다고 생각합니다. 냉동공학 연구실에서 지낸 시간들이 저에게는 이젠 잊을 수 없는 추억으로 남게 될 것입니다.

부족한 논문이 완성될 수 있도록 아낌없는 지도와 격려로 저를 이끌어 주시고, 학생보다는 먼저 진정한 인간이 되도록 도와주신 오후규 교수님께 진심으로 감사드립니다. 아울러, 연구 과정 동안 저의 학문적 부족함을 일깨워주셨을 뿐만 아니라, 제자를 사랑하시는 마음으로 항상 관심을 가져주신 김종수 교수님, 그리고 항상 가까이 계시면서 관심과 배려로 힘이 되어주신 김영수 교수님, 김종수 교수님, 최광환 교수님, 윤정인 교수님, 김윤필 교수님, 정석권 교수님께 감사드리며, 논문의 완성을 위해서 많은 조언으로 좋은 결실을 맺도록 힘써주신 이수대학교 냉동공학과 오종택 교수님, 서강대학교 정시영 교수님, 생산기술 연구원에 김영률 박사님과 김선창 박사님, 실험실 선배님과 후배님의 안위를 챙기시고, ORE의 영원한 발전을 위해서 많은 노력을 아끼지 않는 박기원 교수님, 후배들을 올바른 길로 이끌어 주시는 김민용 교수님께 진심으로 감사드립니다.

변함없는 도움과 관심을 주신 동명대학교 구학근 교수님, 노건상 교수님, 김종률 교수님, 지금은 고인이 되신 한국 해양대학교의 김성규 교수님, 정재천 선배님, 아진산업의 이상훈 선배님, 냉동공장의 박영덕 기사님, 한국가스 안전공사의 권옥배 박사님, 일본 사가 대학교의 배상철 선배님, TOP RACE의 이동건 선배님께 감사의 말씀을 드립니다. 그리고, 실험실 생활동안 늘 힘이 되

어주신 육현형, 종렬형, 오경형, 승준형, 춘근형, 기수형, 대열형, 광일형, 철민형, 병환형, 박진식, 임재학, 김경민, 이호림, 홍진우, 문정욱, 최영석, 정진호, 김형철, 백승문, 최이철, 이상재, 윤국영, 강영주, 윤한주, 장승환, 윤찬일, 박재홍, 임용빈, 권용하, 최봉석, 안상영, 김세웅, 안수현, 이호생, 차동안, 방기석, 이동휘, 이용언, 류태근, 김대희, 최선북, 최호식, 이광배, 전철호, 민경현, 류근태, 이승환 후배님들 그리고 많은 선배님과 여수대학교 냉동공학과 91학번 동기들에게 감사를 드립니다.

힘든 시절 친부모님처럼 사랑으로 키워 주신 자상한 외할머니, 말없이 항상 그 자리에서 지켜봐 주신 외삼촌과 외숙모, 그리고 5대 독자라는 무거운 짐을 지고 있는 경록이, 멀리 타지에서 열심히 살아가는 정언이에게 감사드립니다.

무뚝뚝하지만 동생이 올바른 길로 갈 수 있도록 노력하는 큰형, 동생이 잘 못했더라도 꾸중하지 않고 친구같은 둘째형, 예림이랑 예성이 키운다고 바쁜 와중에도 안부를 묻는 큰형수, 씩씩하고 똘똘한 두영이의 건강을 위해서 희생하는 둘째 형수, 지금의 내가 있도록 옆에서 사랑과 행복을 아낌없이 주고, 이 세상 누구보다도 소중하며 사랑스러운 나의 색시 수정이에게 고마운 마음을 전합니다.

마지막으로 그 어떠한 말로도 고마움을 표현할 수 없지만, 박사학위 논문을 성공적으로 마무리할 수 있도록 옆에서 보필해주시고 마음이 여린 장인 어른과, 아들처럼 밝은 얼굴로 날 대해주시고, 귀하게 키운 딸의 무한한 행복을 저에게 맡겨 주신 장모님께 진심으로 깊은 감사드립니다. 아울러, 자수성가하셔서 아들 셋을 상성하게 키우시고, 항상 부족한 막내 아들 잘되라고 보살펴주신 아버지와, 마음이 넓어서 남들에게 많이 베푸시고, 좋은 길로 갈 수 있도록 인도해 주시며, 내 인생의 버팀목인 어머니에게 머리 숙여 깊은 감사의 말씀을 드리며, 이 결실과 영광을 바칩니다.